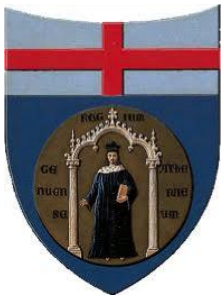

UNIVERSITY OF GENOA

MASTER'S PROGRAM IN BIOENGINEERING

Thesis submitted in partial fulfillment of the requirements for the title of

Master of Bioengineering

Investigating electrographic signatures of sleep

Gianluca Federici

14/06/2023

Thesis advisor: Prof.ssa Michela Chiappalone

Thesis co-advisor: PhD. Vinicius Rosa Cota

Contents

Introduction

The sleep-wake cycle (SWC) is a circadian neurobiological rhythm of major importance across several animal species, humans included [1]. It is characterized by a recurrent alternation of brain states (or stages) with distinct behavioral and electrophysiological features [2]. In a simplified manner, the states within the sleep-wake cycle can be classified into three main states: 1) wakefulness (WK) with desynchronized low-amplitude local field potentials (LFP) and active movement; 2) slow wave sleep (SWS) with synchronized high-amplitude LFP in lower frequencies (delta range) and absence of movement, and; 3) rapid eye movement sleep (REM) with low-amplitude LFP or synchronization in the theta range with deeply reduced muscular tonus and absence of behavior. Differently from the lay notion of a brain "shut down", SWC is in fact a result of complex interactions of neurobiological phenomena serving multiples purposes indispensable for homeostasis and life in general [3]. These molecular and cellular processes result in the production of stereotypical electrophysiological oscillations, the synchronization of which is highly descriptive of the effectiveness of the interaction between areas. Among others, these interactions underlie cognitive processing during both wakefulness and sleep. Particularly, the triple coordination between oscillations of different frequencies (slow oscillation, spindle and ripple) during SWS is a key biomarker for the consolidation of memory traces and the migration of information from hippocampal to cortical areas [4], [5], [6]. So, considering the importance of sleep in the support of core neural functions (such as those related to brain plasticity), taking SWC into account may be beneficial to the development of personalized solutions in neuroengineering. For this purpose, scientists at the University of Genova and Italian Institute of Technology in the framework of the EC-funded grant 'MoRPHEUS' (Motor Rehabilitation Plasticity Hacking by Engineered Stimulation of the Brain During the Sleep-wake Cycle) thought of developing a new neuroprosthetic approach that incorporates a programmable and multi-resolution closed-loop architecture capable of coordinating targeted stimulation during sleep. The goal is to reintegrate sleep in individuals who have suffered from brain damage, such as stroke, with the aim of promoting brain plasticity to facilitate recovery. This thesis has been developed within the MoRPHEUS project and it has a dual objective. Firstly, it aims to identify SWC-related electrophysiological biomarkers (that may represent privileged windows of plasticity for the delivery of therapeutic technological intervention). Secondly, to develop of a new 'sleep stage detection' algorithm that will allow to highlight possible dysfunctions in sleep. After a careful review of the current state of the art, I chose the neural synchronization patterns which are linked to

the SWC as biomarkers. To do that, I personally implemented three techniques: (i) spindle detection, (ii) SWC stage detection and (iii) phase-amplitude coupling (PAC) detection. Spindles are important synchronized events across SWC for memory consolidation (SO-spindle-ripple coupling). SWC stages detection is needed to divide the signal into three main stages (WK, SWS, REM). PAC is the tool that we have chosen to assess the neural synchronization profiles of each major stage and during specific temporal windows in which sleep spindles occur. Once we have identified how the synchronization of brain waves varies during the sleep of a healthy subject, we have developed a new algorithm that, based on these synchronizations, can subdivide it into its different stages (WK, SWS, REM). This is interesting because, when used in animals in which we submitted a stroke model, we can observe the repercussions of this brain injury on the SWC. The thesis is organized as follows:

- **Chapter 1** will provide an overview of the current state of the art in sleep neurophysiology, plasticity and its biomarkers. Subsequently, neurological diseases and their association with sleep will be discussed.
- **Chapter 2** will be dedicated to materials and methods. In this chapter, I will be discussing the state-of-the-art techniques for spindle detection, SWC stages detection and PAC. Additionally, I will describe the datasets that have been used in this study.
- **Chapter 3** will be dedicated to all the analyses that have been conducted for spindle detection.
- **Chapter 4** will be dedicated to all the analyses that have been conducted for SWC stage detection.
- **Chapter 5** will be dedicated to all the analyses that have been conducted for PAC.
- **Chapter 6** will include the results obtained by the analyses shown in the previous three chapters.
- **Chapter 7** will present the novelty, namely the development of a new sleep stage detection algorithm that will allow to highlight dysfunctions in sleep.

Chapter 1

Sleep Neurophysiology

1.1. Nervous system

The nervous system encompasses all the nerve cells present in the human body. Its primary function is to facilitate communication with the external world, while also regulating several internal mechanisms. The nervous system takes in information through our senses, processes the information and triggers reactions, such as making your muscles move or causing you pain.

The nervous system can be divided into two parts, the central nervous system (CNS) and the peripheral nervous system (PNS), so called due to their anatomical location within the body.

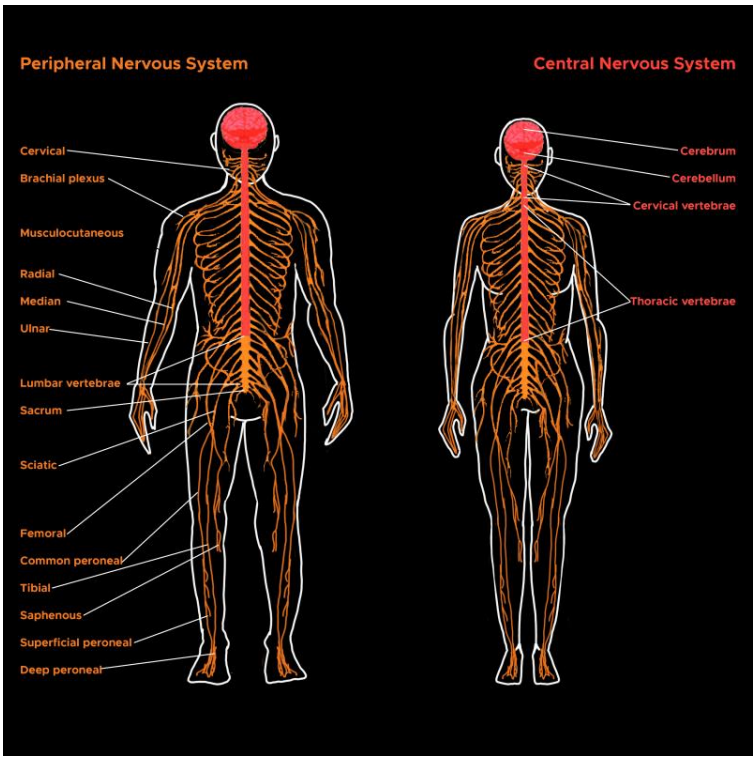

Figure 1 - Illustration of peripheral and central nervous systems. Brain, spinal cord, nerves [7].

The CNS comprises the nerves in the brain and spinal cord, which are protected by the skull and vertebral canal; the CNS is responsible for processing and interpreting information received from the sensory organs and for controlling body responses to stimuli. The PNS, on the other hand, is composed of nerves and ganglia that transport information between the CNS and body organs. Furthermore, the nervous system can be categorized as voluntary and involuntary, regardless for the location in the body. The voluntary nervous system, also known as the somatic nervous system, controls conscious actions that can be influenced, such as movements of limbs and other body parts. On the other hand, the involuntary nervous system, also known as the vegetative or autonomic nervous system, regulates unconscious processes in the body that cannot be consciously controlled such as heart rate, digestion, respiratory rate, and blood pressure. In general, the nervous system is an incredibly complex system, but for the purposes of this thesis, it is sufficient to focus on neurons and the brain. [8]

1.1.1. Neurons

The neuron is the main functional unit of the nervous system. It is the neurons that, by sensing changes in the environment and communicating them among themselves, can control the responses of our body. Thus, they are responsible for the processing of information in the brain. [9] Although neurons can have different morphologies, they all contain four common regions: soma (the cell body), the dendrites and the axon terminals, each of which with their respective functions. The axon transmits efferent signals, the dendrites receive afferent signals from their surroundings while the soma contains the nucleus and other organelles necessary for neuronal function.

Action Potential

When neurons are excited, they can generate an action potential, or electrochemical signals, which propagates along the axons until it reaches synaptic terminations. When a neuron is not transmitting any nerve impulses, the potential is in a resting state. During the resting state, the action of a protein called the sodium-potassium pump maintains a charge difference across the neuron's cellular membrane by actively transporting sodium ions from the inside to the outside of the cell and potassium ions from the outside to the inside [10]. This charge difference generates an electrical potential called the resting membrane potential, which is approximately -65 mV [8]. The modification of the resting potential due to a depolarizing stimulus is called an action potential. The action potential takes place if the stimulus reaches the threshold value, which corresponds, approximately to-55 mV. During the action potential, several zones can be recognized (Figure 1):

- Depolarization, changing the membrane's potential from -60 mV to +40 mV primarily caused by sodium influx.
- Repolarization, a return to the membrane's resting potential, primarily caused by potassium efflux.
- After-hyperpolarization, a recovery from a slight overshoot of the repolarization.[9]

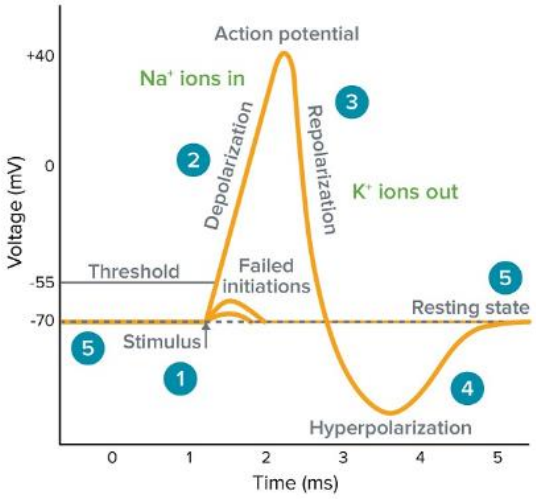

Figure 1 – Action potential

During the depolarization and repolarization phases, no further action potential can be generated, although the applied stimulus. This period is called the absolute refractory period (ARP). The ARP is crucial because it ensures that action potentials are transmitted in only one direction along an axon. Following the ARP, during hyperpolarization, the relative refractory period (RRP) occurs. During this period, a second action potential can be generated only by applying stimuli with an intensity higher than the that generated the previous potential. Once the action potential has reached the end of the axon, the information contained within it must be transferred to another neuron. This transfer occurs at specialized sites that the English physiologist Charles Sherrington called "synapses" in 1897.

Background Activity

Background activity refers to the continuous and irregular spontaneous activity of the central nervous system (CNS) in the absence of external stimuli. This activity is characterized by low-

frequency action potentials, typically between 1 and 10 Hz, that occur randomly in different regions of the brain, it constitutes a sort of background noise. Background activity has been observed in all vertebrates, from fish to mammals, including humans [11]

Synchronized spontaneous activity.

Spontaneous synchronized activity is the one occurring in a particular region of the brain activate simultaneously in a synchronized manner. The synchronized spontaneous activity we are interested in for our research is the local field potential.

Local field potential

LFPs are typically obtained by low pass filtering the raw neural signals (below ∼300 Hz) and reflect summed synaptic activity from a local neuronal population (within a radius of at least a few hundred micrometers) around the recording electrode. Depending on the size and placement of the extracellular electrode, the volume of neurons that contribute to the measured signal varies substantially. With very fine electrodes, the local field potentials reflect the synaptic activity of tens to perhaps thousands of nearby neurons only. Local field potentials are thus the electric fields that reflect a weighted average of input signals on the dendrites and cell bodies of neurons in proximity of the electrode. The reliability of such a relationship, however, progressively decreases with increasing the electrode size, by lumping together electric fields from increasingly larger numbers of neurons. This is why the scalp EEG, a spatially smoothed version of the local field potential at numerous contiguous sites, has a relatively poor relationship with spiking activity of individual neurons. In the case of burst activity, where multiple neurons synchronize their firing, a wave-like pattern can be observed in the local field potential (LFP) with periods of bursts alternating with periods of silence. Thus, the resulting LFP appears as waves, which are commonly referred to as brain waves. There are different types of brain waves that will be discussed in *paragraph 2.5* (figure 2).

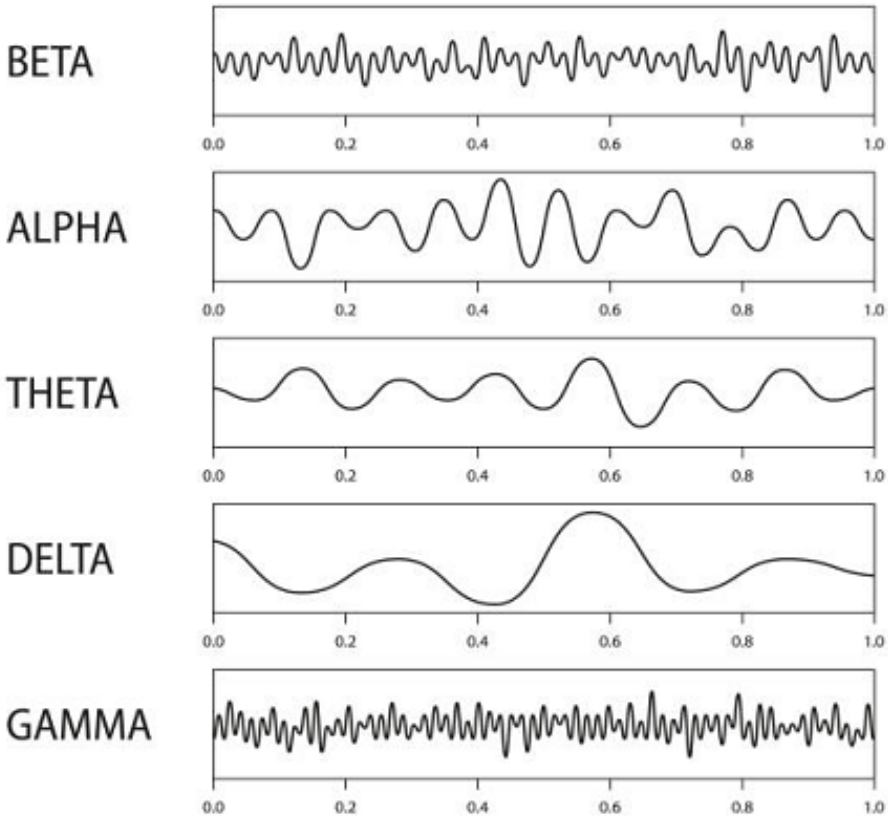

Figure 2 - Brain wave samples with dominant frequencies belonging to beta, alpha, theta, and delta bands and gamma waves.

1.1.2. Brain

The brain represents 2% of the human body weight and it is widely considered the most intricate of all biological systems, consisting of over 100 billion neurons in its mature state. The brain is an organ composed of nervous tissue that commands task-evoked responses, movements, senses, emotions, language, communication, thinking, and memory. The brain can be divided for simplicity into three primary brain vesicles that differentiate into five secondary brain vesicles. In the subdivision, I have included the main anatomical structures that play a fundamental role in sleep. [12]

1. Forebrain. The forebrain is by far the largest brain division, in fact it includes the cerebrum and consists of two parts:
    - Telencephalon: Cerebral cortex, Hippocampus, Amygdala
    - Diencephalon: Thalamus, Hypothalamus Epithalamus (pineal gland)

2. Midbrain. The midbrain is the area of the brain that connects the forebrain to the hindbrain. The midbrain and hindbrain together compose the brainstem
    - Midbrain
3. Hindbrain.
    - Metencephalon: Cerebellum, Pons
    - Myelencephalon: Medulla [12]

The three main parts of the human brain are the cerebrum, cerebellum, and brainstem (figure 3).

Cerebrum

The cerebrum governs motor and sensory information, conscious and unconscious behaviors, feelings, intelligence, and memory. The left hemisphere is responsible for speech and abstract thinking, while the right hemisphere controls spatial thinking. Motor and sensory neurons descending from the brain cross to the opposite side in the brainstem, meaning that a stroke affecting the left-brain hemisphere will result in motor and sensory deficits on the right side of the body. Two very important structures within the cerebrum are the thalamus and hypothalamus. Sensory neurons, in fact, bring sensory input from the body to the thalamus, which then relays this sensory information to the cerebrum. For example, hunger, thirst, and sleep are under the control of the hypothalamus.

The cerebrum comprises four lobes: the frontal, parietal, temporal, and occipital lobes, each of which with distinct functions.

- The frontal lobe controls motor function, language, and cognitive processes, such as memory.
- The parietal lobe is responsible for interpreting vision, hearing, motor, sensory, and memory functions.
- The temporal lobe is crucial for understanding spoken and written language (Wernicke area), retaining memories, processing emotions, and plays a significant role in hearing and spatial and visual perception.
- The occipital lobe contains the visual cortex and is responsible for interpreting visual information.

Cerebellum

The cerebellum controls the coordination of voluntary movement and receives sensory information from the brain and spinal cord to fine-tune the precision and accuracy of motor activity.

Additionally, the cerebellum aids in various cognitive functions, such as attention, language, pleasure response, and fear memory.

Brainstem

The brainstem acts as a bridge connecting the cerebrum and cerebellum to the spinal cord. It contains principal centers that perform autonomic functions such as breathing, temperature regulation, respiration, heart rate, wake-sleep cycles, coughing, sneezing, digestion, vomiting, and swallowing. The brainstem contains both white and gray matter [12].

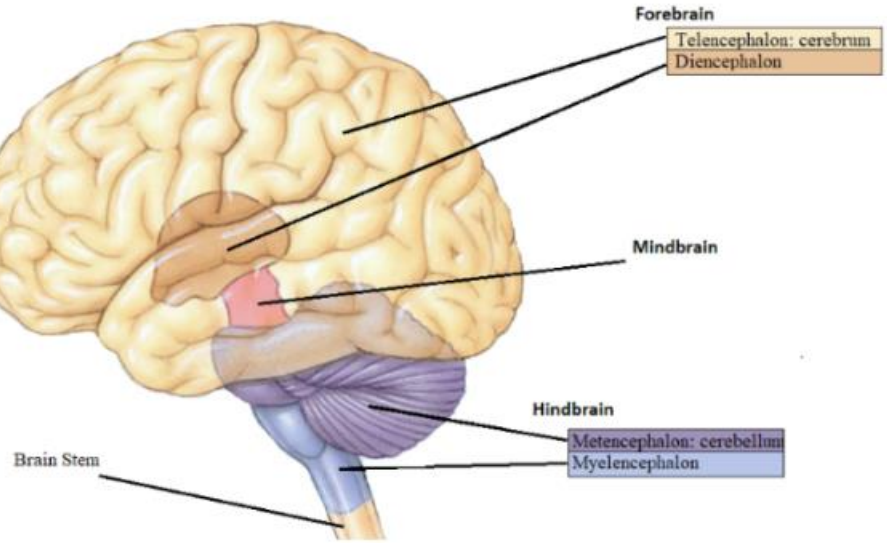

Figure 3 – Brain structures

1.1.3. Brain structures involved in sleep.

There are several brain structures that are involved in sleep (figure 4). The hypothalamus, a small structure deep inside the brain, contains groups of nerve cells that act as control centers affecting sleep and arousal. Within the hypothalamus, the suprachiasmatic nucleus (SCN) is a cluster of thousands of cells that receive information about light exposure directly from the eyes and regulate the circadian rhythm. Some people with damage to the SCN sleep erratically throughout the day because they are not able to match their circadian rhythms with the light-dark cycle. The brain stem, which includes the pons, medulla, and midbrain, communicates with the hypothalamus to control the transitions between wake and sleep. The brain stem also plays a special role in REM sleep; it

sends signals to relax muscles essential for body posture and limb movements, so that we don’t act out what happens in our dreams. The thalamus acts as a relay for information from the senses to the cerebral cortex (the covering of the brain that interprets and processes information from short to long-term memory). During most stages of sleep, the thalamus becomes quiet, letting you tune out the external world. But during REM sleep, the thalamus is active, sending the cortex images, sounds, and other sensations that fill and produce our dreams. The pineal gland, located within the brain’s two hemispheres, receives signals from the SCN and increases production of the hormone melatonin, which helps you to sleep once the lights go down. The basal forebrain and midbrain also play roles in promoting sleep and wakefulness. The basal forebrain releases adenosine (a chemical by- product of cellular energy consumption) which inhibits wake-promoting neurons in the hypothalamus and brainstem. The amygdala, an almond-shaped structure involved in processing emotions, becomes increasingly active during REM sleep in which there is a "dissipation" of emotional charge, in response to previous emotional experiences (of the day or of previous periods). This results in less subjective emotionality the following day. [13]

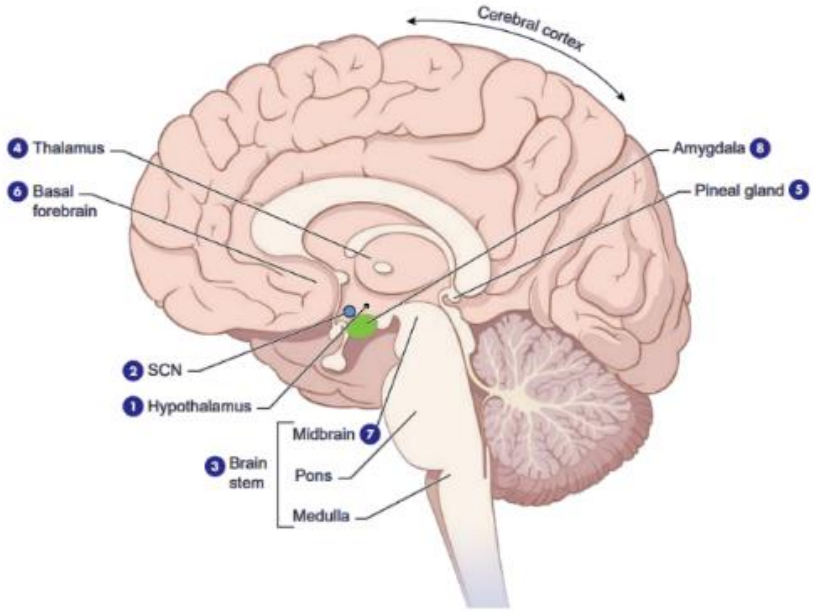

Figure 4 –Brain structures involved in sleep.

1.1.4. Sleep - wake generating systems.

In most complex organisms there are two mechanisms that regulate most physiological processes: homeostasis and circadian regulation. Homeostasis is the tendency towards a state of equilibrium. On the other hand, the circadian regulation serves to change the level of each variable for optimal functioning at the proper time of the day. Also, the sleep-wake system is regulated by the interplay of these two major processes, one that promotes sleep (process S, the homeostatic drive for sleep) and one that maintains wakefulness (process C, regulated by the circadian system). Wakefulness is generated by an ascending arousal system from the brainstem that activates forebrain structures to maintain wakefulness. This idea, originally put forward by Morruzzi and Magoun (1949), has more recently been refined by proposing that the transmission of information within the brain can follow two different branches [14]. The first branch is an ascending pathway from the brainstem to the thalamus in which the thalamic relay neurons are activated by the neurons located in the brainstem. These last, which are crucial for transmission of information to the cerebral cortex, are mainly the pedunculopontine and laterodorsal tegmental nuclei (PPT/LDT) that produce specific neurotransmitters, such as acetylcholine. These relay neurons are important because when they are activated, they send reinforcing signals to the cerebral cortex, to help maintain a state of attention and wakefulness. Neurons in the PPT/LDT are most active during wakefulness and REM sleep, which is characterized by cortical activation, loss of muscle tone, and active dreams. During non-REM sleep, when cortical activity is slow, these neurons are much less active. The second branch of the ascending arousal system bypasses the thalamus; in fact, this pathway originates in cell groups in the upper brainstem that contain the monoamine neurotransmitters (norepinephrine, serotonin, dopamine, and histamine), enters the hypothalamus, rather than the thalamus, where it picks up inputs from nerve cells that contain peptides (orexin or hypocretin and melanin-concentrating hormone). These inputs then traverse the basal forebrain, where they pick up additional inputs from cells containing acetylcholine and gamma-aminobutyric acid. At last, all these inputs enter the cerebral cortex, where they diffusely activate the nerve cells and prepare them for the interpretation and analysis of incoming sensory information. Sleep process S is regulated by neurons that shut down the arousal systems, thus allowing the brain to fall asleep. Many of these neurons are found in the preoptic area of the hypothalamus and are called “hypnogenic neurons”. These neurons produce chemicals that inhibit the activity of neurons involved in vigilance and wakefulness. The sleep-generating system also includes neurons in the pons that intermittently switch from NREM to REM sleep over the course of the night. These neurons send outputs to the lower brainstem and spinal cord that cause muscle atonia and chaotic autonomic activity that characterize REM sleep. Other

outputs are sent to the forebrain, including activation of the cholinergic pathways to the thalamus to activate the EEG. So, process C is a circadian-regulated wake-promoting system that acts to counteract process S, promoting wakefulness and alertness. As bedtime approaches, the wake-promoting effects of process C begin to decline, facilitating sleep consolidation and reducing the need for sleep throughout the night. With sufficient sleep, the homeostatic drive for sleep is reduced, and the circadian waking drive begins to increase, resetting the cycle. In the absence of process C, total sleep time remains the same but becomes randomly distributed throughout the day and night, indicating that process C also serves to consolidate sleep and wake into distinct episodes. Moreover, by synchronizing with the circadian system, process C helps to coordinate sleep-wakefulness cycles with environmental light-dark cycles. This process is illustrated in figure 5, depicting the typical sleep-wake pattern with black and white bars representing sleep and wakefulness, respectively. The blue line indicates the baseline condition of 8 hours of sleep and 16 hours of waking. When the blue line increases, the model is awake, and when it reaches the upper threshold (represented by the upper black sinusoidal line), the model goes to sleep, and the line decreases. This cycle continues until the lower threshold is reached, and the model awakens again. [15].

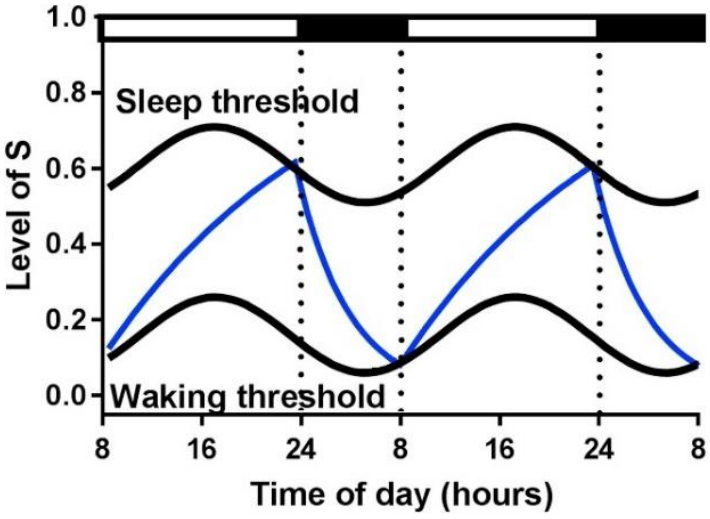

Figure 5 - The two-process model of sleep regulation

1.2. Sleep

Sleep is defined as a natural and reversible state of reduced responsiveness to external stimuli and relative inactivity, accompanied by a loss of consciousness. Sleep occurs in regular intervals and is

homeostatically regulated, i.e., a loss or delay of sleep results in subsequently prolonged sleep [16]. Sleep deprivation and disruptions can lead to severe cognitive and emotional problems. Sleep is believed to be a universal phenomenon among vertebrates, including birds, fishes, and reptiles, and similar sleep-like states have been observed in invertebrates such as flies, bees, and cockroaches [16]. According to the US National Sleep Foundation, an adult (26-64 years old) should get approximately 7 to 9 hours of sleep per night in order to promote a good health [17]. However, sleep is much more than a number of hours; in fact, during sleep, we cycle through different sleep stages that are essential for various aspects such as plasticity, memory consolidation, and the enhancement of the immune system's efficacy etc.. Sleep in mammals consists of two main sleep stages: slow-wave sleep (SWS) and rapid-eye-movement (REM) sleep, which alternate in a cyclic manner.

1.2.1. Sleep - wake cycle

The Sleep-Wake Cycle (SWC) is a circadian rhythm of paramount significance in numerous species of animals, including humans. It is defined by the recurrent alternation of brain states, each of which exhibits unique behavioral and electrophysiological characteristics. The regulation of sleep occurs at the genetic, biological, and cellular levels. Multiple brain regions, such as the basal forebrain, thalamus, and hypothalamus, participate in controlling this vital state. Interactions between different brain regions and communication between cortical areas and the periphery occur through various neurotransmitters, which either enhance wakefulness or promote sleep. [18]
These states can be divided into three categories (Figure 6).

- Wakefulness (stage W) is a state in which the individual is conscious, alert, and awake. During the wake state neurons in the cerebral cortex fire irregularly so the brain activity during this stage is characterized by low-amplitude, high-frequency fluctuations, desynchronized brain waves and active movements. This state is crucial for activities such as learning, decision making, and problem solving. The wake stage can be further divided into two sub-stages based on whether the eyes are open or closed. During eye-open wakefulness, beta waves (13-40 Hz) predominate, whereas alpha waves (7 - 13 Hz) become the predominant pattern when individuals close their eyes and become drowsy.[19]
- NREM is characterized by synchronized high-amplitude LFP in lower frequencies (delta range) and absence of movement. This stage presents irregular occurrence of various striking EEG events with a progressive apparition of spindles then slow waves with sleep deepening. NREM sleep is classified into the actual consensus of three stages N1 to N3 [20].

- **N1 (5**%). N1 (Stage 1 Sleep) is the initial stage of NREM sleep, it is considered the lightest stage of sleep and has the lowest awakening threshold. It constitutes around 5% of total sleep time and lasts for 1 to 5 minutes. During this stage, more than 50% of the alpha waves are replaced with low-amplitude mixed-frequency (LAMF) activity as observed in EEG recordings called theta waves of low voltage (4-8 Hz). Muscle tone is present in the skeletal muscles and breathing is regular. [19]
- **N2 (45%).** In stage N2 of sleep, characterized by deeper sleep, heart rate and body temperature decrease. The most important and characteristic brain waves in this stage are sleep spindles (10-15 Hz), ripples (140-200 Hz) and K-complex. The focus of this thesis will be the investigation of the function and significance of sleep spindles and ripples. These high frequency oscillations, primarily generated in the thalamus for sleep spindles and in the hippocampus for ripples, have been shown to play a crucial role in memory consolidation and the strengthening of neural connections. Stage N2 lasts around 25 minutes in the first sleep cycle and becomes longer with each subsequent cycle, eventually making up about 45% of total sleep time. Bruxism, or teeth grinding, may also occur during this stage.[19]
- **N3 or SWS (25%).** N3, also known as slow-wave sleep (SWS), due to the high prevalence of slow waves, is the deepest stage of sleep with the highest awakening threshold. It is characterized by delta waves (1-4 Hz), which are signals with low frequency and high amplitude and by slow wave oscillations (0.5-2 Hz). [10] These oscillations are generated in the cortex and play a crucial role in the physiological and functional processes of sleep. As people age, they tend to spend less time in N3 and more time in N2 sleep. If someone is awakened during N3, they may experience sleep inertia, which is a phase of mental fogginess that lasts for 30 minutes to an hour. N3 is important for the body's tissue repair, bone and muscle growth, and immune system strengthening. This stage is also associated with sleepwalking, night terrors, and bedwetting. [19]

- **Rapid Eye Movement Sleep (REM)** was previously known as paradoxical sleep, because REM actually resembles the waking EEG more closely than NREM sleep. REM is characterized by low-amplitude local field potentials (LFP) or synchronization in the theta range (4-8 Hz), is accompanied by deeply reduced muscular tonus and absence of behavior [19]. During REM sleep, distinct sawtooth waves can be observed, which are characterized by rapid and regular amplitude fluctuations. These waves are distinguished by their sharp

and contoured shape resembling the teeth of a saw, and they are commonly found in the theta frequency range [21]. This stage begins approximately 90 minutes after sleep onset and gets longer throughout the night, with the first period lasting around 10 minutes and the final period lasting up to an hour. REM is associated with sensory arousal resistance and spontaneous awakening in the morning [19].

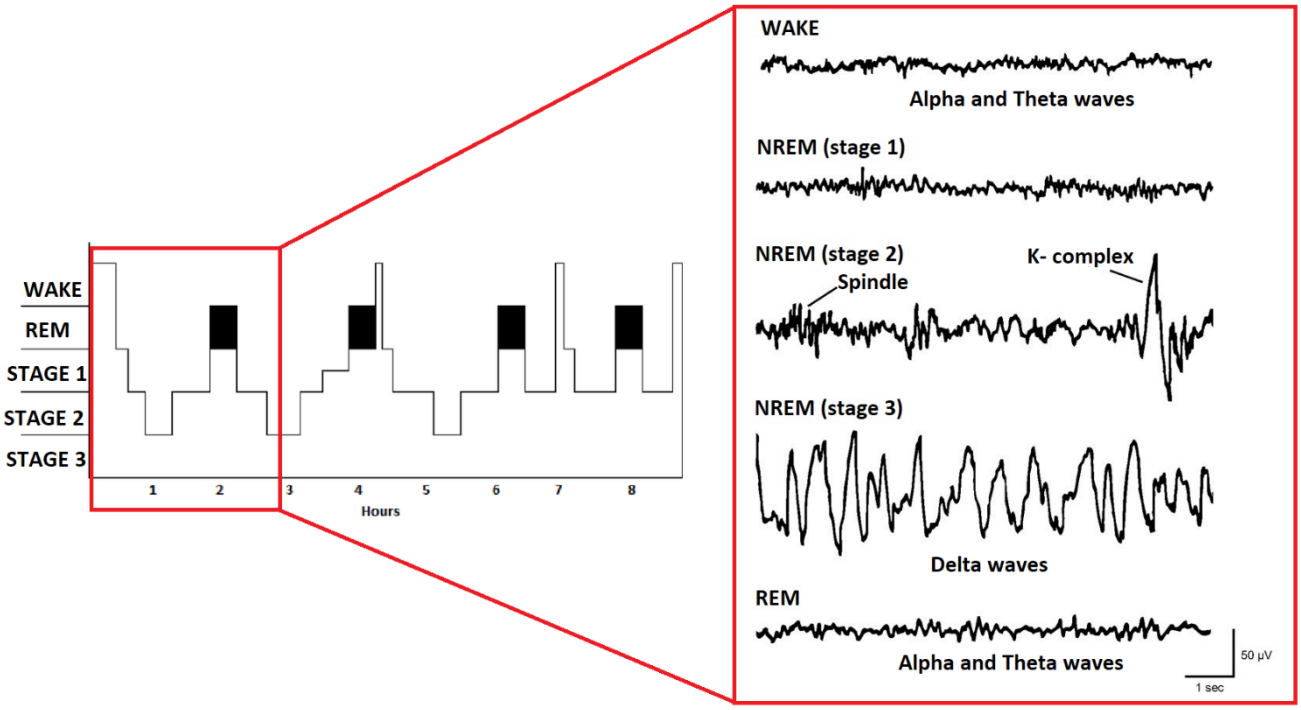

Figure 6 - EEG signal capture different sleep stages during NREM and REM sleep in human.

1.2.2. Sleep wake cycle from human to animal model

Despite significant progress in our understanding of the stages of the sleep-wake cycle, the exact function of sleep remains unclear. However, advancements have been made in uncovering the brain mechanisms that regulate sleep and wakefulness using animal models, typically rodents. While sleep architecture is conserved across species, there are differences in sleep patterns between humans and rodents due to the differences in complexity of the central nervous system. Firstly, the organization of the sleep-wake cycle is reversed in rodents compared to humans. Specifically, rodents are nocturnal animals; they are awake during the dark phase and asleep during the light

phase. Moreover, humans have monophasic sleep, meaning that, sleep is usually taken in one session during a 24-h period (i.e., during night). Conversely, rodent sleep is polyphasic and relatively fragmented [22]. Lastly, while NREM sleep in humans, as we mentioned, is conventionally divided into 3 stages, in rodents this distinction is not used [23] and it is often considered by default as a uniform state and most scientific articles use the terms “SWS” and “NREM” indifferently, which may lead to misinterpretation when comparing human and rodent literature. In fact, when researchers attempt to perform a direct comparison of sleep properties across species, rodents sleep is compared to the sole human stage 2 of NREM sleep [24], making difficult any further comparison in sleep regulation [25] (published in preprint). However, there are common shared traits among species, such as specific properties associated with the frequency spectrum of distinct sleep states. Recently, there is an increasing number of studies that support the similarity between the sleep-wake cycle in humans and that of mice, contrary to what was previously believed. In a preprint article, several similarities between human and rodent sleep have been found. Some of the similarities are as follows (figure 7):

- In both species, cycles tend to start with N1, followed by N2, N3, and finally REM sleep.
- An increase in REM sleep incidence has also been observed in mice, like what has been reported in human sleep.
- Like in humans, REM sleep in mice occurs in a regular pattern defining sleep cycles that last about 10 minutes, compared to 90 minutes in humans.
- The main difference between mice sleep and human sleep is the duration of individual epochs, which are an order of magnitude shorter in mice. This difference is consistent with theories that suggest that the duration of the sleep cycle and its consolidation depend on a homeostatic "time constant," which is positively correlated with the brain size and the inertia of neural networks.
- The brevity of the NREM sub-stages epochs may explain why these have been neglected in previous mouse studies.
- A sleep stage like human N1 has been identified in rodents.
- Considering these substages greatly improves our understanding of the neuronal mechanisms involved during sleep in relation to memory consolidation and homeostatic synaptic scaling.[25]

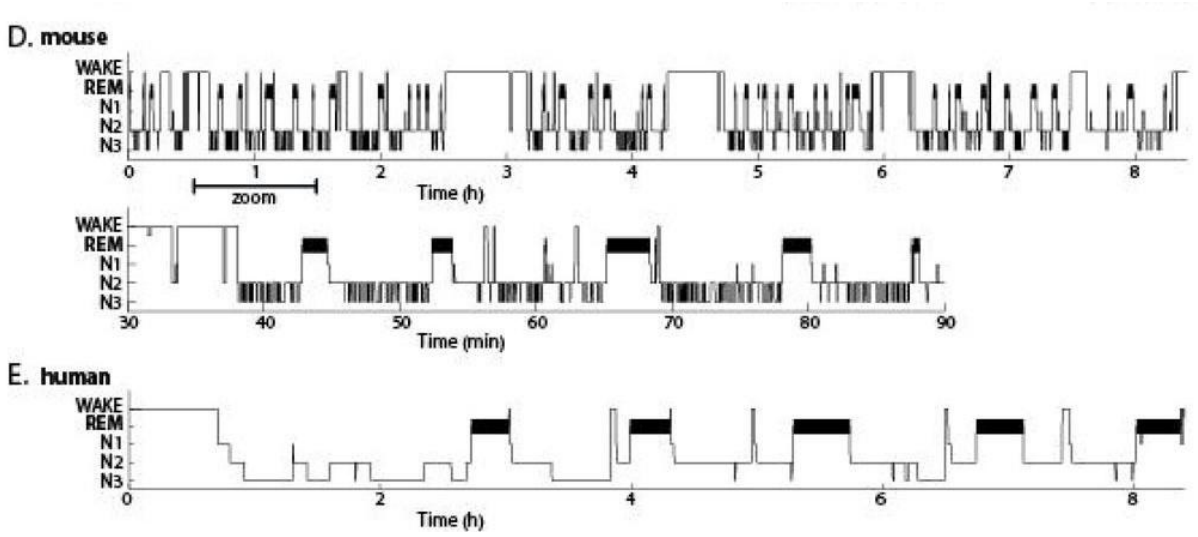

Figure 7 – Comparison between mouse vs human hypnogram

1.3. Sleep and plasticity

1.3.1. Memory consolidation

In the last two decades, research has amassed compelling evidence supporting the role of sleep in cognitive processes related to memory formation and consolidation. Memory formation depends on the ability of the brain to change its structure and function in response to experiences, known as brain plasticity. If sleep plays a critical role in memory consolidation, evidence of sleep-dependent plasticity would strengthen this claim. Memory formation begins with the creation of a memory trace. These memory traces are not immediately stable or long-lasting. They need to undergo a process called consolidation to become more permanent memories. Consolidation involves various changes in the neurons and their connections to solidify the memory trace. At the cellular level, consolidation can involve alterations in gene expression, which means that certain genes may be activated or deactivated to support the storage of the memory. Additionally, there may be changes in the electrical excitability of neurons, making them more likely to fire in response to specific stimuli. Moreover, synaptic connectivity, the strength and structure of connections between neurons, may also be modified to facilitate the storage of the memory trace. Once the memory trace is consolidated, it can be retrieved and accessed. Retrieval involves activating the specific neural circuits associated with the memory. These circuits are capable of storing the memory in a durable and retrievable format, known as a "memory engram" [26] So, in general terms, sleep probably

provides conditions that support the transformation of memory traces into memory engrams, thus supporting the consolidation of memory [16]. Critical for its influential role have been experimental studies showing that, during NREMS, 1) there is a reactivation of neural activity patterns acquired during learning, a first step in transforming memory traces into more enduring formats; 2) there is an enhanced functional connectivity between brain areas implied in learning, brain areas thus cooperate during the transfer of memory-related information; and 3) cueing stimuli during NREMS support memory consolidation, which indicates that sensory experience linked to learning promotes memory trace re-activation. The central postulate to the transfer and transformation of an initial labile memory trace thus implies the existence of a carrier mechanism that specifically routes these memory traces through mechanisms involving synaptic plasticity [16]. The standard two-stage memory model for memory consolidation, originally developed for declarative memory, posits that new memories are initially encoded in a temporary store represented by the hippocampus, before gradually being transferred to a long-term store, mainly represented by the neocortex, or forgotten (figure 8). Therefore, sleep represents an offline mode of brain processing that facilitates memory consolidation, which involves the redistribution of newly encoded memory representations to other neuron networks serving as long-term stores. This system consolidation process primarily occurs during SWS rather than REM sleep. The initial encoding of events happens alongside in neocortical networks and in the hippocampus during wakefulness. The reactivation and redistribution of memories depend on a triple time-locking of sleep-related rhythms between cortex, thalamus, and hippocampus: Slow oscillation, spindle and ripple. Slow oscillations are a type of electrical activity that occurs in the brain during sleep. These oscillations consist of two phases: a hyperpolarizing down-state, during which neurons are silent, and a depolarizing up-state, in which neuronal firing increases to wake-like levels. Slow oscillations synchronize neuronal activity not only in the neocortex, but also in other brain regions such as the thalamus and hippocampus, generating a global temporal structure that enables memory reactivation. The depolarizing up-phases of the slow oscillations repetitively drive the reactivation of hippocampal memory representations together with sharp-wave ripples in the hippocampus and thalamus-cortical spindles. This synchronous drive allows the formation of spindle-ripple events, in which sharp-wave ripples and associated reactivated memory information become nested into single troughs of a spindle. [4]

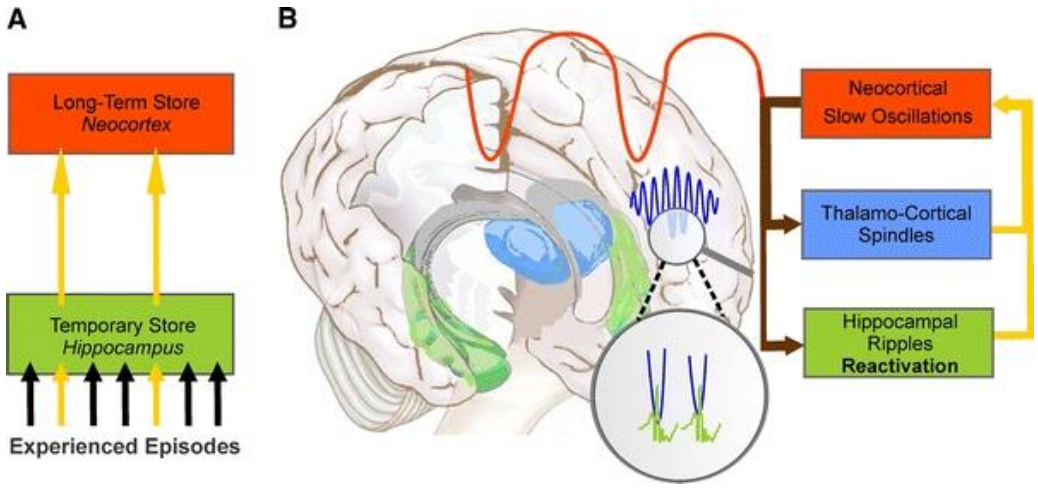

Figure 8 - Active system consolidation during sleep.

Memory

When we refer to memory, we are discussing a complex system that can be divided into declarative and nondeclarative memory. Declarative memory involves conscious recollection of facts, events, and information that can be consciously and intentionally recalled. It can further be subdivided into:

1. Episodic memory: It refers to the ability to recall specific personal experiences and events, such as remembering a particular birthday party or a vacation.
2. Semantic memory: It involves the storage of general knowledge, concepts, and facts that are not tied to personal experiences. For example, knowing that Rome is the capital of Italy or understanding the concept of gravity.

Non-declarative memory, also known as procedural memory or implicit memory, is responsible for acquiring and utilizing skills, habits, and associations without conscious awareness or intentional retrieval. It involves the learning and retention of motor skills, such as riding a bicycle or playing an instrument. These skills become automatic with practice and do not require conscious effort to execute.

1.3.2. Biomarkers

The primary biomarkers that we have chosen to analyze for this work are patterns of neuronal synchronization that occur during the sleep-wake cycle. Neuronal synchronization can be defined as

a correlated appearance in time of two or more events associated with various aspects of neuronal activity. Neuronal synchronization can be distinguished into long and short-range synchronization. Long-range synchrony is usually detected with two or more electrodes placed at some distance apart. It leads to brain activity that is correlated to long distances and can be seen using both local filed potential (LFP) and electroencephalogram (EEG) recordings. The local or short-range synchrony can be detected either with one relatively large field potential electrode, or with two or smaller intracellular or extracellular unit (action potential) recording electrodes located at short (less than 1 mm) distances from each other. During the sleep-wake cycle, neuronal synchronizations are referred to as normal thalamocortical oscillations, also known as sleep or wake oscillations. These oscillations are generated through both local and long-range synchronization and are frequently associated with rhythmic oscillations of neuronal activity, including slow oscillation, delta, spindle, beta, gamma, and ripples. The patterns and the dominant frequencies of these oscillations are defined by the specific mechanisms involved and depend on the functional state of the brain. Normal oscillatory activities include slow (0.1–15 Hz, present mainly during slow-wave sleep or anesthesia), and fast (20–600 Hz) activities. The fast activities can be present in various states of vigilance and frequently coexist with slower rhythms. The various oscillatory rhythms generated in the thalamocortical system can be divided in two main classes: intrinsic, generated by a single neuron as a result of an interplay between specific intrinsic currents [e.g., thalamic delta oscillation], and extrinsic, or network oscillations, which require the interaction of excitatory and inhibitory cells within a neuronal population (e.g., spindle oscillation). Intrinsic neuronal currents contribute to the generation of network oscillations [27]. The main oscillations involved in SWC are:

1. Slow oscillation
2. Sleep spindle
3. Ripple
4. Delta oscillation
5. Theta oscillation
6. Gamma oscillation

Slow oscillation

During slow-wave sleep and some types of anesthesia, the dominant pattern of brain activity is a slow oscillation with a low frequency (0.3-1 Hz), in which the cortical network alternates between silent and active states, each lasting 0.2-1 s (figure 10). Silent periods are characterized by the

absence of synaptic activity, while active periods involve intensive synaptic activity leading to the generation of fast oscillations within the thalamocortical system. Slow oscillations have an intracortical origin, and each cortical slow wave originates in a particular location and propagates to involve other cortical regions. The survival of slow oscillations after extensive thalamic lesions in vivo and in cortical in vitro preparations, and the absence of slow oscillation in the thalamus of decorticated cats point to an intracortical origin of this rhythm. [27]

Sleep Spindle

Sleep spindles are a well-recognized burst-like sequence of 11-16 Hz sinusoidal cycles found in the electroencephalogram (EEG) of sleeping mammals with a duration ≥0.5 s (figure 9, 10). These spindles are categorized into two types: "fast" (generally >13 Hz) and "slow" (generally <13 Hz). Thalamic circuits are the major site of origin for sleep spindles, with the thalamic reticular nucleus (TRN) acting as a "pacemaker" or "nucleus reticularis", these spindles then propagate to the cortical surface, where they play a role in regulating and coordinating sleep-related brain activity. They are present throughout NREM, but best visible during N2, while being absent during N1 and REM. Discrete spindles dominate in the N2 stage of human NREM, with 2-8 spindles/min in N2 and 1-6 spindles/min in N3, and total counts of spindles per time spent in N2 in a night amount to 1,000-2,000. The density, amplitude, and duration of spindles increase over successive NREM cycles in humans. 50-70% of all sleep spindles are temporally coupled to the cortical slow oscillations in both humans and mice. Sleep spindles have been proposed as prime candidates in the process of hippocampal-dependent memory consolidation, as they promote synaptic plasticity and favor the induction of associative forms of long-term synaptic plasticity. [27]

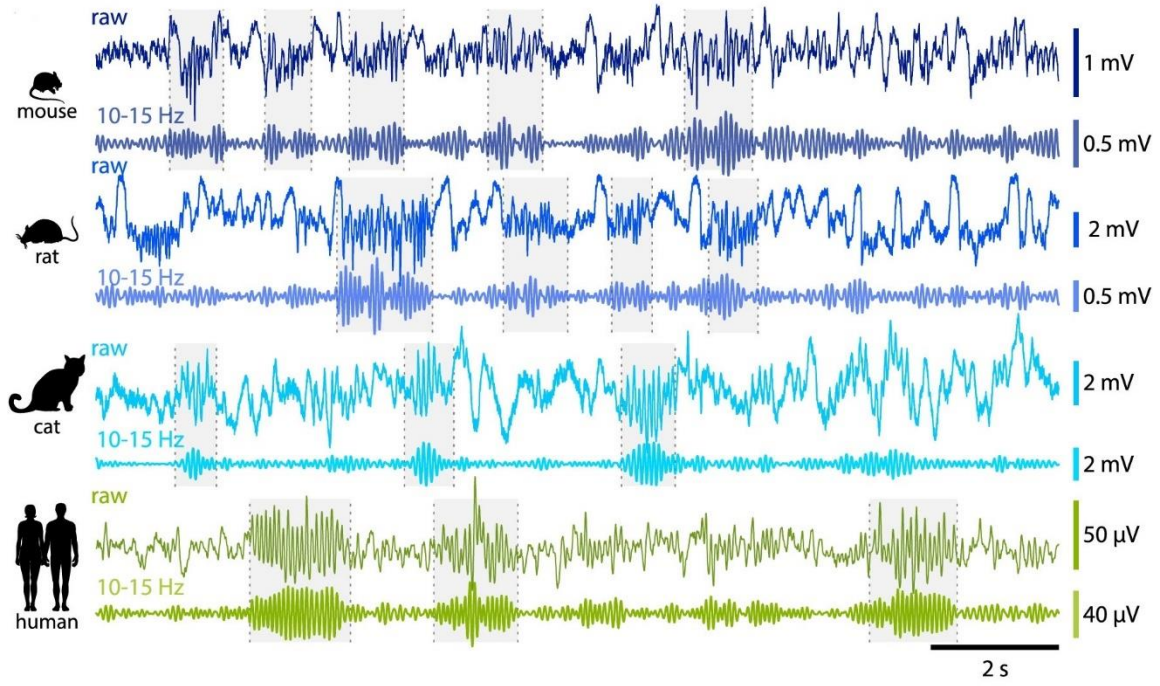

Figure 9 - Electrophysiological manifestations of sleep spindles across mammalian species. Representative 15-s traces of non-rapid-eye-movement sleep (NREMS) from mouse barrel cortex, rat hindlimb cortex, cat (area 5, parietal-associative cortex, local field potential recordings in deep layers), and human.

Ripple

Ripples are brief high-frequency oscillatory neural activities in the brain, lasting less than 150 ms, with a range of 140 to 200 Hz in rodents and 80 to 140 Hz in humans (figure 10). They were first identified in the rodent hippocampus. Sharp-wave ripples (SWRs) occur during both wakefulness and sleep states. During wakefulness, SWR replay is believed to support memory retrieval for processes such as decision-making. During SWR replay, groups of neurons in the hippocampus rapidly replay past experiences in split-second bursts. This replay of past experiences can aid in memory-guided decision making by allowing the brain to rapidly retrieve relevant information from past experiences. In contrast, SWR replay during sleep is geared to gradually consolidate a memory trace into a broader framework of existing memories. [28]

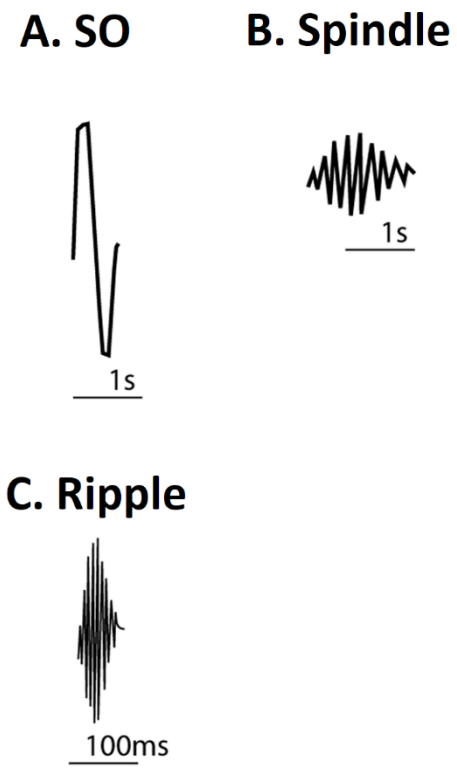

Figure 10 - Graphical representation of a slow oscillation (A) of a spindle (B) and a ripple (C)

Delta oscillation

Delta oscillations (1–4 Hz) are commonly observed in both humans and animal models during slow wave sleep (SWS) and other states of diminished consciousness, such as anesthesia, generalized epileptic seizures, coma, and the vegetative state. However, recent studies have challenged the correlation between high amplitude delta oscillations and unconsciousness. For example, prominent delta activity has been observed during conscious states in conditions such as epilepsy, postoperative delirium, and powerful psychedelic states. Additionally, clinical reports from various disorders have documented awake and conscious patients with high amplitude delta oscillations [29]. It is thought that the delta oscillation has two different components, with one originating in the neocortex and the other in the thalamus. It has been proposed that synaptic plasticity associated with slow and delta oscillations could contribute to the consolidation of memory traces acquired during wakefulness. [27]

Gama oscillation

Gamma oscillations are rhythmic fluctuations in local field potentials (LFPs) that span a broad range of frequencies (~25–100 Hz). Gamma oscillations are prominent across multiple brain regions including the hippocampus, where they are believed to play a role in attentional selection and memory operations [30]. Accumulating evidence suggests that the broad range of frequencies of oscillations that are described as gamma rhythms may actually be two functionally distinct rhythms, low (~25–50 Hz) and high (~55–120 Hz) gamma [31]. Gamma rhythms play a crucial role in hippocampal memory processing, Sensory perception and problem solving [31]. Gamma activity can exhibit coherence, or synchronized patterns of activity, at both cortical (outer layer of the brain) and subcortical (below the cortical layer) levels during wakefulness and NREM sleep. [32] This coherence of gamma activity is believed to facilitate the integration or "binding" of information from different brain regions, thereby enhancing perception.

Theta oscillation

The 4-12 Hz theta (θ) rhythm represents a highly consistent EEG oscillation observed in the mammalian brain during both waking and REM sleep states. This theta rhythm is characterized by regular and rhythmic patterns of electrical activity, which can be reliably recorded from various regions of the brain. The hippocampus is the main structure involved in the generation of this oscillation. In addition to the hippocampal formation, theta frequency oscillations have been observed in several other structures, including the subicular complex, entorhinal cortex, perirhinal cortex, cingulate cortex, and amygdala. These structures are thus the main current generators of the extracellularly recorded theta field. However, none of these cortical structures can generate theta activity on their own [21]. The theta oscillation is hypothesized to play a fundamental role in mammalian spatial navigation and memory [33]

1.4. Sleep and neural disorder

Traumatic brain injury (TBI), defined as an alteration in brain function or other brain pathology caused by an external force, is a common injury and results in 2.5 million emergency room visits annually. Even in its mildest form (generally known as “concussion”), individuals with TBI can suffer from persistent sequelae that prevent the return to normal physical, cognitive and emotional functioning, all of which are important components of overall recovery. Sleep–wake disturbances are among the most prevalent and persistent symptoms following TBI. Studies indicate that 30–

70% of TBI survivors across the entire injury spectrum experience disordered sleep after injury. The most common sleep–wake disturbances are insomnia and hypersomnia/pleiosomnia (an increased need for sleep), followed by sleep-related breathing disorder, circadian rhythm disorder, and parasomnia/movement disorders. Although sleep–wake disturbances after TBI have long been recognized in humans, the underlying neurologic mechanisms have yet to be clearly established. Only recently studies have utilized animal models of TBI that can provide mechanistic insight into these sleep–wake disturbances [34]. So, having confirmed that after a traumatic brain injury (TBI), the normal functioning of sleep, as well as its functions, is compromised, recent studies have focused on methods to enhance sleep in order to facilitate recovery after brain injury. Now it is clear that one of the main functions of sleep is to regulate neuroplasticity. Therefore, optimizing sleep processing during rehabilitation has the great potential to improve recovery. As we explained in paragraph 2.3.1, sleep has been closely linked to memory consolidation (especially studied for hippocampal-cortical interactions, i.e., declarative memory). Sleep is also known to enhance motor memories. Thus, scientific research in recent years has been questioning which characteristics of sleep are altered by experimentally induced stroke. Recent works have shown that the balance between SO and delta-waves (δ) determines whether there is an enhancement of skill or, instead, forgetting. Recordings in stroke patients and animal models of stroke have shown that the microarchitecture of NREM sleep is modified: in fact, it has been observed a reduction of coupling between sleep spindles and SO and an increase of delta-waves. With recovery of motor function, there has been a redistribution of sleep spindles towards a more physiological state, characterized by an increase in precise spindle-SO coupling and a reduction in local δ-waves [35]. Additionally, the relation between sleep spindles and sleep stability suggests that aberrant sleep spindle function may accompany if not causally underlie sleep disturbances. Furthermore, the dependence of sleep spindles on intact TC circuits indicates that altered sleep spindles may sensitively report on diseases with perturbed TC function, such as epilepsy, age-related pathologies, and neuropsychiatric disorders. Novel studies emphasize a link between sleep spindles and neurodevelopmental disorders [36],[37] which substantiates their dependence on brain maturation (sect. VII). Additional reported alterations of sleep spindles in mood and anxiety disorders document that sleep spindles may provide insights into cognitive impairments on a broad scale of TC dysfunctions [38] [37]. There are also noteworthy studies on traumatic head insult, coma [39] and pediatric cardiac arrest [40] which report that recovery of N2 and the reappearance of sleep spindles correlate positively with the restoration of cognitive ability. While there is thus a broad potential for sleep spindles as causal factors or as biomarkers for disease, it is also clear that altered sleep spindle parameters need to be

more finely resolved to move towards a diagnostically more useful level. Figure 11 provides an overview illustrating the dependence of spindle activity on various diseases.

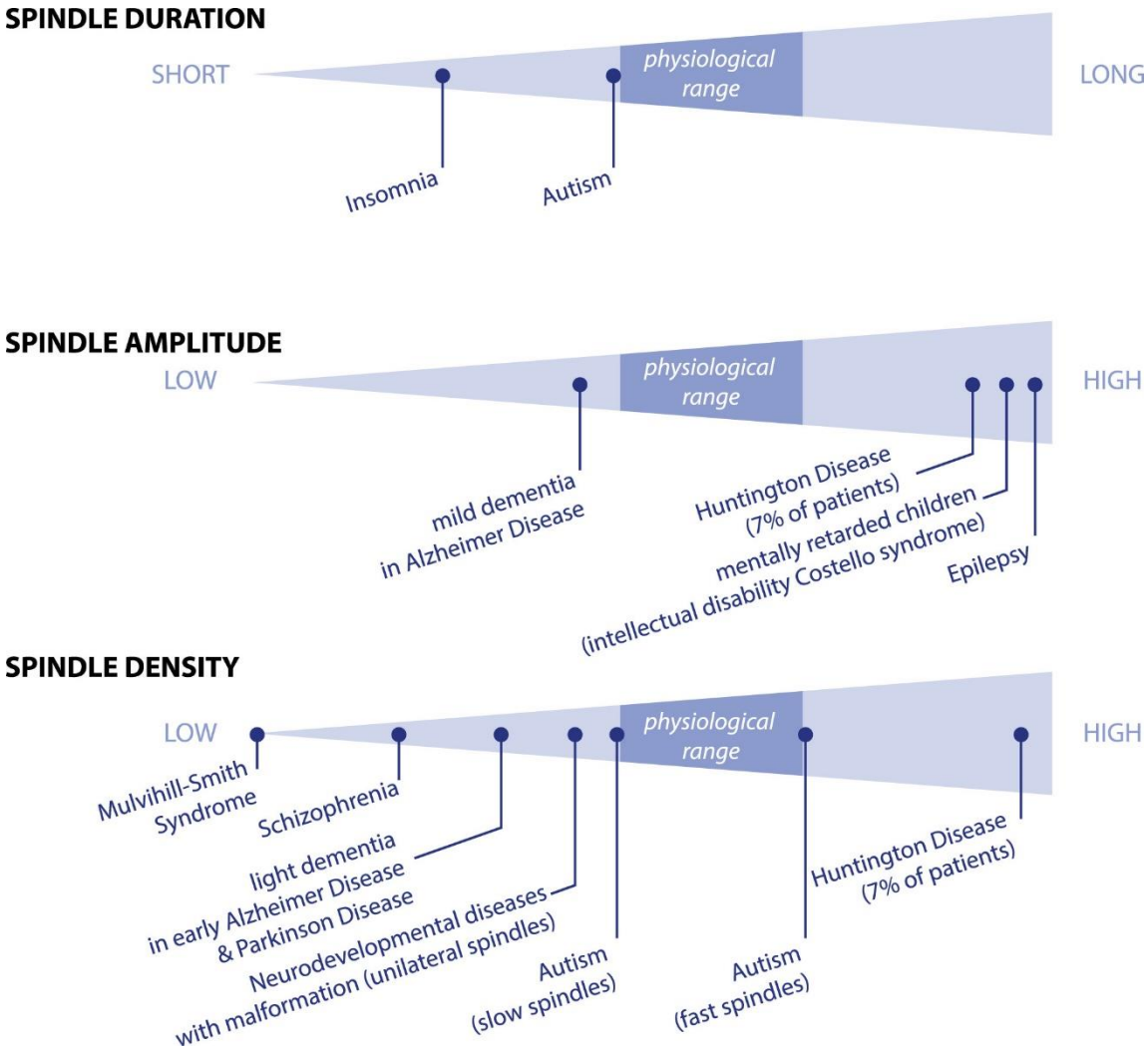

Figure 11 - Overview of sleep spindle modifications with disease. Alterations are indicated relative to a physiological range that is centered within a range of possible alterations in the weaker (left) and stronger (right direction). Points connected to lines refer to semiquantitative changes relative to the physiological range.

So, understanding the relationship between sleep and brain damage opens up avenues for potential therapeutic interventions. Restoring and optimizing sleep patterns may help mitigate the risk of brain damage and promote brain health. Non-pharmacological approaches, such as cognitive-behavioral therapy for insomnia (CBT-I) or continuous positive airway pressure (CPAP) therapy for sleep apnea, have shown promising results in improving sleep quality and mitigating associated

cognitive impairments. These interventions aim to address the underlying causes of sleep disturbances and promote healthy sleep habits. Emerging research also suggests that targeted interventions, such as closed-loop transcranial electrical stimulation, specifically targeting sleep-related brain oscillations, could potentially enhance sleep-dependent processes and facilitate recovery from brain damage. By modulating neural activity during specific sleep stages, these interventions aim to promote neuroplasticity, memory consolidation, and brain repair mechanisms.

Chapter 2

Materials and Methods

2.1. Electrophysiological recordings

Two LFP recordings were used for this study, one obtained by Prof. Vinicius Rosa Cota and the team at the University of Sao Joao del-Rei (UFSJ) in Brazil for the spindle detection [41], and the other obtained from an open-source database resulting from the study of Barger and colleagues [42]. The latter recording was used for SWC stage detection and PAC analysis.

2.1.1. Datasets for spindle detection

I will now introduce the protocol of the experiments led by Vinicius Rosa Cota and the team at the University of Sao Joao del-Rei (UFSJ) in Brazil. All experimental procedures were previously approved by the Ethics Committee on the Use of Animals (CEUA). These experiments are the ones that produced the dataset on which I have later worked on for the spindle detection. The dataset is composed of 56 male Wistar rats kept in a 12-hour light-dark cycle. The rats were randomly divided into five groups:

- Control group (CTRL, n = 14)
- Surgical control group (SHAM, n = 9)
- Non-periodic stimulation group (NPS, n = 13)
- Social interaction group (CTRL/SI, n = 14)
- Sleep monitoring group with simultaneous NPS stimulation (SWC/NPS, n = 6).

As this thesis focuses on the study of the electrophysiology biomarkers of sleep, only the group related to sleep will be used in the next analyses. These groups were monitored by electro physiological recording (EMG and LFP) and their behavior was filmed over the course of 8 consecutive days for a period of 6 h/day (10 am to 4 pm). On odd days (1st, 3rd, 5th, and 7th), recordings were conducted without the application of NPS, whereas on even days (e.g., 2nd, 4th, 6th, and 8th), NPS was delivered throughout the entire recording period (figure 12). The recording that will be used for

future analyses is without NPS. For each animal, three electrodes of two different types were implanted in the following locations for local field potential (LFP) recording:

- Prefrontal cortex
- Hippocampus
- Thalamus

One electrode was a self-tapping bone screw positioned in the right parietal cortex. The other two electrodes were Teflon-coated stiffened stainless-steel monopolar wires, which were implanted into the thalamus (AP = +3.0 mm, ML = +2.6 mm, DV = − 6.4 mm) and hippocampus (AP = +2.8 mm, ML = +1.5 mm, DV = − 3.3 mm) in the right hemisphere. Additionally, to detect muscle tone during different sleep-wake cycle states, two electrodes with rounded tin tips welded to stainless steel wires were inserted into the neck muscles for differential electromyographic recording. LFP signals were filtered at 0.3–300 Hz and amplified with a 2000 V/V gain, EMG signals were filtered at 30–300 Hz and amplified with a 1000 V/V gain. Both signals were then digitized at a sampling rate of 1000 Hz using an off-the-shelf amplifier system (model #3500, A-M Systems, Sequim, WA, USA) connected to a 12-bit resolution analog to digital converter (PCI 6023E, National Instruments, Sao˜ Paulo, SP, Brazil). [41]

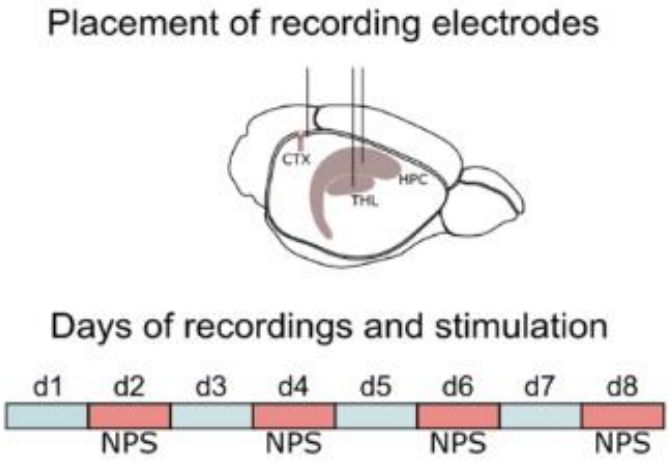

Figure 12 – Procedure of the experiments led by Cota et al,.

2.1.2. Dataset for SWC and PAC analysis

I will now introduce the protocol of the experiments led by Zeke Berger and the team. All experimental procedures were previously approved by the Animal Care and Use Committee at the University of California, Berkeley. These experiments are the ones that produced the dataset on which I have later worked on for the PAC analysis. The dataset is composed of 10 Adult C57BL/6 mice. Recordings were made with the mice in their home cages placed in sound-attenuating boxes. Five 4-hour recordings were collected from each of 10 mice, and two 24-hour recordings were collected from five of those mice. For 24-hour recordings, recording started at 19:00 following 24 hours of habituation and lasted 48 hours. For four-hour recordings, recording started at 13:00 following two hours of habituation. For and EMG recordings, a reference screw was inserted into the skull on top of the right cerebellum. EEG recordings were made from two screws on top of the left and right cortex, at anteroposterior –3.5 mm and medio-lateral +/-3 mm (figure 13). Two EMG electrodes were inserted into the neck musculature. The signals were filtered 1-500 hz. Both signals were then digitized at a sampling rate of 512 Hz. [42]

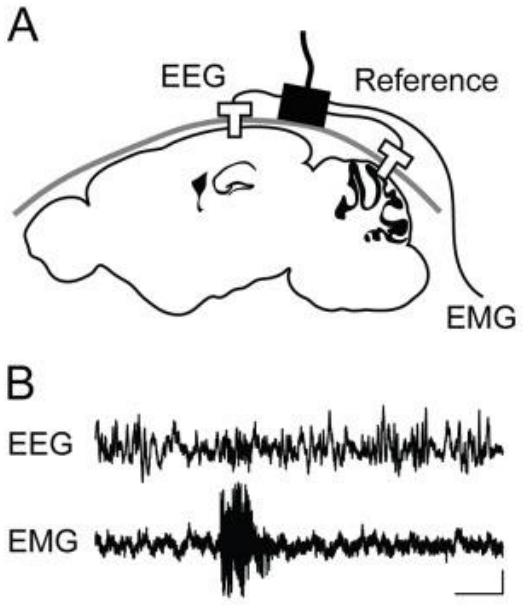

Figure 13 - Overview of the signal collection process for sleep scoring in mice.
A: schematic of EEG and EMG recordings. An EEG electrode is inserted in the anterior cortex, a reference electrode is placed in the cerebellum, and an EMG electrode is inserted into the neck musculature. B: sample EEG and EMG recordings.

2.2. Spindle Detection

In this paragraph, I will discuss the gold standard methods used for detecting spindles and specifically those that have been selected by me. The spindles in human and rodent electroencephalograms (EEG) are characterized by amplitude, duration, frequency, and density. Currently, visual detection by an expert is considered the gold standard for quantifying human spindles. The reliability of visual detection between experts is generally considered to lie at >80% and improves further once the number of included expert scorers is larger and consensus rules are applied. However, visual scoring is slow, feasible only for limited data sets, prone to errors, and bears the risk of subjective judgements based on variable expertise. Therefore, automated methods are being developed to detect spindles more accurately and reliably. The first step in automated detection is to extract nonstationary phasic events within the sigma frequency range that cross a minimal threshold amplitude, followed by additional criteria depending on the choice of the thresholding method. There are three main types of automatic algorithms for spindle detection: fixed or adaptive thresholds and time-frequency analysis. Fixed thresholding methods use a fixed amplitude threshold value to detect spindles, while adaptive thresholding methods vary the amplitude threshold according to the local amplitude characteristics of the EEG signal, resulting in higher accuracy and reduced false detections. Time-frequency analysis methods analyze the time-varying frequency content of the EEG signal to identify spindles with variable frequency content. However, this method is computationally intensive and requires careful selection of the time-frequency analysis technique [43]. In this paragraph, I will describe which algorithms have been selected. After careful research of the current state of the art regarding methods for spindle detection, approximately 10 papers were selected. Subsequently, out of these 10, we have chosen to implement four of them:

1. "San Francisco" algorithm
2. "Boston" algorithm
3. Spindler
4. DDA algorithm

The San Francisco and Boston algorithms are named after the locations where the studies that developed these methods were conducted. Specifically, the San Francisco algorithm was developed as part of a study conducted in San Francisco, while the Boston algorithm was developed in a study conducted in Boston. The San Francisco and Boston algorithms follow a similar routine while Spindler and DDA algorithms are based on two very different approaches. Our proposal was to

identify a reliable and efficient tool for our own investigations. We did this by implementing and testing three algorithms, verifying the coincidence between the classifications, and choosing the fastest among the ones with the best coincidence. We have seen there is a considerable degree of coincidence, particularly if the algorithms share the same computational approach). The tested algorithms were compared to this established gold standard and met the criteria for approval. In fact, they have been published in reputable journals and utilized in various studies. In the following paragraphs I will explain the strategy of each of the algorithms.

2.2.1. San Francisco

The San Francisco algorithm utilizes a fixed threshold based on the mean and standard deviation of the local field potential (LFP) signal during NREM sleep. In particularly, to detect spindles, the Local Field Potential (LFP) underwent several preprocessing steps. Firstly, the LFP was z-scored in each channel and then averaged across all good channels. The resulting average LFP was filtered in spindle band 10-15 Hz. This filtering process involved two independent zero phase-shifted filters, namely a high-pass Butterworth filter and a low-pass Butterworth filter. Independent zero phase-shifted filters refer to the application of filters that do not introduce any delay in the filtered signal. This means that the filter does not cause a time shift in the output signal compared to the input signal. The high-pass filter used was a 6th order Butterworth filter with zero phase-shift and a cutoff frequency of 10 Hz. This was followed by the low-pass filter, an 8th order Butterworth filter with zero phase-shift and a cutoff frequency of 15 Hz. The order of the filters was determined using a conventional minimum-order design approach. The design aimed to achieve a maximum passband ripple of 3 dB and a minimum stopband attenuation of 15 dB (assumed to be 7 Hz for the high-pass filter and 19 Hz for the low-pass filter). After filtering, a smoothed envelope of the signal was computed using the magnitude of the Hilbert transform, convolved with a Gaussian window of 200 ms. This smoothed envelope was then used to determine two thresholds for spindle detection, based on the mean (μ) and standard deviation (σ) of the spindle band LFP. The upper threshold was set as $\mu + 2.5 \times \sigma$, and the lower threshold was set as $\mu + 1.5 \times \sigma$. In Figure 10, the horizontal dashed lines represent these threshold values used for detecting the spindle period. To identify spindles, epochs were considered where the spindle power exceeded the upper threshold for at least one sample and also exceeded the lower threshold for at least 500 ms. Each epoch that exceeded the lower threshold was marked as the start and stop of a spindle. The duration of each spindle was determined based on this start and stop values. The detections are constrained in amplitude and time features for improved performance: minimum duration of spindles, minimum separation between events,

minimum amplitude (detection threshold), and maximum amplitude to exclude artefacts (figure 14). [44]

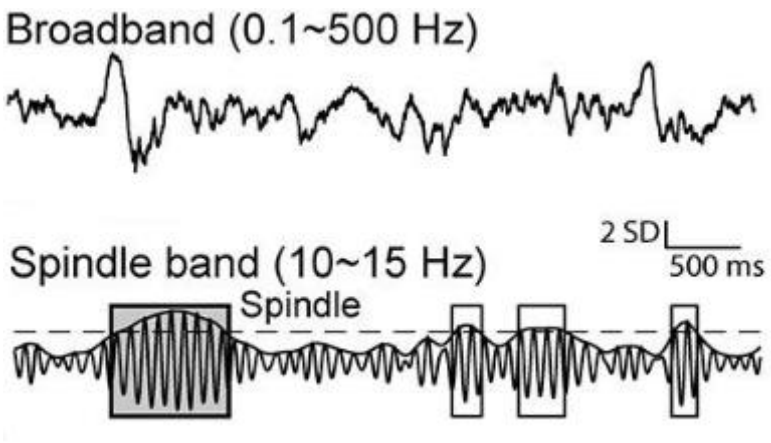

Figure 14 - San Francisco Routine

2.2.2. Boston

The Boston algorithm follow a similar procedure to the San Francisco method, relying on a fixed threshold approach. The routine followed a series of steps to analyze the raw EEG record. Initially, the raw EEG record was subjected to band-pass filtering between 10 and 15 Hz, as this frequency range encompasses the peak mouse spindle (~11 Hz). To perform the band-pass filtering, a Butterworth filter was employed with the following parameters: First stopband frequency of 3 Hz, first passband frequency of 10 Hz, second passband frequency of 15 Hz, second stopband frequency of 22 Hz, with stopband attenuation levels of 24 dB. Next, the root-mean-square (RMS) of the filtered EEG data was calculated using a 750 ms window. This step aimed to smooth the trace and generate a signal envelope. The 750 ms window size was selected to minimize the erroneous detection of short, spike-like artifactual signals as spindles. Following the RMS calculation, the values were cubed to enhance the separation between noise and signal on the y-axis and facilitate the placement of thresholds. A two-threshold approach was implemented to establish inclusion criteria for spindle detection, incorporating several user-defined parameters. The threshold values were determined based on the mean cubed RMS transform value of the entire trace, encompassing all behavioral states. The approach involved a lower threshold (1.2× mean cubed RMS; default) and an upper threshold (3.5× mean cubed RMS; default). Initially, the detection algorithm utilized the upper threshold value to identify potential spindle peaks in the cubed RMS (envelope) record. Subsequently, the lower threshold was applied to determine the start and end of each event,

considering temporal criteria (>0.5 seconds and <10 seconds; default) for inclusion in the detection process. The utilization of mean-based thresholds allowed for appropriate scaling of the calculated thresholds to account for changes in signal variability and amplitude across different animals. The specific multipliers used to define these thresholds were determined through systematic modification to optimize agreement between spindle detections by the algorithm and human scorers in preliminary work (figure 15). [45]

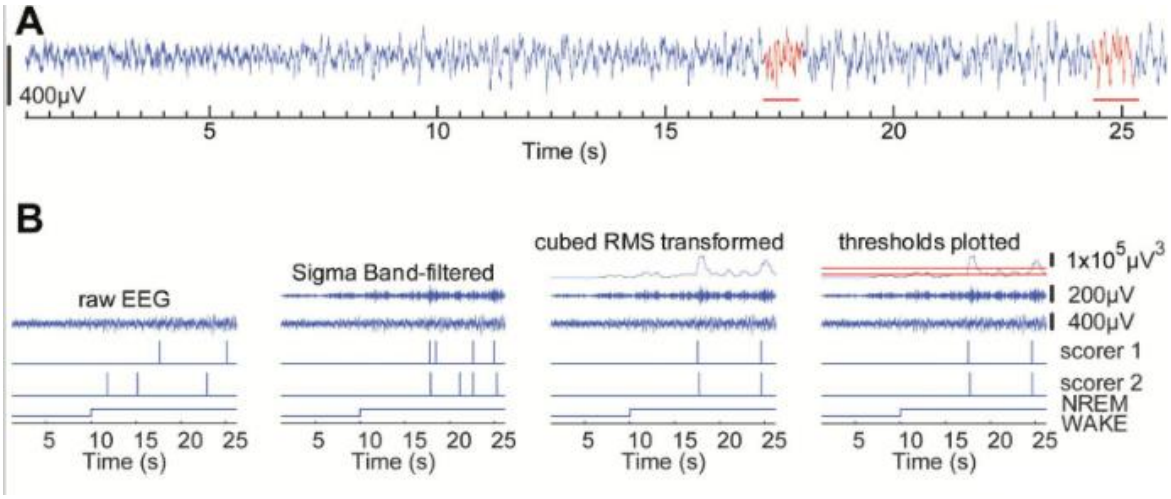

Figure 15 - Boston Routine.
(A) Representative example of mouse cortical EEG data illustrates the difficulty in identifying sleep spindle activity (red horizontal line) in raw data. (B) Representative example of comparison of manual detection of sleep spindles between two experienced scorers. Agreement between detected events between scorers was very low using only the raw EEG trace but was greatly improved with availability of additional data processing, including (1) band-pass filter, (2) cubed RMS transform, and (3) thresholds plotted.

2.2.3. Spindler

Spindler is an advanced algorithm designed for the analysis of EEG signals, specifically aimed at detecting and analyzing spindle events. The algorithm operates on a single channel of raw EEG data and employs several steps to accurately identify spindles. Initially, the EEG signal is subjected to a band-pass filter to isolate the frequency band associated with spindles. In the specific case of the article, the band of interest is set between 10 and 15 Hz. This filtering operation allows focusing on the relevant frequencies for spindles and reduces interference from other brain activities Next, the filtered signal is decomposed using a technique called "Matching Pursuit" (MP) with Gabor atoms.

The MP algorithm selects the most suitable Gabor atoms to approximate the EEG signal and detect spindle characteristics. Gabor atoms are sinusoidal functions modulated by a Gaussian window and are characterized by parameters such as frequency, duration, phase, and amplitude. The Spindler algorithm utilizes a specific dictionary of Gabor atoms defined in the pre-defined settings table. Once the signal is decomposed into Gabor atoms, a threshold is applied to detect the presence of spindles. The threshold, referred to as Tb, is a measure indicating the density of Gabor atoms in each time window. If the density exceeds the threshold, the presence of a spindle in that specific time window is considered. This approach allows for precise identification of spindles in the brain signal (figure 16) [45].

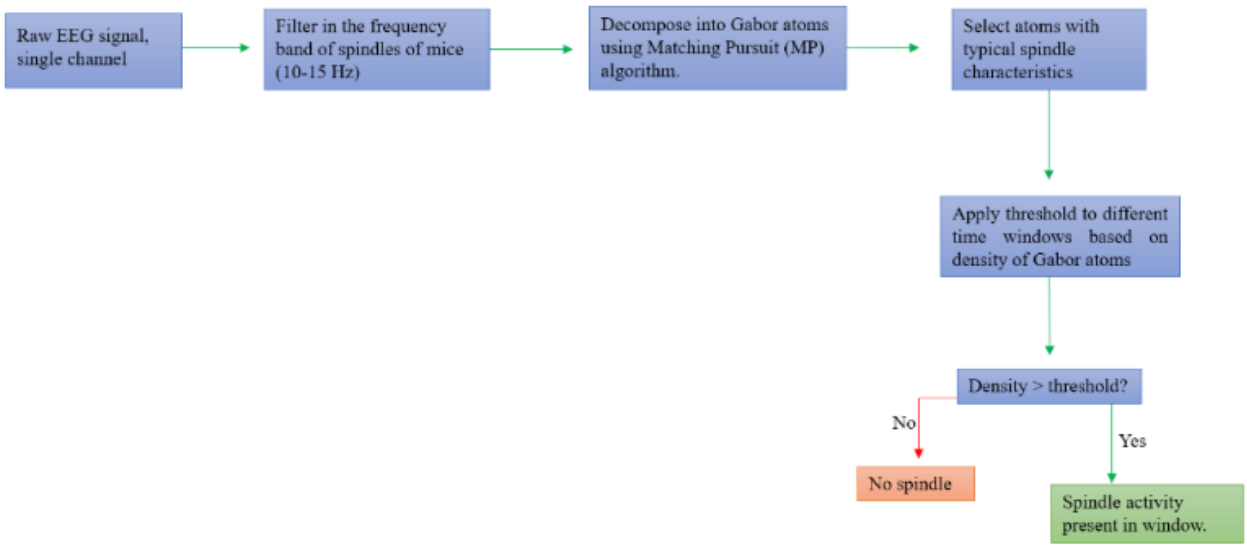

Figure 16 - Spindler Routine

2.2.4. DDA

Finally, DDA is an alternative approach for sleep spindle detection using a nonlinear time-domain algorithm in real time. The algorithm uses an embedding to reveal the nonlinear invariant properties of an unknown dynamical system (here the brain) from a single time series (here intracranial recordings). DDA combines delay and differential embeddings in a functional form. The delayed embedding technique is used to create a representation of an EEG signal in a higher-dimensional space. This allows for better capturing of the signal's structure and dynamics, making it easier to analyze. The differential embedding technique uses the difference between signals to create a new set of data from the original signal. This allows for the analysis of variations and differences within

the signal, contributing to better identification of relevant patterns, in this case spindles. To identify sleep spindles, the DDA algorithm uses a detection criterion based on the presence of peaks in the signal and a set of parameters including their amplitude, duration, and frequency [46]. To ensure the implementation of the DDA algorithm, which is exclusively compatible with Linux operating systems, I installed Linux as a dual boot on my personal computer. Through various modifications, I have successfully executed the code; however, I have encountered a persistent issue that remains unresolved. Specifically, the code detects spindle occurrences beyond the temporal scope of the recording. For instance, it identifies spindles even at the timestamp of 1782.9 seconds (approximately 30 minutes), despite the recording's actual duration being limited to 900 seconds. As a result of this predicament, our research focus has shifted towards the implementation and analysis of the three previously mentioned methods. This approach will allow for a comprehensive comparison and selection of the most suitable spindle detection algorithm, as elaborated upon in Chapter 3.

2.3. Sleep wake cycle stage detection

In the traditional sleep staging methods, sleep stages are classified based on monitoring signals, which is time-consuming, laborious, and prone to the subjective influence of sleep experts. Therefore, many efforts have been put into developing automatic sleep staging methods. The staging algorithms can be roughly divided into two categories, traditional machine learning-based algorithms, spectral analysis algorithms and deep learning-based algorithms that use artificial neural networks. In this paragraph, I will describe which algorithms have been selected after a thorough review of the current state-of-the-art in the field. For the stage detection I’ve been implemented three methods:

1. Gervasoni code [47]
2. Accusleep [42]

2.3.1. State Space

The algorithm consists of describing the SWC as a dynamical system in which the trajectory is computed from LFP spectral content (figure 17). First, all data segments with amplitude saturation were discarded from the working dataset (representing <1% of the total duration in each rat). After a sliding window Fourier transform was applied to LFP signal using a 2 sec window with a 1 sec step, so for each second of brain activity, we have information about the frequency spectrum of that

second. Then, two spectral amplitude ratios were calculated by integrating the spectral amplitude (absolute value) over selected frequency bands for each data window: 0.5-20/0.5-55 Hz for ratio 1 and 0.5-4.5/0.5-9 Hz for ratio 2. These two amplitude ratios are heuristically chosen based on a careful parameter search that aimed to achieve the best separation of states. The ratios are designed to produce normalized values that range from 0 to 1. For each animal, principal component analysis (PCA) was applied to the same spectral amplitude ratio obtained from all LFP channels to reduce the dimensionality. The first principal component (PC) was used as an overall ratio measure, explaining 80% of the variance. Resulting PCs were further smoothed with a Hanning window of 20 sec to reduce within-state variability. These two ratios were used to construct the 2-D state space in which each point represents 1 sec of ongoing brain activity. Such neurodynamical representation results in clear cluster of points which can be automatically (or manually) detected, and which were empirically demonstrated to correspond to each one of the major sleep stages. The density of points therefore reflects the relative abundance of the different brain states, and the distance between two consecutive data points reflects the speed of spectral changes. [47]

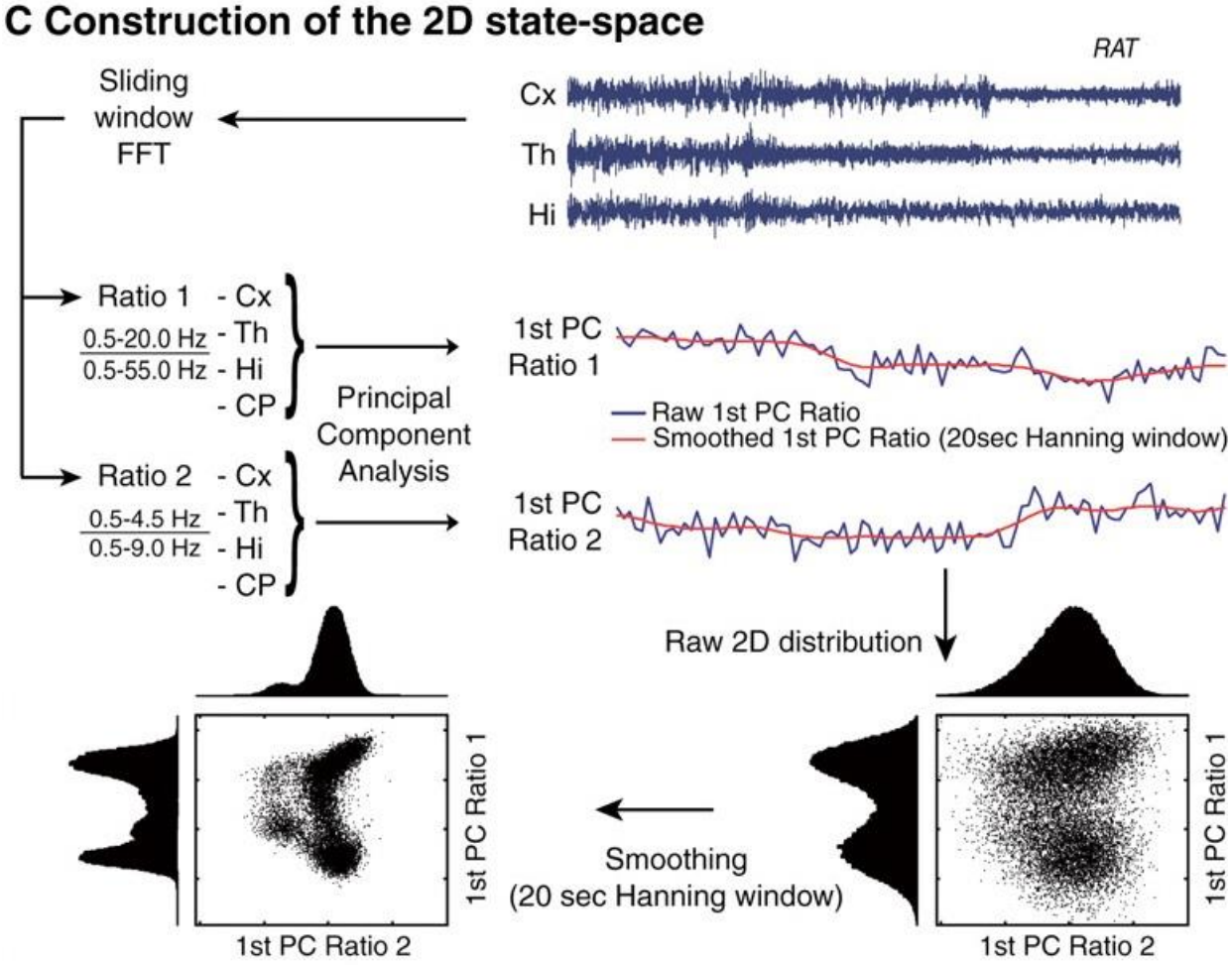

Figure 17 - Construction of the 2-D state space

For each animal, enhanced maps were generated by dividing the point density of 2-D maps (density plot) by the square of the average spectral change speed at each bin (speed plot). The density of each point in the 2D map is calculated by counting the number of points present in a certain area around the point in question and dividing that number by the considered area. The velocity, on the other hand, is calculated as the distance between a point in one time window and the corresponding point in the next time window, divided by the duration of the time window. This velocity is calculated for each point, and the square of average of the velocities of all the points is used as the denominator for the division. Subsequently, main clusters were identified starting from the enhanced maps. Subsequently, the main clusters and their transitions were identified starting from the enhanced maps. Trajectories connecting different clusters were considered valid if they lasted for at least 60 seconds and spent at least half of the preceding 30 seconds in the initiating cluster

and half of the subsequent 30 seconds in the terminating cluster. So, the 2-D state space method allows for the detection of a finite number of clusters (figure 18) that correspond to the distinct behavioral states observed in freely moving rats. Specifically, this method enables the unambiguous identification of most behavioral states, including QW, SWS, REM, and WT, as well as the elusive transient state known as IS (Intermittent State). IS is a transitional state that occurs between SWS and REM episodes. [47]

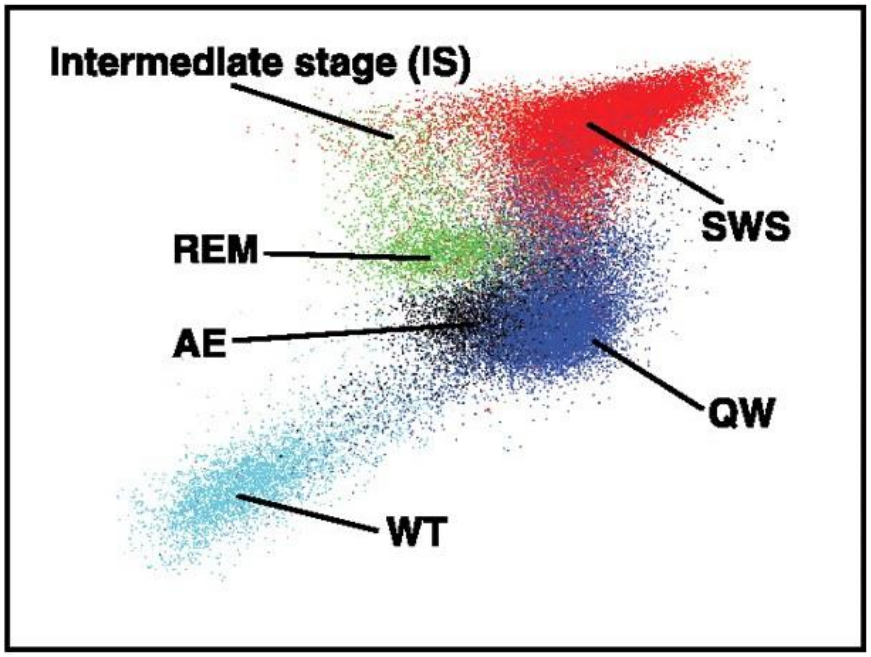

Figure 18 - Global brain states and two-dimensional state space.
The plot displays two chosen LFP (Local Field Potential) spectral amplitude ratios. Each data point represents a 1-second window for which the amplitude ratios were calculated. The clustering observed in the plot corresponds to distinct states within the system. This representation provides insights into the global brain states and their organization in a two-dimensional state space.

2.3.2. Accusleep

Accusleep is a MATLAB Graphical User Interface (GUI) that incorporates an automated sleep scoring system utilizing a neural network (SS-ANN) and mixture z-scoring. Mixture z-scoring is a novel standardization approach that addresses the problem of distributional shift in sleep scoring. Specifically, two sources of distributional shift are observed in sleep scoring datasets: nuisance variability and class balance variability. Class balance variability is often the substance of the

scientific inquiry that a classifier is meant to support. An experimental intervention, such as a drug, is expected to alter the amount of time spent in one or more sleep states and classification algorithms for sleep scoring are to be used to detect this change. In contrast nuisance variability should be removed so that observations from different subjects can be compared. Common sources of nuisance variability in the context of sleep scoring include the use of different types of recording equipment and different implantation sites for recording electrodes. The simplest form of nuisance variability is an affine transformation. Both types of variability may coexist within a single dataset.
If the distributions of measurements from two subjects differ only by an affine transformation, then after applying z-score normalization, the distributions will be identical and have a mean of 0 and a standard deviation of 1. However, if there are other sources of variation in the distribution, z-score standardization may not be appropriate.[42]

$$Z = \emptyset - \mu/\vartheta \tag{1,1}$$

The main difference between the standard z-score formula and the mixture z-score formula relates to how the mean and standard deviation used for normalization are calculated. In the standard z-score formula, the mean μ and standard deviation σ of measurements Φ are calculated for the entire dataset, without considering differences between classes. This can lead to issues when class distributions are different. The mixture z-score formula, on the other hand, involves calculating the mean and standard deviation separately for each class and then combining them based on class probabilities to obtain the mixture mean and standard deviation. However, the technique of mixture z-scoring requires knowledge of the class of each observation. The mixture z-scored values ZM corresponding to measured feature values Φ are computed as:

$$Zm = \frac{\phi - \omega^T \hat{u}}{\sqrt{\omega^T(\hat{\sigma}^2 + (\hat{u} - \omega^T \hat{u})^2)}} \tag{1,2}$$

μˆ and σˆ are vectors of label-conditioned means and standard deviations, respectively. The conditioning on labels means that mixture z-scoring requires some labeled data. w is a fixed vector that sums to 1, which represents the proportions of the class labels for the values Φ. So, the Accuasleep algorithm functions as follows: The EEG and EMG signals are loaded along with the pre-labeled classes or by labeling a small number of epochs for each class using the user interface, approximately 10 minutes of labeled data. This enables the computation of the z-mixture parameters for that subject. After the z-mixture parameters have been computed for that subject, the sleep state

can be automatically labeled using SS-ANN. When processing additional data for the same subject, it is not necessary to manually label all epochs again. Simply load the raw data, load the z-mixture parameters for that subject, and then apply automatic classification using the neural network model [35]. The SS-ANN architecture is designed to process grayscale images. The input of the network consists of grayscale images with dimensions of 185 × 13 pixels. These images represent 32.5-second periods of the standardized joint EEG/EMG spectrogram, centered on each epoch. The intensity of the pixels corresponds to the spectral features of the signal during that time period. A spectrogram is essentially a visual representation of the frequency components of a signal in the time domain. It is a 2D representation that shows how the spectral intensity varies over time. SS-ANN utilizes three convolution-ReLU-maxpool modules with batch normalization, followed by a linear classifier. Convolution is an operation that involves applying a filter or kernel to a sliding window within the input image to compute local features. The Rectified Linear Unit (ReLU) activation function is applied after the convolution to introduce non-linearity, retaining only positive values and nullifying negative values. Max pooling is the dimensional reduction operation that follows the convolution and ReLU activation. The pooling layer reduces the spatial size of the output by selecting the maximum value within a sliding window. This helps to reduce the number of parameters and extract the most relevant features. Batch normalization is used to normalize the data within each batch during the training of a neural network. A batch is a set of training samples that are processed simultaneously during the training process of a neural network. After the three convolution-ReLU-maxpool modules with batch normalization, a fully connected layer is used, followed by a softmax layer for obtaining output probabilities, and finally a classification layer for assigning the final classification label to the input sample. The convolution layers have filter size 3, with 8, 16, and 32 filters per layer. The max pooling layer has a size of 2 and a stride of 2. The network is trained using stochastic gradient descent with momentum and a mini-batch size of 256 for 10 epochs. The learning rate starts at 0.015 and is reduced by 15% each epoch. Prior to training, the classes are balanced by randomly oversampling the classes with fewer examples to match the number of examples in the largest class. After the classification step, sleep stages are further refined by assigning bouts shorter than 5 seconds to the surrounding stage. [42]

2.4. Phase amplitude coupling

Neuronal oscillations of different frequencies can interact with one another. The interaction of rhythms in different bands is commonly called “cross-frequency coupling” (CFC).

There are many types of interaction:

1) Phase-phase coupling (PPC)
2) Amplitude-amplitude coupling (AAC)
3) Phase-amplitude coupling (PAC)

The type that interests us is the last one. In the phase-amplitude coupling or nesting, the amplitude of high-frequency oscillations is modulated by the phase of low-frequency rhythm. The best-known example of this type of CFC occurs in the hippocampus, where the theta (5–10 Hz) phase modulates the gamma (30 –100 Hz) amplitude (this nesting plays a role in sequential memory organization and maintenance of working memory). PAC has been reported in species such as mice, rats, sheep, monkeys and humans and in brain regions other than the hippocampus, such as the basal ganglia and the neocortex. New evidence supports the idea that this type of coupling presents a functional role in the execution of cognitive functions and memory processes. For quantity this nesting we have a MI (modulation index), the greater is this number the greater is the coupling. [48]

2.4.1. Algorithm

To assess the neural synchronization, I've implemented the code described in a paper by Tort et al [48]. This code consents us to quantify the nesting of phase - amplitude frequencies by calculating the MI and to compute the comodulograms. The difference between MI and comodulograms is that the MI show the coupling of one frequency with another frequency, instead the comodulograms is the same thing but for all the frequencies. To calculate the MI index, the following operations are performed: The unfiltered LFP signal (xraw(t)) is filtered for the two frequency bands of interest (fp and fA), resulting in filtered signals denoted xfp(t) and xfA(t). The Hilbert transform is applied to the filtered signals xfp(t) and xfA(t), obtaining their respective phases φfp(t) and φfA(t), and amplitudes AfA(t) and AfP(t). We are interested in the phase of the low-frequency wave and the amplitude of the high-frequency wave. The phase φfp(t) is then divided into a certain number of equal-size bins. For each phase bin, the mean amplitude corresponding to that phase bin is calculated. This allows us to obtain an average amplitude value of the high-frequency wave for each phase bin of the low-frequency wave. This is useful because it helps to identify any relationships between the phase and amplitude of the waves at specific moments of the phase cycle. Lastly, the mean amplitude is normalized by dividing each bin value by the sum over the bins. (Figure 19)

$$P(j) = \frac{\langle A_{f_A} \rangle_{\phi_{f_p}}(j)}{\sum_{k=1}^{N} \langle A_{f_A} \rangle_{\phi_{f_p}}(k)} \quad (1,3)$$

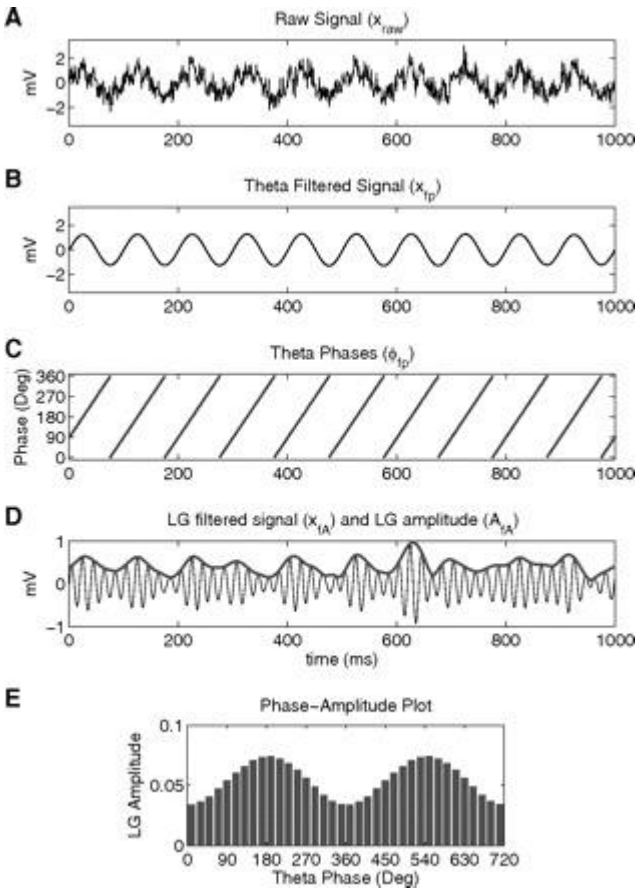

*Figure 19 - Steps in the computation of the phase-amplitude plot and modulation index (MI). The raw signal (*A*) is filtered at the phase (*B*) and amplitude (*D*, thin line) frequency ranges of interest. Next the phase (*C*) and the amplitude (*D*, thick line) time series are calculated from the filtered signals by using the Hilbert transform. A composite phase-amplitude time series (ϕ_{fp}, A_{fA}) is then constructed and used to obtain the mean amplitude distribution over phase bins (*E*; 2 cycles shown for clarity). The MI is obtained by measuring the divergence of the observed amplitude distribution from the uniform distribution. See text for further details. LG, low-gamma (30–60 Hz).*

The modulation index (MI) is then calculated, and its relation to the deviation from the uniform distribution of amplitude with respect to phase is analyzed. If there is no phase-amplitude coupling between two frequencies fp and fA, the distribution of amplitude across phase bins is uniform, meaning that the amplitude of fA is the same for all phases of the fp oscillation. If there is phase-amplitude coupling, the distribution of amplitude deviates from the uniform distribution, meaning that the amplitude of fA varies non-uniformly with respect to the phase of the fp oscillation. The MI is defined to quantify the deviation of this amplitude distribution from the uniform distribution. Specifically, the MI is calculated as a constant multiplied by the Kullback-Leibler (KL) distance

between the observed amplitude distribution and the uniform distribution. The KL distance is a measure of the difference between two probability distributions, and the MI is a measure of the strength of the phase-amplitude coupling. If the amplitude is uniformly distributed across phase, the MI is zero, while if the amplitude is concentrated in a single-phase bin, the MI is equal to 1. So, The MI is defined by dividing the KL distance of the observed amplitude distribution (P) from the uniform distribution (U) by log (N). Log (N) is the maximal possible entropy value, which happens precisely for the uniform distribution [when we have P(j) = 1/N for all bins j]. The Shannon entropy of a uniform distribution, in which each bin has the same probability of occurrence, is maximum and equal to log(N), where N is the total number of bins in the distribution. This is because in a uniform distribution, there is no information that can be used to predict which bin will be chosen, which means that there is maximum uncertainty. Instead, when the distribution is highly concentrated in a specific bin, the entropy will be low because the most likely choice is easily predictable.

$$M = \frac{D_{KL}(P,U)}{log(N)} \tag{1,4}$$

Although the MI measure is able to examine only two frequency ranges at a time [i.e., an (fp, fA) pair], it can be used to construct a phase-amplitude comodulogram plot, a tool that simultaneously reports the level of coupling among multiple bands. The comodulogram is obtained by scanning frequency band pairs and applying the CFC measure to each one of them. Although computationally expensive, this analysis is ideal for searching for phase-amplitude couplings when no a priori assumptions are made about the phase-modulating (fp) and the amplitude-modulated (fA) frequency bands. The results are described using a pseudocolor plot that indicates the level of coupling between several narrowed-filtered frequency bands pairs. Typically, the abscissa represents the frequencies analyzed as fp, whereas fA is represented in the ordinate axis; that is, hot colors in a given coordinate (x, y) of the bidimensional map indicate that the phase of the x frequency modulates the amplitude of the y frequency. Figure 20 illustrates an example of the application of the comodulogram plot to mouse 2 on day 3 of the Barger dataset. This analysis focuses specifically on a window of rapid eye movement (REM) phase. [48]

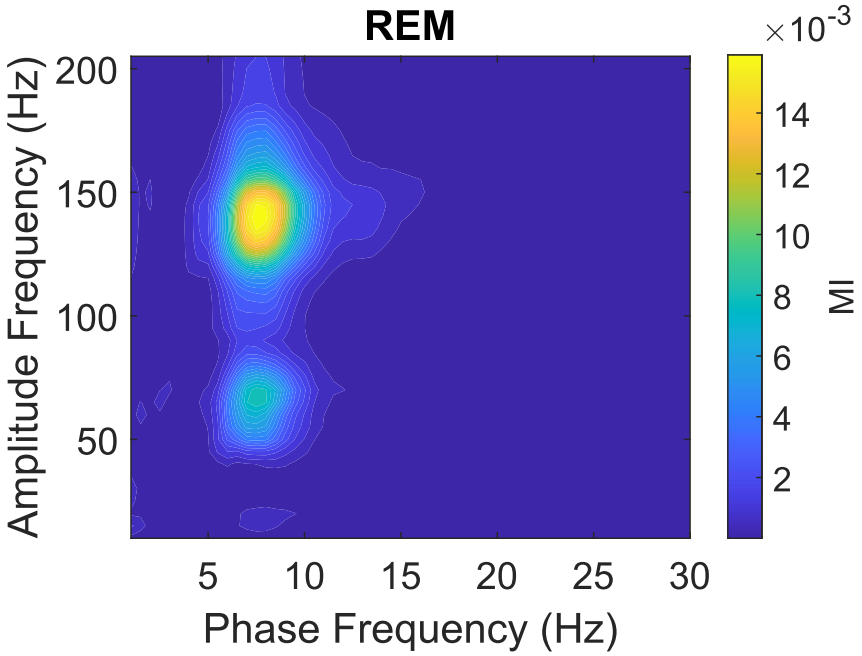

Figure 20 - Comodulogram that illustrates the characteristics of gamma amplitude modulation by theta-phase during the REM (Rapid Eye Movement) phase.

Chapter 3

Sleep Spindle Analysis

3.1. Comparison

Once all three algorithms were implemented, each of the three algorithms was applied to recordings of three different rats. Four 15-minute segments of recordings containing sleep spindles were extracted from each rat, first from the CTX channel and then from the THL channel. The HPC (hippocampus) channel was not selected for this analysis because sleep spindles are thalamocortical events, and the information in the hippocampus was not considered relevant for this particular analysis. Figure 21 displays an example of spindle detection using the three algorithms, San Francisco, Boston, and Spindler, respectively. The figure also includes the envelope and raw data for the analyzed time window. Spindles are depicted in a triangular shape, as illustrated in Figure 22, which provides a zoomed-in view of Figure 21.

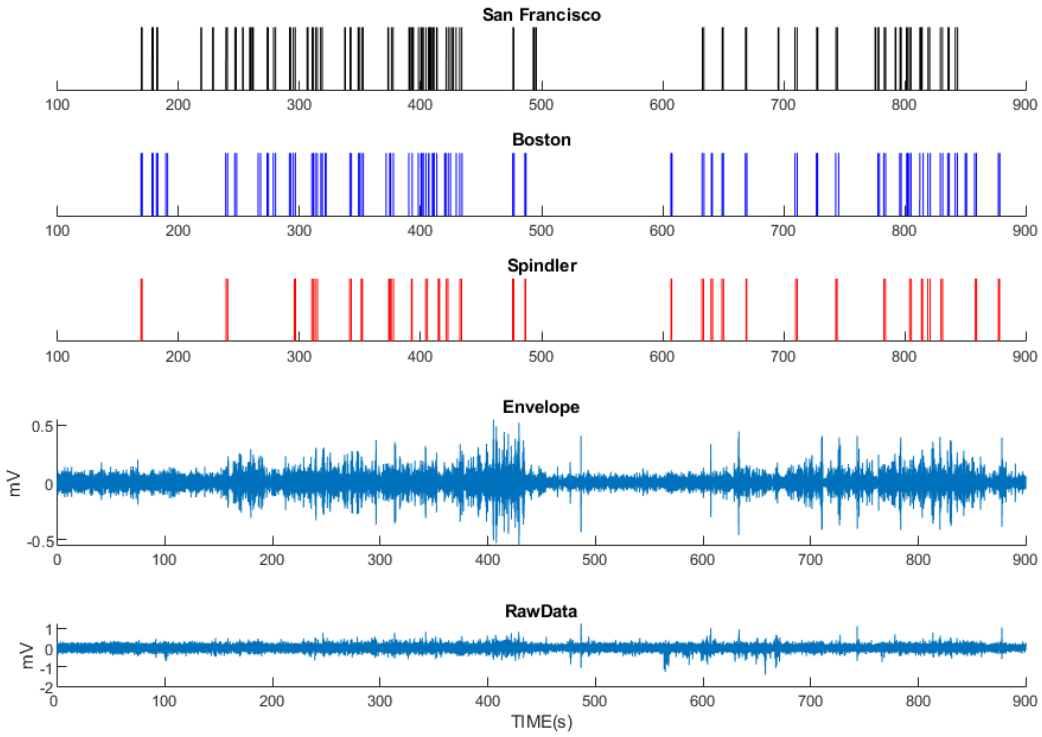

Figure 21 – Spindle Detection rat 1, last 15 minutes of recording. Each spindles are represented as rectangles.

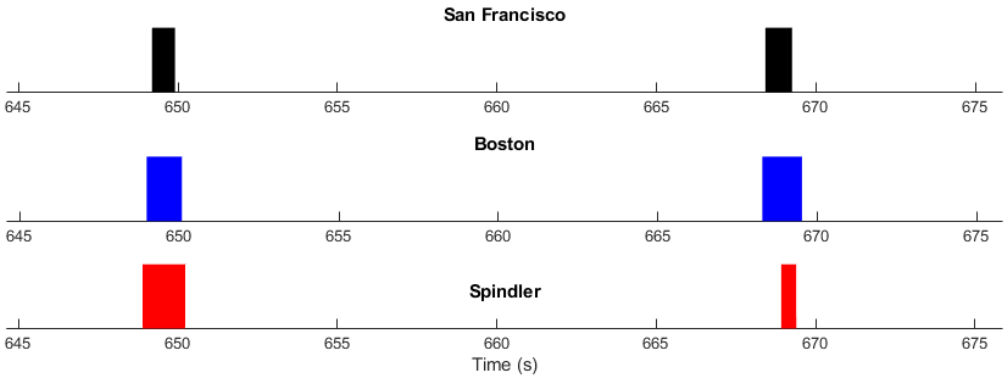

Figure 22 - Zoom.

Next, a MATLAB script was written to determine the correlations between the different pairs of algorithms. This was done because, in the absence of a ground truth to compare results with, if the detected sleep spindles from different algorithms match, it indicates a high level of reliability in the results. Once the common detected spindles for each pair of algorithms were calculated, the Jaccard index was computed to analyze the correlation between the three different algorithm pairs. The Jaccard index, in fact, allows us to quantify the degree of similarity between the sets of detected spindles generated by each algorithm. This analysis provides insight into the consistency and reliability of the results generated by each algorithm and can aid in identifying the most effective algorithms for spindle detection in the given dataset. The Jaccard coefficient is defined as the size of the intersection divided by the size of the union of the sample sets:

$$J(A,B) = \frac{|A \cap B|}{|AUB|} \qquad (1,5)$$

The index ranges from 0 to 1, where values closer to 1 indicate a higher degree of similarity between the two sets of data being compared. To express the similarity measure as a percentage, it is possible to multiply the Jaccard index by 100. This allows for a more intuitive interpretation of the similarity metric, with higher percentage values indicating a greater degree of overlap between the two sets of data. From the figures 23, 24, it can be observed that the algorithm pair with the highest similarity in the CTX and THL channels is San Francisco and Boston, with respective average correlation of 77.9% and of 72.8% and an interquartile range (IQR) from 73.6% to 82.2%

and from 68.84% to 75.70%. This indicates that the results produced by the two algorithms are very similar to each other in the majority of cases. Therefore, for subsequent analyses, we focused exclusively on one of these two algorithms. Specifically, San Francisco was selected due to its faster computational speed compared to Boston (figure 25, 26)

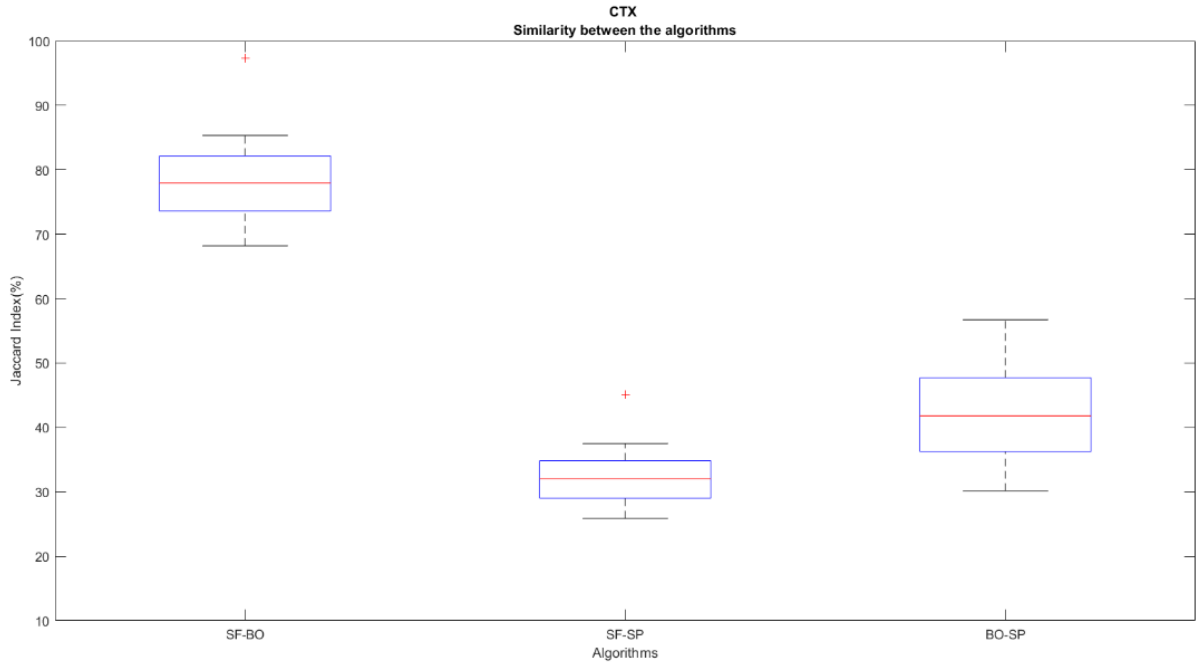

Figure 23 - similarity between the algorithms CTX

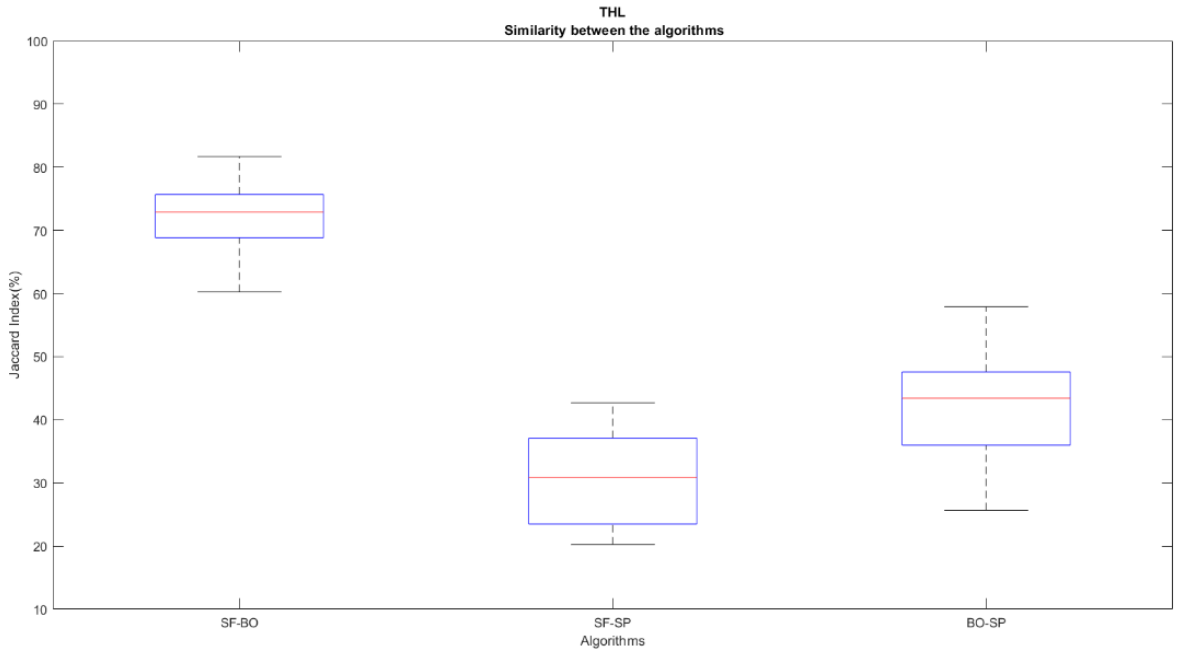

Figure 24 - similarity between the algorithms THL

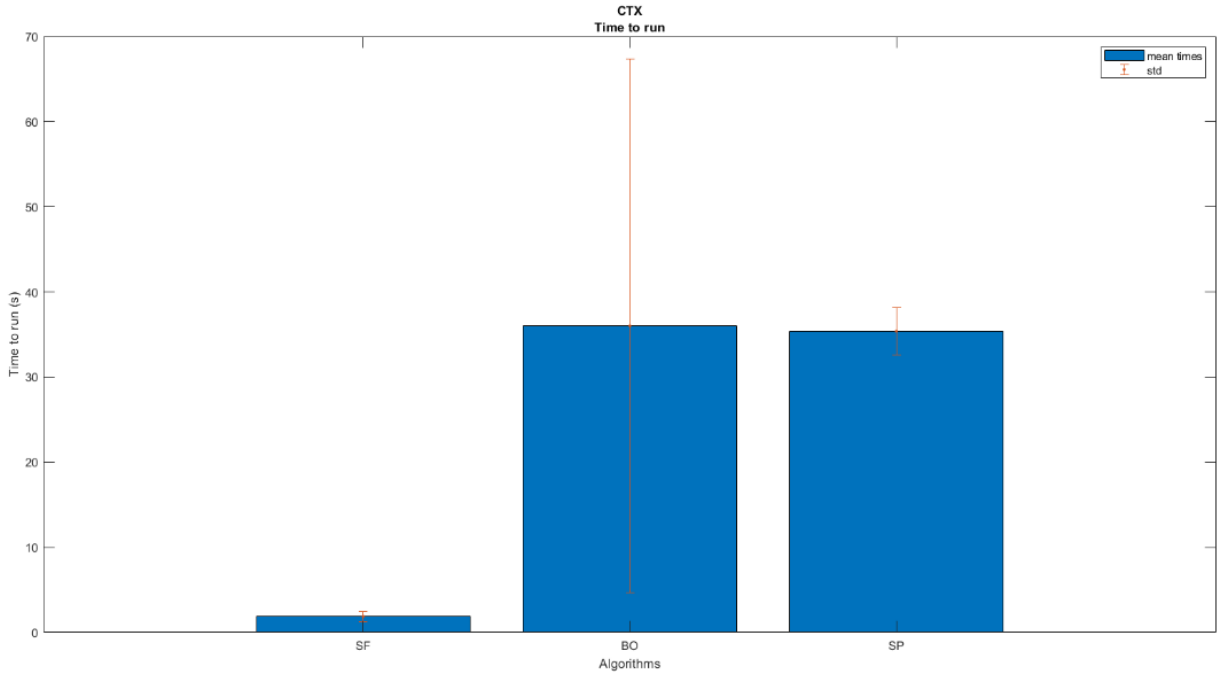

Figure 25 – time to run algorithm on CTX channel

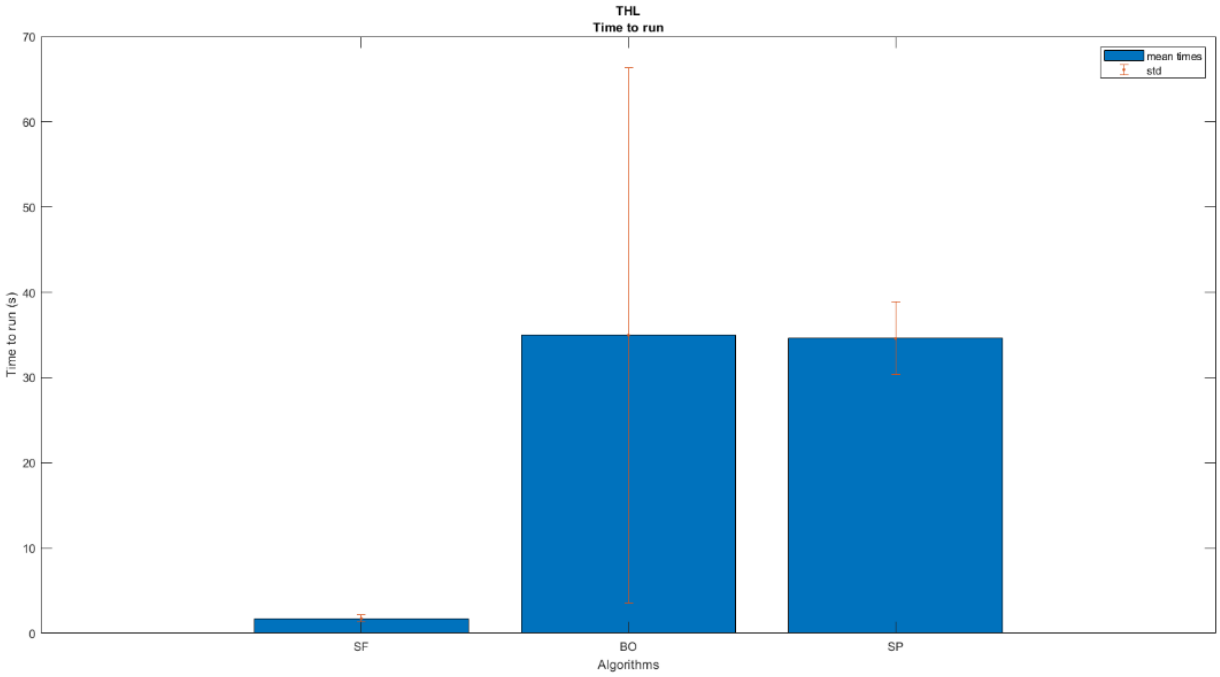

Figure 26 – time to run on THL channel.

3.2. Adjust parameters.

Despite the two algorithms having a similar routine and even if they approximately find the same number of spindles (60 vs 61), by comparing them we notice that the time frames in which spindles are detected don't perfectly match every time. As we can see from the figure 27, 28 (especially in the frame 370-440 seconds), the main error is the unresolved clustered spindle by Boston's algorithm.

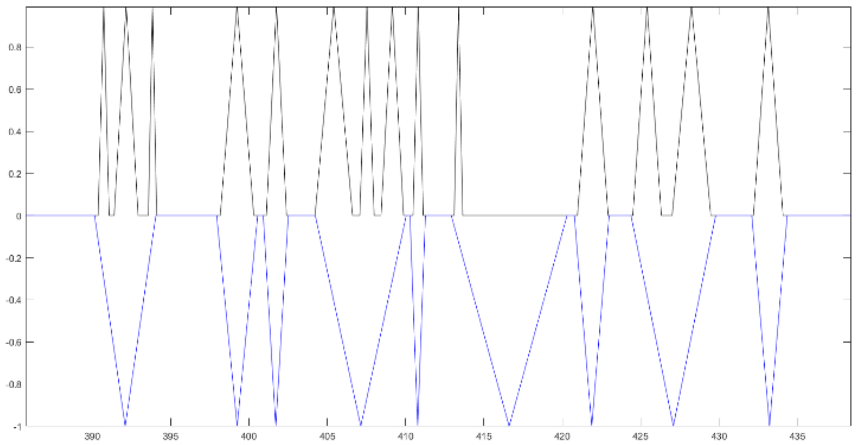

Figure 27 - unresolved clustered spindle *CTX channel*

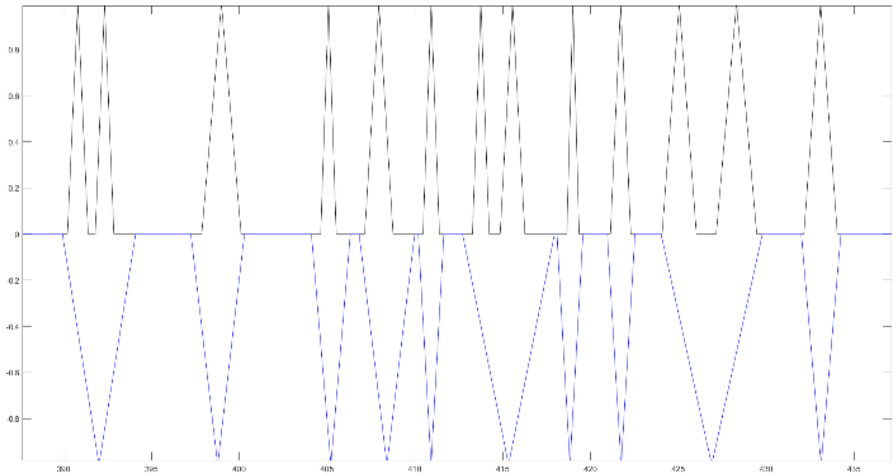

Figure 28 - unresolved clustered spindle *THL channel*

However, this is not an unexpected error. Indeed, as the code developers write in the paper, the unresolved clustered spindle is the principal error of this method; that is to say, where a human scorer could discern multiple spindles close together, but the algorithm counted only one. In fact, for example, when San Francisco detected 3 spindles close together, Boston classified them in only one big spindle. To solve this error, the author recommends decreasing the value of ISI from 0.3 as far as 0.01. I've tried it but there were no changes. Then, to attempt to solve this problem, I've checked the parameters of the two algorithm and tried to detect the main differences between them. Down below you find a summary table with the main parameters compared [Table 1]. One difference that in my opinion could be the reason of the unresolved clustered spindle problem is linked to the parameter of the spindle. In fact, when I've checked it, I've noticed that Maximum spindle length (MSL) and Inter-Spindle Interval (ISI) are different for each algorithm. By lining the maximum spindle length and ISI of the two algorithms the result was not the expected one. By entering the San Francisco's values of ISI and MSL in Boston algorithm the number of spindles decrease from 60 to 50 and in the erroneous time frame (370-440 seconds) the unresolved clustered spindle problem doesn't' occur since there are not spindle anymore. I've tried to do the opposite thing, that is entering Boston values in San Francisco's algorithm, and I've noticed an increase of the number of spindles from 61 to 66 and an increase of the main error. Subsequently, Vinicius and I have decided to change approach. Instead of working directly on spindles' parameters, we've tried to focus on the upper and the lower thresholds (that are different) The Boston threshold values were derived from the mean cubed RMS transform value of the entire trace (all behavioral states) and included both a lower threshold (1.0× mean cubed RMS; default) and upper threshold (2.5× mean cubed RMS; default). While the two thresholds of San Francisco algorithm are based on the mean (m) and standard deviation (s) of the spindle band LFP; the upper and lower thresholds were set $\mu + (1.5)\ \sigma$ and $\mu + (2.5)\ \sigma$, respectively. So, since the setting of these thresholds is based on different strategies, I've changed only the set values. Increasing the two San Francisco's thresholds, the result, as we expected, is that the number of spindles decrease. By setting the lower and the upper threshold value to 2 and 3, 42 spindles have been detected instead of 60. Since these changes worked, I've tried to modify the lower threshold of Boston. I've done it because the lower threshold was used to determine the start and end of each event while the upper threshold value identify putative spindle peaks. So, the lower threshold determined if these putative spindles met our temporal criteria. Increasing Boston's lower threshold to 2.8 and keeping the upper one on the same value we notice a decrease of the maximum spindle length. If we compare the obtained results to the ones achieved by modifying San Francisco's thresholds we notice a clear improvement of the

unresolved clustered spindle problem (figure 29,30). In fact, in the erroneous time frame, how we can see, we have a 1 to 1 matching between the spindle of the two algorithms. In the end, modifying the upper and lower thresholds, we've managed to reach an almost 1 to 1 correspondence. We can conclude that the perfect convergence between the results of the two algorithms is possible by modifying the parameters.

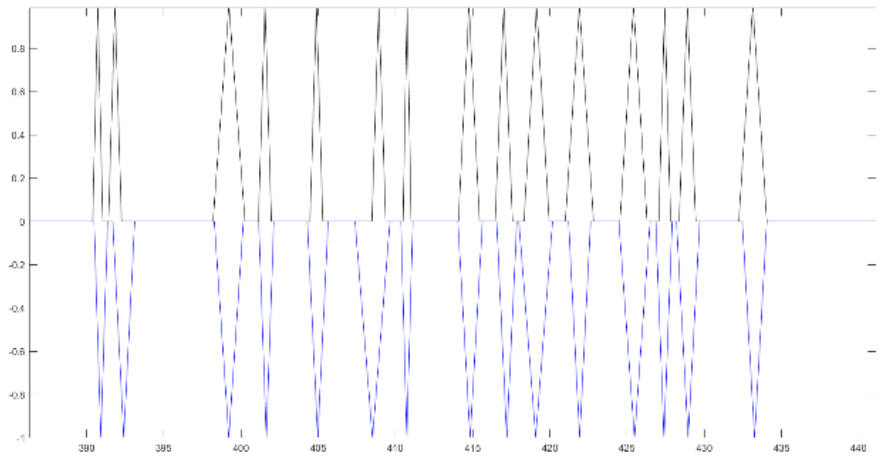

Figure 29 - resolved clustered spindle *CTX channel.*

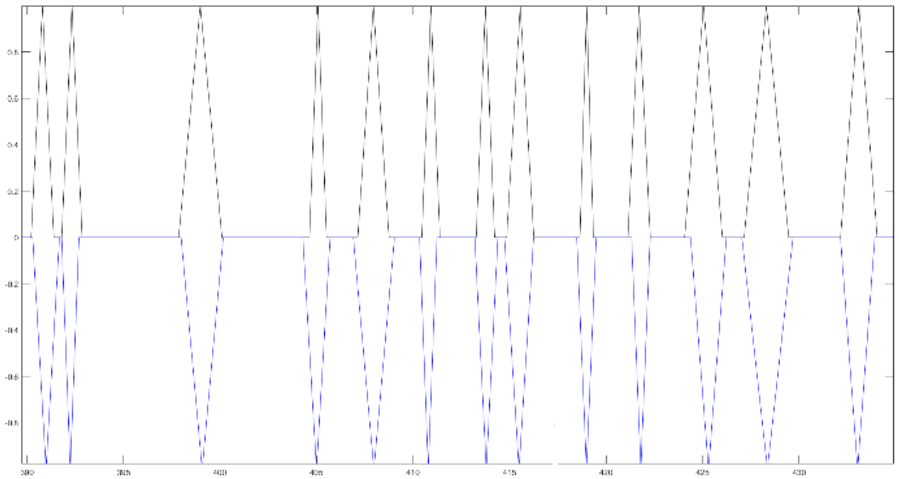

Figure 30 - resolved clustered spindle *THL channel.*

In conclusion, we found that changing parameters in filter-based routines heavily influence the results obtained. By modifying the upper and lower thresholds, we were able to achieve an almost 1 to 1 correspondence in our results. We also observed that the choice of method can impact the

results obtained, and further investigation into the differences across routines is necessary. However, when parameters are appropriately adjusted, the routines can be considered comparable, providing evidence of validation. Overall, our findings emphasize the importance of carefully selecting parameters and methods in the analysis of electrophysiological data.

	San Francisco	**Boston**	**Spindler**	**DDA**
Minimum spindle length	0.5 s		0.5 s	
Maximum spindle length	2.5 s		3 s	
ISI (Inter-Spindle Interval)	0.3 s	0.1 s	0.3 s	0.3
Lower Threshold (default)	$\mu + (1.5) \times \sigma$	1.0× mean cubed RMS		
Upper Threshold (default)	$\mu + (2.5) \times \sigma$	2.5× mean cubed RMS		

Table 1 – Parameters Spindle

	San Francisco	Boston	Spindler
Response	Butterworth	Butterworth	
Digital type	IIR	IIR	FIR
Order High pass Butterworth filter	6	Minimum-order designs	
Order Low pass Butterworth filter	8	Minimum-order designs	
First stopband frequency	7	3	
First stopband frequency	10	10	11
Second passband frequency	15	15	17
Second stopband frequency	19	22	
Stopband attenuation levels	15	24	53
Passband Ripple	3	1	

Table 2 – Filter table

Chapter 4

Sleep wake cycle stage detection

4.1. Analysis

For the detection of SWC stages and construction of hypnograms, we first applied toolbox package which is termed AccuSleep [42] and then we also used the State Space algorithm [47] .

4.1.1. Comparison

After implementing the two algorithms for SWC stage detection on the entire dataset (10 mice), a script was developed to verify their agreement. The aim of using and comparing both approaches is twofold. Firstly, since a ground truth was not available, it was necessary to compare the two algorithms in order to deduce their accuracy. Additionally, while the State Space algorithm has been utilized in various studies (including some of our own), it has not been compared to other approaches for further validation. The results show an agreement of 85.1 % ± 3.07. Figure 31 shows an example of hypnograms obtained from the two distinct SWC staging algorithms for mouse 09 day 5. The hypnogram is a graph that represents the sleep stages as a function of time. Both show a health polyphasic alternation of WK (green), SWS (red), and REM (blue), with REM always following SWS (except for a few short episodes in the state space algorithm which are most probably detection artifacts), as expected. Qualitatively, there is also a strong agreement between approaches, even though they rely on very different computational methods (expert-trained machine learning versus spectral content).

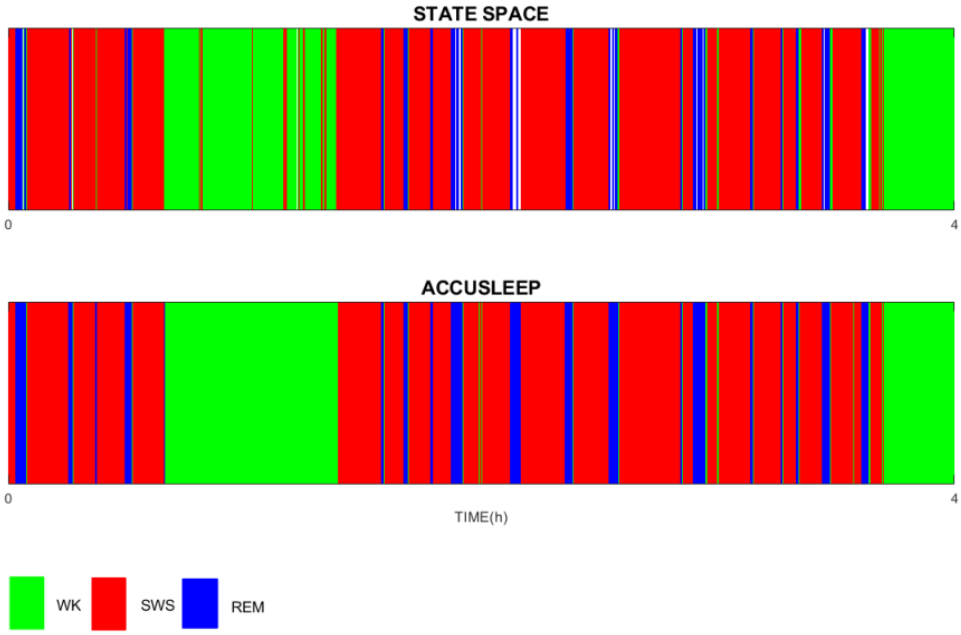

Figure 31 - SWC stage detection algorithms compared.

For further validation, the state space of mouse 09 day 5 was implemented, in which each individual point was colored according to the information obtained from the AccuSleep classification. As can be observed from the figure 32, the colors match the locations accurately.

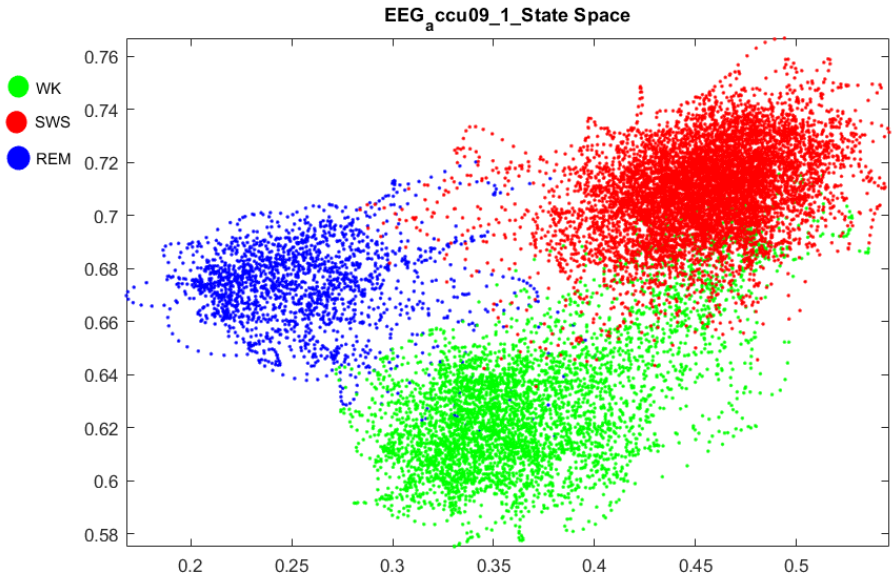

Figure 32 - Classification of Accusleep in the state space created in Gervasoni algorithm. The colors match the locations well, this suggests that the two algorithms used are reliable.

Chapter 5

Phase amplitude coupling analysis

5.1. Construction of a Ground Truth

Once the code written by Tort et al. was downloaded, the first step was to test it by creating a ground truth for testing and implementing the code. The following steps were carried out:

1. Create a simple LFP with a sinusoidal slow oscillation (spindle) of 10 Hz.
2. Create short snippets of ripple (200 Hz) that lasts 40 ms
3. Create a coupled LFP in which (2) is always in the same place (phase)
4. Create a uncoupled LFP in which (2) is not in the same place (phase)
5. Add noise for see if there is still modulation.
6. Compute MI and comodulogram for both of them
7. Verify if MI of signal (3) >> MI of signal (4)

The result is that the comodulogram of the LFP coupled show a strong nesting between a high frequency of 200 Hz and 10-50 Hz low frequency (figure 32) while the LFP uncoupled comodulogram shows that there isn't any nesting as we expected (figure 33). Then, we add noise to verify if there is still modulation and what we noticed is that there is a strong nesting between the low frequency of spindle (10 Hz) and the high frequency of ripple (200 Hz) (figure 34). So, the amplitude of the ripple is modulated by the phase of the spindles. While, in the LFP uncoupled with noise (figure 35) we can notice that there isn't still any coupling within these pair of frequency.

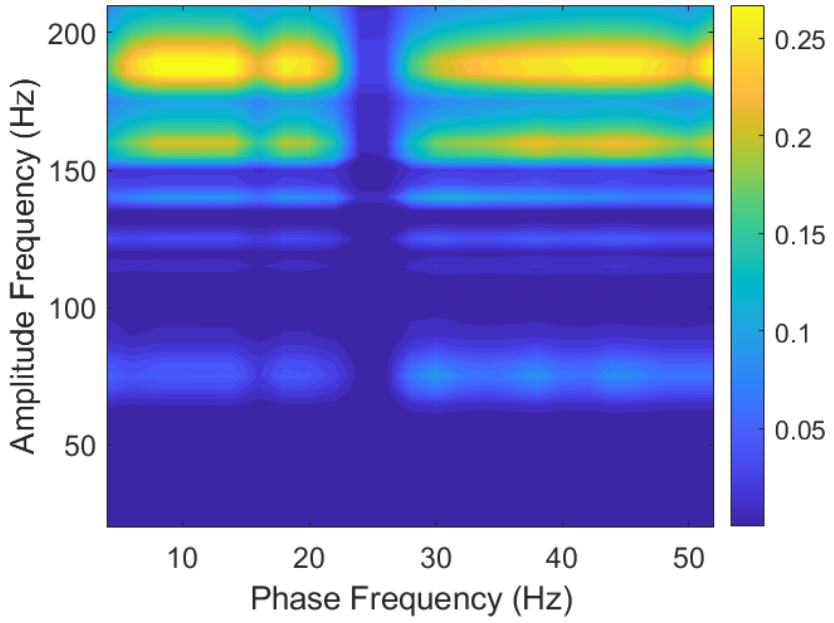

Figure 33 – Comodulogram LFP coupled.

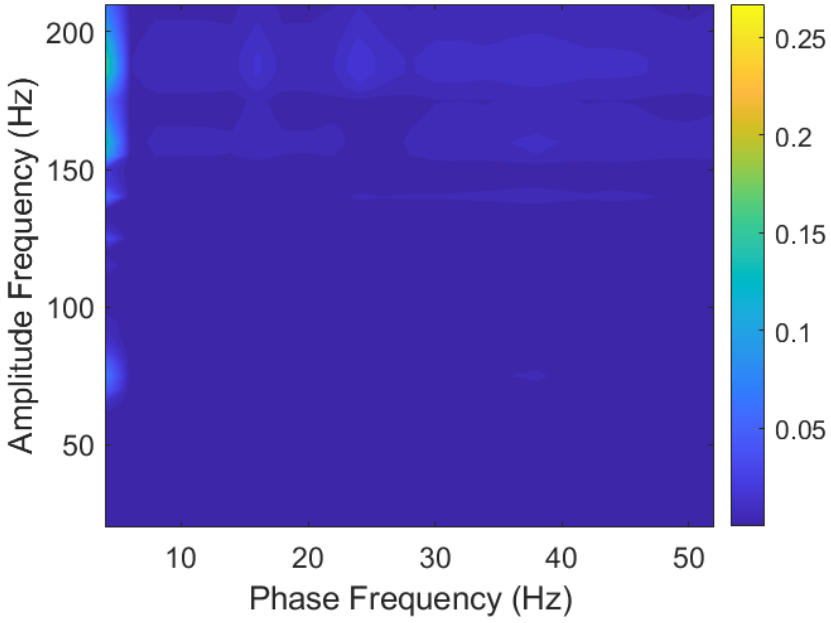

Figure 34 – Comodulogram LFP uncoupled.

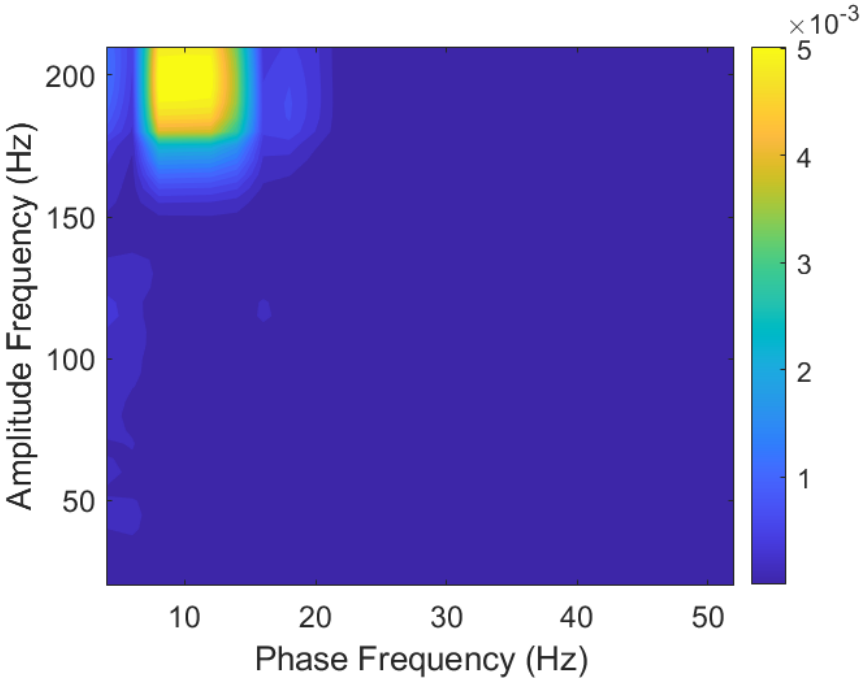

Figure 35 – LFP couled with noise

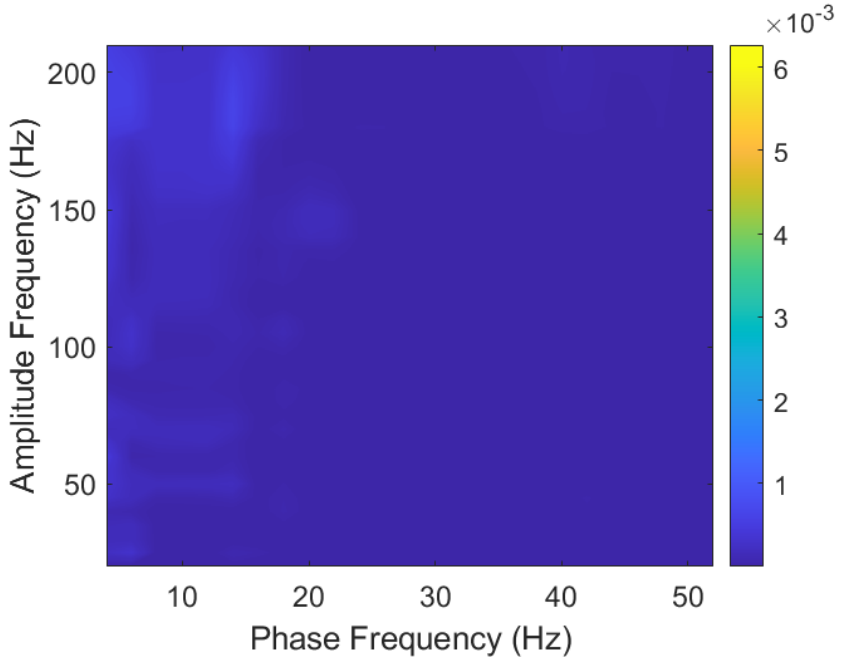

Figure 36 – LFP uncoupled with noise.

5.1.1. Profiling the coupling pattern

Once the selected algorithm was confirmed to be functional, it was applied to the Barger dataset [35]. We calculated the coupling between phase frequencies 1-30 Hz and amplitude frequencies 10-210 Hz for 10 mice using the modulation index (MI) routine of Tort et al. for study the general pattern on SWC. After the comodulograms were built, we chose specific frequency of pairs for statistical comparison. They were chosen for both their neurobiological relevance and also for the qualitative differences that could be observed by the visual inspection of the comodulograms. Table 3 summarizes pairs of frequency assessed in this study.

Identifies	*Frequency used for phase (low)*	*Frequency used for amplitude (high)*
A	Theta (7.5 Hz)	High gamma (140 Hz) / ripples
B	Theta (7.5 Hz)	Low gamma (70 Hz)
C	Slow wave (1 Hz)	Theta (11 Hz) / spindles
D	Slow wave (1 Hz)	High gamma (150 Hz) / ripples
E	Theta (11 Hz) / spindles	Low gamma (70 Hz)
F	Delta (2.5 Hz)	Theta (11 Hz) / spindles
G	Slow wave (1 Hz)	Higher gamma (200 Hz) / ripples

Table 3 - Pairs of frequencies assessed by PAC.

Chapter 6

Results

6.1. SWC strongly modulates PAC patterns.

Having obtained information on the sleep state of the mice with Accusleep, I selected 30 seconds of REM, NREM, and wake for each of the 10 animals to see if there was a recurrent pattern in the co-modulogram. Stage-specific comodulograms of a representative animal (mouse 9 day 5) are displayed on figure 36,37,38, which shows some regions that are strongly modulated across sleep, such as coupling between theta and gamma (low and high).

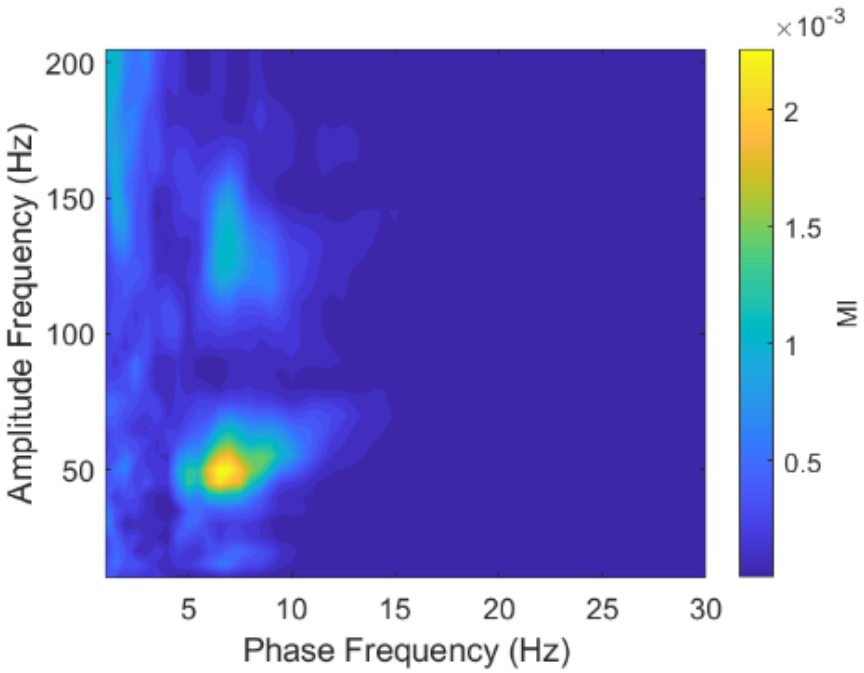

Figure 36 – comdulogram that rappresent 30 second of WAKE

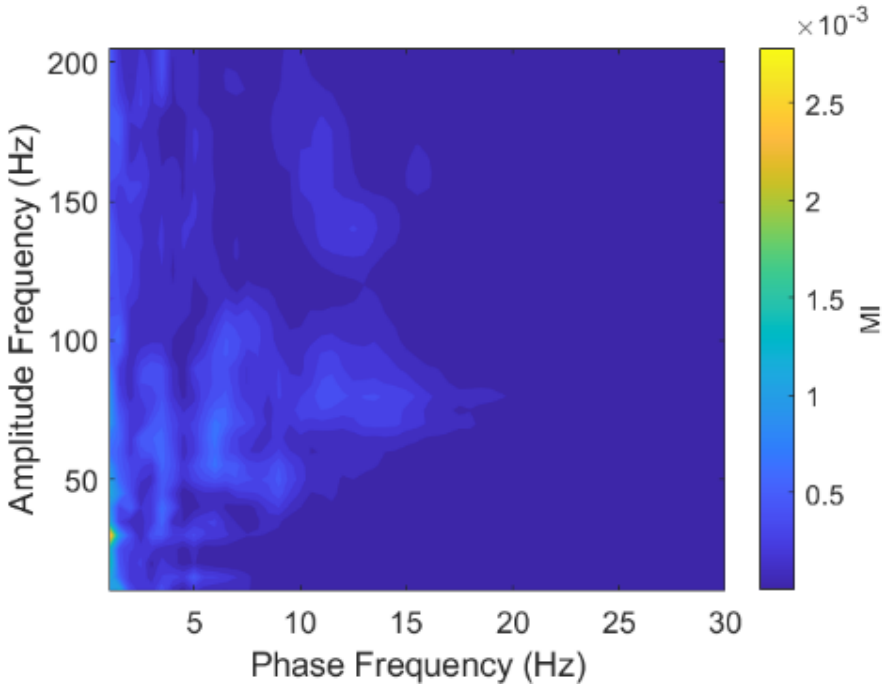

Figure 37 – comdulogram that rappresent 30 second of SWS

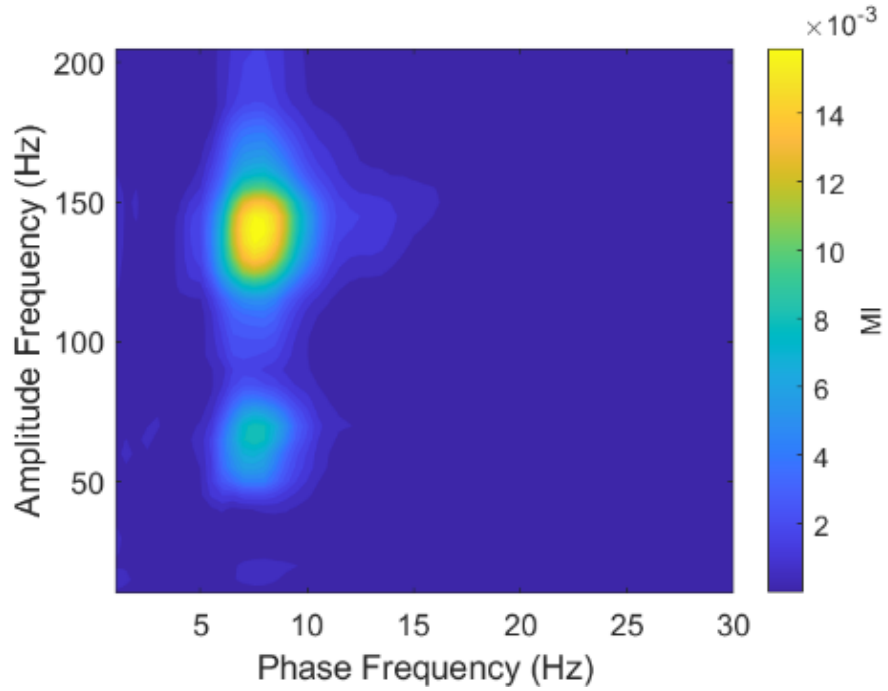

Figure 38 – comdulogram that rappresent 30 second of REM

After creating the comodulograms, MI values, related to the selected frequency pairs, were extracted from them for each of the three sleep stages (REM, NREM, and wakefulness). The aim was to visualize how the patterns of neural synchronization vary across the sleep-wake cycle in these 10 animals. Group measures of specific frequency pairs can be found in the curves of Figure 39 (comparisons between WK and SWS), Figure 40 (SWS and REM) and Figure 41 (WK and REM). Each panel (A to G) corresponds to a specific frequency pair (as described in Table 3) and shows all animals (light gray lines) and the mean with SEM (bold red lines). As it can be seen, the average MI for several frequency pairs displayed differences with statistical significance when comparing distinct stages (***$p < 0.001$; **$p < 0.01$; *$p < 0.05$; paired t-test). The paired t-test one tail is used to compare the differences between paired observations from two groups and evaluate if these differences are statistically significant. It is a statistical test that determines whether there is a significant difference between the means of two paired groups or conditions. One-tailed because we are specifically interested in determining if there is a significant difference in a particular direction. In our study, we specifically aimed to compare the coupling between specific frequency pairs in pairs of two phases at a time (WK vs SWS; SWS vs REM; WK vs REM). Therefore, we employed the paired t-test as an appropriate statistical test for our research objective. From start, it is clearly apparent that the PAC between the phase of theta range and the amplitude of the gamma range (both high and low; Figures 34 and 33, panels A and B, respectively) are strongly increased during REM sleep in comparison to both WK and SWS. These same couplings also show to be slightly increased in WK when compared to SWS (Figure 32, panels A and B). Interpretation of such results is straightforward and can be related to the acquisition of memory traces by active exploration during WK and posterior consolidation during sleep, both processes in which theta and gamma oscillations play important roles [49]. Particularly, theta is a very stereotypical electrophysiological signature of REM and can be clearly noticed in raw tracings. Such observation is in line with other studies on theta-gamma coupling dynamics [50] and is reviewed in [51] on the context of High Frequency Oscillations. Although theta is a rhythm generated within hippocampal circuitry, its influence in cortical areas (such as the prefrontal region) can be captured by cortical electrodes such as those used in the acquisition of the recordings. Additionally, PAC values between delta and theta are clearly increased during SWS when compared to both WK (Figure 32, panels C and F) and REM (Figure 33, panels C and F). In fact, delta waves are the predominant rhythms observed during this stage.

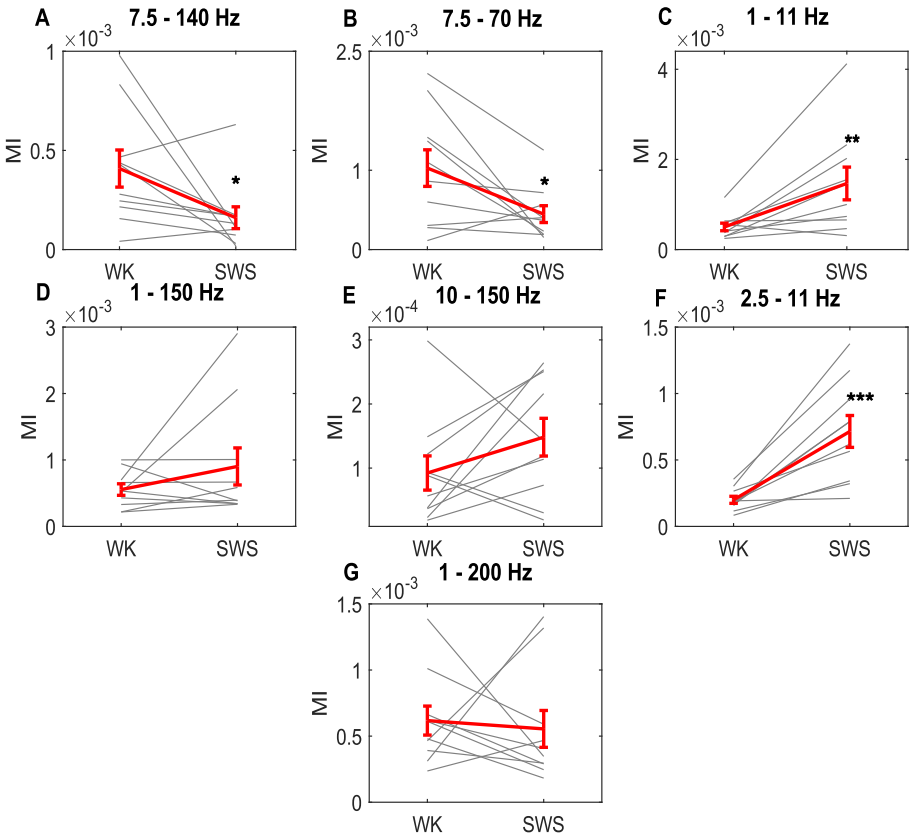

Figure 39 - Group measure of PAC for all different pairs of frequencies considered, comparing WK to SWS (***p < 0.001; **p < 0.01; *p < 0.05; paired t-test).

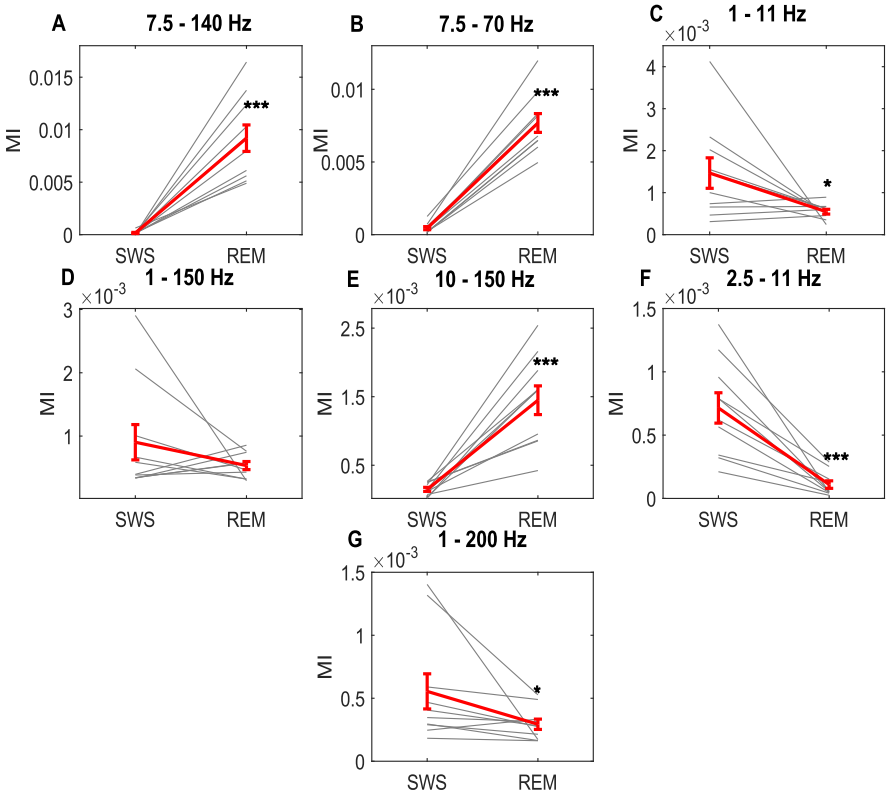

*Figure 40 - Group measure of PAC for all different pairs of frequencies considered, comparing SWS to REM (***p < 0.001; **p < 0.01; *p < 0.05; paired t-test).

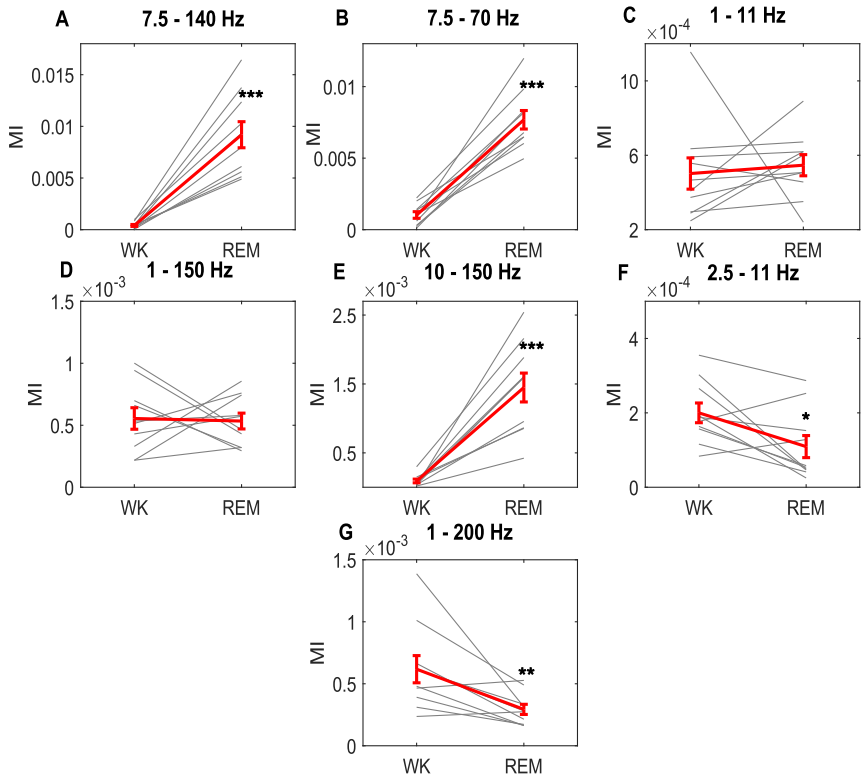

Figure 41 - Group measure of PAC for all different pairs of frequencies considered, comparing WK to REM (***p < 0.001; **p < 0.01; *p < 0.05; paired t-test).

From this analysis, we can conclude that SWC strongly modulates PAC patterns, as summarized in Table 4. The arrows in Table X indicate changes during SWS or REM compared to WK. The PAC modulation discovered in this study can serve as a basis for future sleep staging algorithms.

Pair	*SWS*	*REM*
A	↓	↑
B	↓	↑
C	↑	-
D	-	-
E	-	↑
F	↑	↓
G	-	↓

Table 4 – Significant PAC alterations referenced to WK.

6.2. PAC does not reveal SO-spindle-ripple coordination.

After identifying typical patterns of neural synchronization across the SWC, we investigated whether PAC could also discern triple coordination of SO-spindle-ripple. However, we found inconsistencies in this regard. As we expected based on literature, Delta-Theta PAC (suggesting SO-spindle coupling) increased during SWS compared to WK and REM. However, Theta-Gamma PAC (suggesting spindle-ripple coupling) did not increase during SWS, which was unexpected since these coupling known to occur during this stage. To achieve this, we computed the MI values in 30-second excerpts of LFP. However, it is important to note that we did not use single comodulogram points for this analysis. Instead, we calculated the MI values within frequency ranges that better represented the oscillations of interest: 0 – 2 Hz for slow oscillations, 7 – 15 Hz for spindles, and 140 – 200 Hz for ripples. Figure 42 shows a representative animal to illustrate the results of this analysis. Here, hypnograms are depicted as a temporal sequence of color-coded SWC stages (WK: green; SWS: red; REM: blue) and spindles are indicated as dots in the uppermost portion of the hypnogram. In the bottom of hypnograms, black tracings depict the MI values computed across time each 30 s. Top hypnogram is superimposed with slow-oscillation and spindle PAC and bottom hypnogram with spindle and ripple PAC.

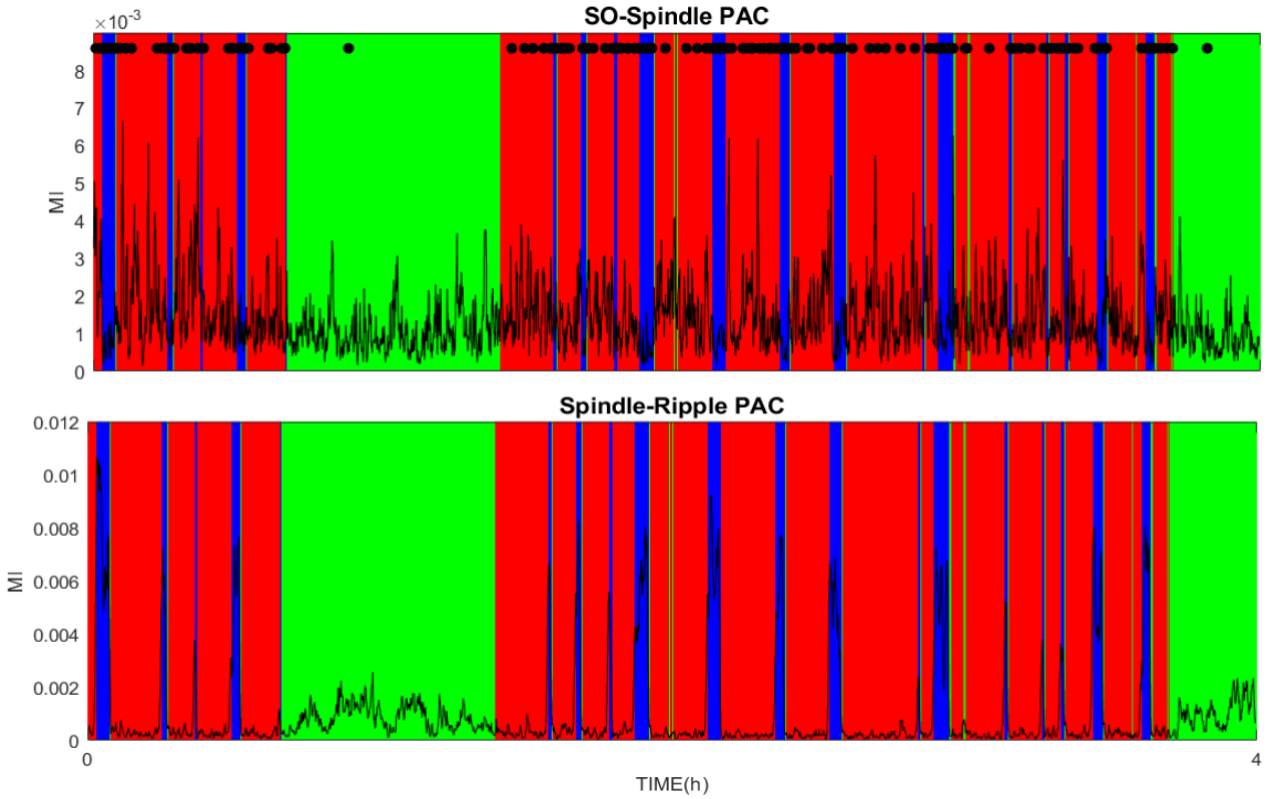

Figure 42 – Hypnogram with spindles and MI (top MI of SO -spindle, down MI of spindle-ripple)

Some clear features are immediately distinguishable from these plots.

1. As expected, the MI curve of SO-spindle shows peaks during SWS (in red) and decreases during REM (in blue) on the upper hypnogram.
2. Unexpectedly, the MI curve of spindle-ripple shows peaks during REM (in blue) and flattens during SWS (in red) on the lower hypnogram.

   This unexpected pattern suggests that what we are observing may not be the coupling of spindle-ripple activity, but rather that of theta-gamma activity because these two activities share a portion of frequency ranges and theta-gamma activity is known to be prominent during the REM phase.

3. As expected, spindles are primarily observed during slow wave sleep (SWS), with possible detection artifacts during wakefulness (WK).
4. Surprisingly, a significant number of spindles are also observed during rapid eye movement (REM) sleep stage.

This observation may be explained by either the similarity in frequency ranges between spindles and theta waves, which can potentially cause interference, or by the possibility that the spindles are

erroneously marked as occurring in the REM stage, when in fact they belong to the transition zone between REM and SWS. To better understand and address the issue observed, we plotted the spindles in the state space and examined whether many of them fell in the REM phase, or if they were related to transitions. Our findings revealed that with the classical notation of spindle frequency range between 7-15 Hz, many spindles occurred during the REM phase (figure 43).

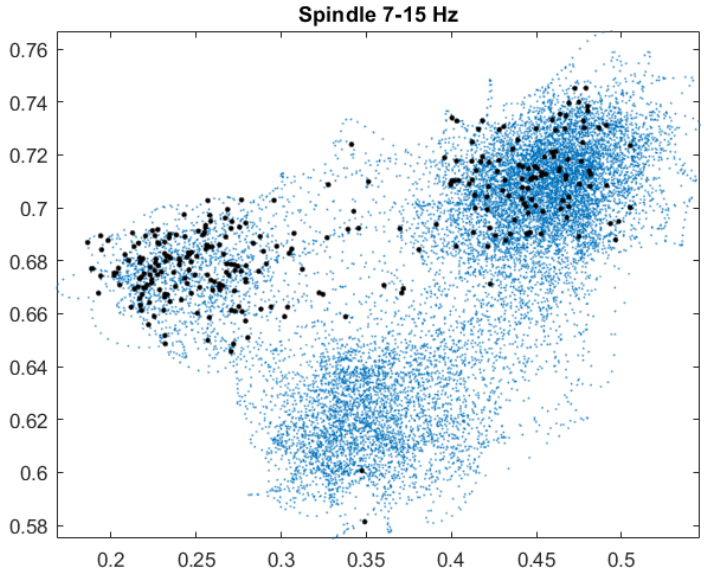

Figurer 43 – State space with spindle

So, to verify if this was due to the similarity in frequency ranges between spindles and theta waves, we chose to reduce the spindle range due to suspected contamination. The decreasing spindle frequency range significantly reduced the number of spindles during the REM phase, as shown in Figure 44. This supports the notion suggested by recent literature that increasing the spindle range can help avoid interference with theta waves. This finding is a novel discovery, as historically the literature has described spindle frequency ranges between 7-15 Hz [52], whereas it may be more appropriate to use a range of 10 or 12-15 Hz. Therefore, in response to the question of whether the spindles reveal SO-spindle-ripple coordination, the answer is likely negative.

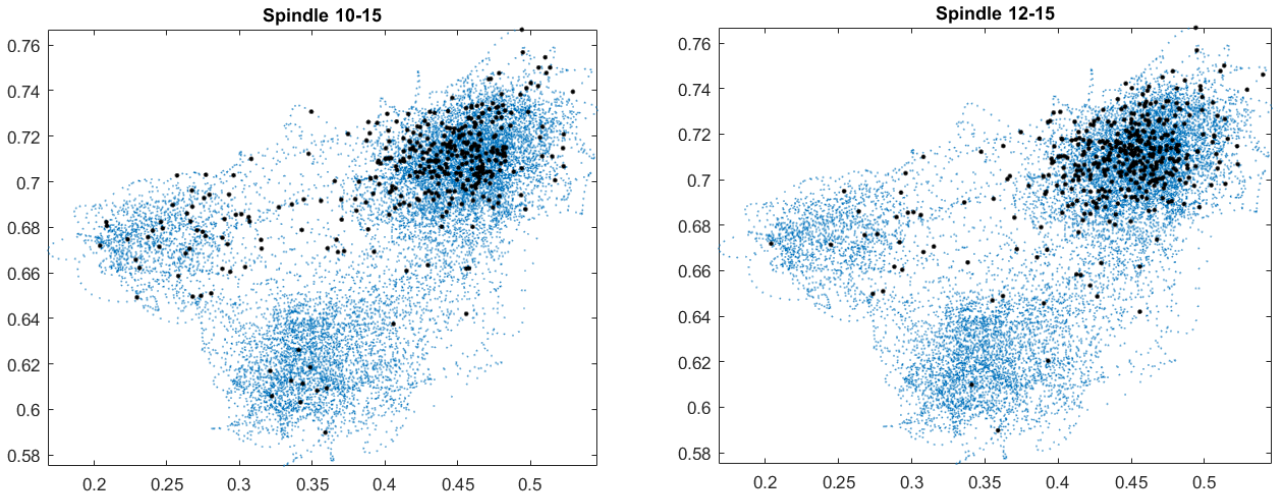

Figure 44 - Narrowing spindle range greatly reduces number of spindles in REM phase.

Subsequently, I conducted additional analyses to verify whether the suspicion that PAC could not detect the triple coordination of SO-spindle-ripple was true. I performed the statistical analysis again from scratch, but this time I didn't just take random 30-second windows of recording where the animals were in WK-SWS-REM (figure 44,45,46). I extracted 30 seconds of SWS but centered on the spindles, 30 seconds of REM in which no spindle was identified, and 30 seconds of WK in which no spindle was identified. Then, I constructed 30 comodulograms and performed the statistical analysis with these new points (table 5)

Identifies	*Frequency used for phase (low)*	*Frequency used for amplitude (high)*
A	Theta (7.5 Hz)	High gamma (140 Hz)
B	Theta (7.5 Hz)	Low gamma (70 Hz)
C	Slow wave (1 Hz)	Spindles (15 Hz)
C	Slow wave (1 Hz)	Spindles (10 Hz)
E	Spindles (13 Hz)	Ripples (140 Hz)
F	Spindles (13 Hz)	Ripples (200 Hz)
G	Slow wave (1 Hz)	Ripples (200 Hz)
H	Delta (2.5 Hz)	Theta (10 Hz)
I	Delta (2.5 Hz)	Spindles (13 Hz)

Table 5 – New pairs of frequency assessed by PAC

Analyzing the SO spindle coupling, we see that it is greater during SWS compared to REM (panel C and D figure 45), as we expected and as we also observed in the previous statistical analysis. However, if we evaluate the spindle-ripple coupling, that was different from what we expected in the previous analyses (because it was greater in REM), we can see that also in this case it is greater in the REM compared to SWS (panel E figure 45). Trying with another pair of points that always represents spindle-ripple (panel F figure 2), we see that it is greater in the SWS phase, but not significantly. In contrast, theta-gamma (panel A and B, figure 45) and delta-theta (panel H and I figure 45) couplings remained consistent with our expectations.

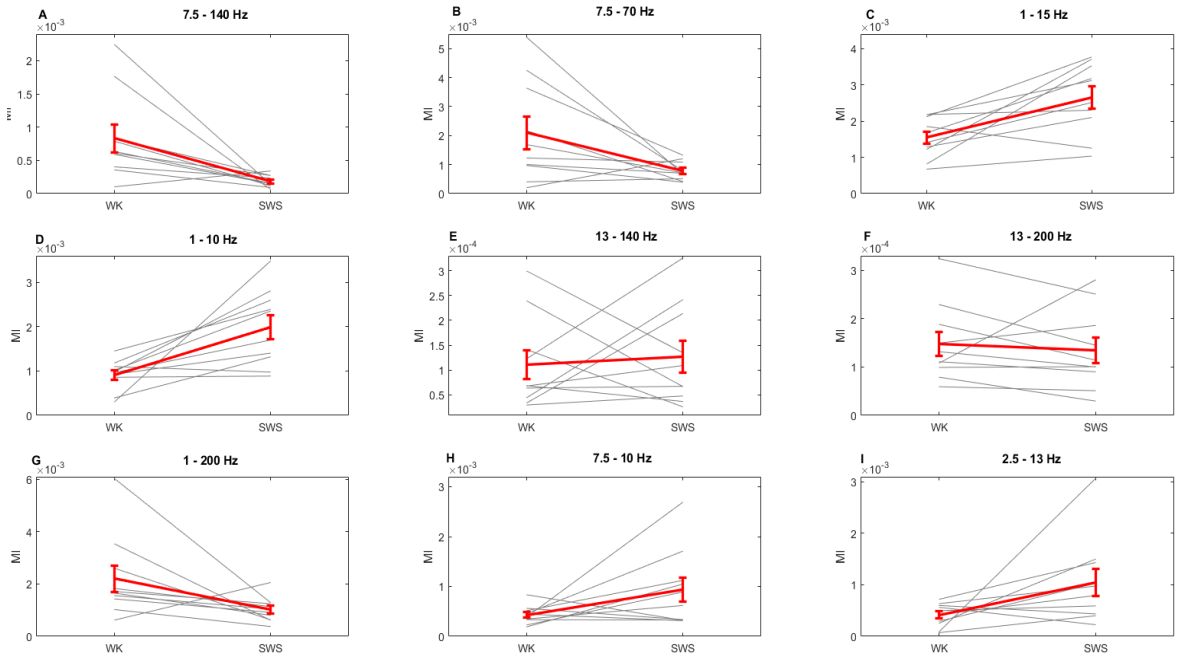

Figure 44 - Group measure of PAC for all different pairs of frequencies considered, comparing WK to SWS

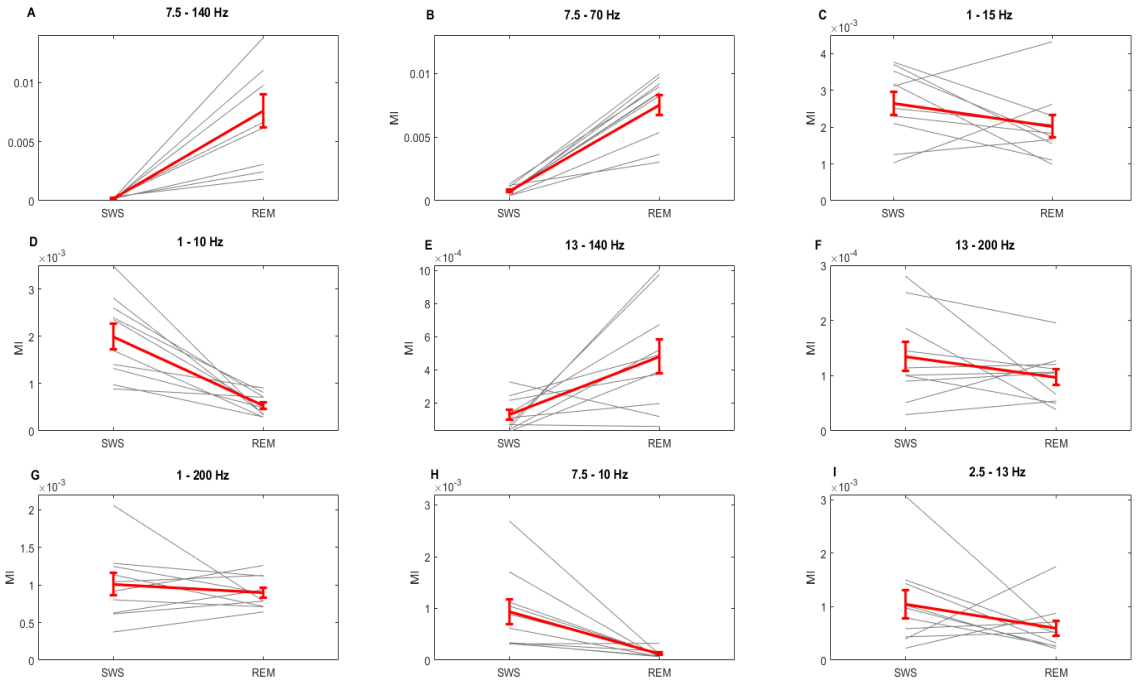

Figure 45 - Group measure of PAC for all different pairs of frequencies considered, comparing SWS to REM

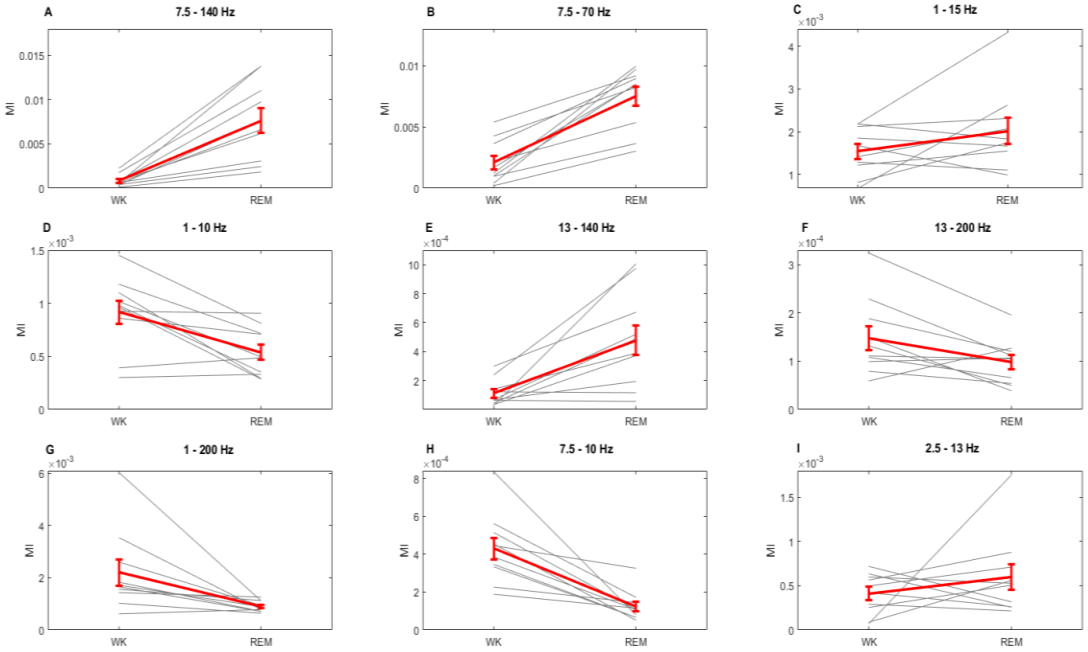

Figure 46 - Group measure of PAC for all different pairs of frequencies considered, comparing WK to REM

Afterwards, I conducted an additional experiment whereby I calculated the MI of spindle-ripple and of SO-spindle using a new spindle frequency range (10-15 Hz) throughout the entire recording and plotted the results on the hypnogram. The findings revealed that there was no significant improvement in the graph depicting the spindle-ripple coupling compared to the results from the previous analysis, wherein the spindle-ripple peaks were observed during REM and not SWS. The experiment was conducted on two different animals, and in the second animal, mouse 4 day 5 (figure not shown), some peaks were observed during SWS, but not enough to discern the states with certainty. The final test I performed was to calculate the MI in 30-second windows, first throughout the whole signal and then only in 30-second windows centered on all spindles (only the spindles that fell into the SWS phase, the spindles that were erroneously in the REM and wake phases were not counted). I expected the coupling of SO-spindles and spindle-ripple to be greater in this second case, but as we can in the table 6, only the coupling of SO-spindles is slightly greater, while the spindle-ripple coupling is not.

Whole rec	*SO-Spindles*	*Spindles-Ripples*	*SWS spindle*	*SO-Spindles*	*Spindles-Ripples*
Mouse 1	0,001537	1,63E-04	Mouse 1	0,00151	1,37E-04
Mouse 2	0,002505	1,42E-04	Mouse 2	0,002988	1,25E-04
Mouse 3	0,001837	1,83E-04	Mouse 3	0,001721	1,63E-04
Mouse 4	0,00156	1,91E-04	Mouse 4	0,001695	1,49E-04
Mouse 5	0,001993	1,52E-04	Mouse 5	0,001999	1,19E-04
Mouse 6	0,002027	1,58E-04	Mouse 6	0,002027	1,58E-04
Mouse 7	0,002512	2,17E-04	Mouse 7	0,002779	1,36E-04
Mouse 8	0,003112	2,84E-04	Mouse 8	0,004311	1,74E-04
Mouse 9	0,001578	2,79E-04	Mouse 9	0,001575	1,63E-04
Mouse 10	0,001704	2,28E-04	*Mouse 10*	0,001686	2,28E-04
	0,002036	2,00E-04		**0,002229**	**1,52E-04**

Table 6 – Comparison of MI Calculation in 30-second Windows: Whole Signal vs. SO-Spindle Centered Windows

Based on all these analyses, it can be concluded that cross-frequency coupling is not effective in capturing the coordination of SO-spindle-ripple. Specifically, it can better discern the coupling of SO-spindles, but not spindle-ripple. It is likely that this is due to the fact that spindle-ripple is very close to theta-gamma, which is much more prominent as a coupling.

6.3. SO-spindle-ripple detection

Since PAC (Phase-Amplitude Coupling) and related measurements such as MI (Mutual Information) not provide a comprehensive quantification of the intricate coordination between slow oscillations, spindles and ripples, an alternative method was implemented to investigate the coordination among these three cerebral waveforms. Initially, the identification algorithms for each event were applied, specifically implementing all three algorithms derived from the aforementioned San Francisco study (spindle detection, ripple detection, SO detection). Each method relied on the same preprocessing steps of the Local Field Potential (LFP). To begin, the LFP was z-scored in each channel and then averaged across all good channels. The resulting average LFP for each method underwent specific band filtering, with ripple analysis utilizing a bandpass filter of 140-200 Hz and slow oscillation analysis utilizing a bandpass filter of 0.1-2 Hz. This filtering process involved the application of two independent zero phase-shifted filters: a high-pass Butterworth filter and a low-pass Butterworth filter. Following filtering, a smoothed envelope of the signal was computed using the magnitude. This smoothed envelope served as the basis for determining thresholds for ripple and slow oscillation detection, based on the mean (μ) and standard deviation (σ) within the specific band LFP [44]. Once the three events (slow oscillations, spindles, and ripples) were identified in the LFP, an analysis of occurrence within temporal windows was performed. For the identification of SO-spindle couplings, the time difference between the peak of the spindle and the up-state of the linked SO was measured for each detected spindle (DTSO-Spindle). Spindle events with DTSO-Spindle falling between 0.5 s and 1.0 s (i.e., within a nesting time window) were considered as SO-nested spindles [44]. Similarly, for spindle-ripple couplings, cortical ripple events showed significant cross-correlation with cortical spindles within 200 to 500 ms prior to the peak of spindle power, similar to the observed coupling between hippocampal ripples and cortical spindles. So the window in question starts 500 ms before the spindle peak and ends with the end of the spindle under consideration [53]. Hence, spindles identified as coupled with ripples were subsequently used to examine potential couplings with slow oscillations, providing a comprehensive overview of the triple coordination (figure 47). The developed method was tested on two dateset: four mice from Barger dataset and two rats from my co-advisor Vinicius

Rosa Cota's dataset. Five tables have been attached, providing relevant results: The first table presents the number of events detected throughout the entire recording, including the counts for SO-spindle couplings, ripple-spindle couplings, and SO-spindle-ripple couplings (table 5). The subsequent two tables represent the analysis of the ground truth for an example animal from each dataset (table 6,7). in Notably, the percentage of spindles coupled with SO in all tested animals was approximately 40%, which aligns with existing literature. For instance, it is known that 50% of all sleep spindles are temporally coupled to cortical SO in both humans and mice [43]. On the other hand, the percentage of ripples coupled with spindles was significantly lower, around 2%, which is consistent with findings in literature. Jan Born's analysis reported an average co-occurrence of ripples with spindles at 7.2 ± 0.6% in the hippocampus [43]. It should be noted that Barger's dataset only includes cortex recordings, which may account for the slightly higher percentage observed. While the percentage that concerns Vinicius Rosa Cota's dataset is closer to Jan Born's since the ripples were detected in the hippocampus. The total number of SO-spindle-ripple couplings (as indicated in Table 7) was also found to be very low, consistent with literature findings that event-based analyses show a low occurrence of SO events co-occurring with spindles and ripples, with a maximum of 3.6 ± 0.4% in recordings from the hippocampus. Regarding the construction of a ground truth, we know from literature that, in an animal with brain damage such as a stroke, the number of SO-spindle-ripple couplings significantly decreases [44]. This information could be very important for constructing a ground truth with which to validate this routine. So, one approach to achieve this purpose is to apply the routine to both a healthy animal and an animal model with induced brain damage. Firstly, the routine is applied to the healthy animal, which serves as a control group. By analyzing the identified couplings between slow oscillations, spindles and ripples in the healthy brain, it is possible to establish a baseline for the expected coordination patterns. Subsequently, the routine is applied to the animal model with induced brain damage. If the number of couplings between the different brain oscillations shows a significant decrease compared to the healthy animal, it provides evidence that the routine is sensitive to changes in coordination and may be effectively capturing the impact of brain damage. However, due to the absence of a dataset consisting of animals with brain injuries, a surrogate ground truth was created using the following approach: The vector containing the spindle events was artificially shifted by 10, 20, 40, and 80 seconds, simulating different temporal delays. By introducing these delays, the aim was to assess the impact on the identified couplings. The observed trend in the decrease of coupling percentage with increasing temporal delay provides valuable insights, particularly in the context of spindle-ripple detection: even with a 10 second delay, the decrease in SO-spindle coupling percentage was

not overly significant, likely due to the presence of many close couplings, while in spindle-ripple detection the percentage of coupling reaches 0% (table 8,9). This analysis suggests that, as the temporal proximity between the events diminishes, the likelihood of their coupling decreases. While this surrogate ground truth cannot directly validate the routine's performance on animals with brain injuries, it offers a reasonable approximation of the expected behavior and helps shed light on the robustness of the method.

Mouse	Spindle	SO	Ripple	SO-Spindle (#)	Spindle-Ripple (#)	SO-spindle-ripple (#)
Mouse 1	1383	3410	2889	**467**	**74**	**8 (4 in SWS)**
Mouse 2	1286	3562	3548	**516**	**32**	**8 (0 in SWS)**
Mouse 3	1313	3442	3260	**539**	**33**	**8 (4 in SWS)**
Mouse 4	1428	3792	4022	**718**	**24**	**3 (0 in SWS)**
Rat 1	2180	3641	4147	**581**	**70**	**21 (all in SWS)**
Rat 2	1535	3046	3972	**506**	**171**	**18 (all in SWS)**

Table 7 - Number of coupling (SO-spindle-ripple)

Shift	Spindle-SO (%)	Ripple-Spindle (%)
	40.12%	2.49%
(+10s)	37.17%	0%
(+20s)	36.70%	0%
(+40s)	35.77%	0%
(+80s)	33.59%	0%
(+160)	33.44%	0%
(+320)	30.02%	0%
(+600)	25.74%	0%
(+1800)	24.18%	0%

Table 8 – Groundtruth mouse

Shift	Spindle-SO (%)	Ripple-Spindle (%)
RAT2	32.96%	11.14%
(+10s)	28.66%	0%
(+20s)	27.62%	0%
(+40s)	25.73%	0%
(+80s)	22.54%	0%
(+160)	20.78%	0%
(+320)	20.33%	0%
(+600)	21.89%	0%

Table 9 – Groundtruth rats

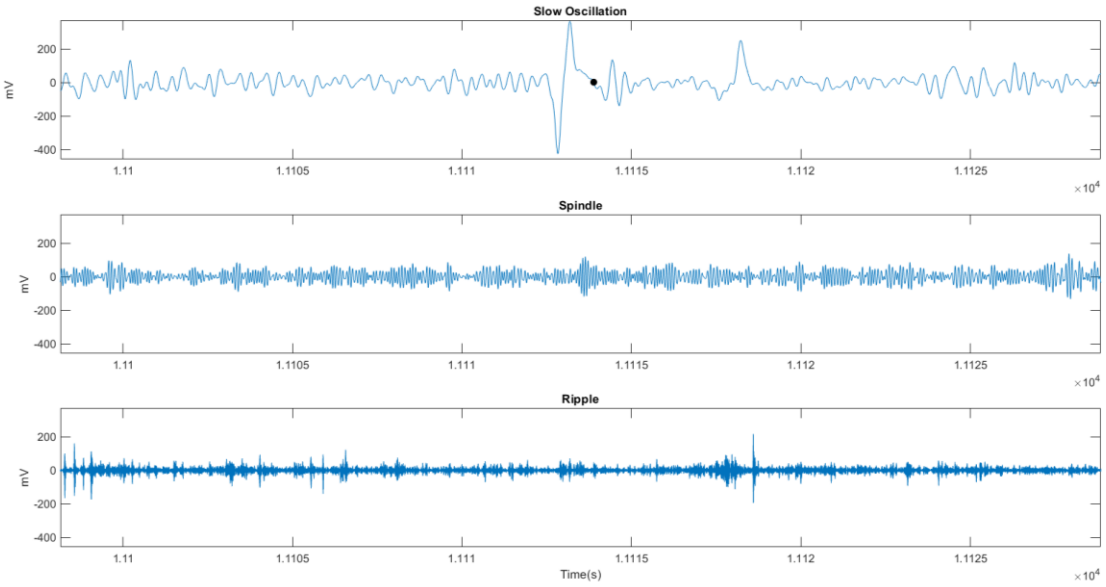

Figure 47 - Triple coordination between SO-spindle-Ripple

Chapter 7

Development of a new sleep stage detection based on PAC

The patterns of modulation identified in this study, summarized in Table 3, have been used as a basis for staging algorithms. Specifically, two types of staging algorithms were developed: a threshold-based method and a neural network-based method.

7.1. Creating a routine for SWC staging using PAC (threshold method).

In the threshold-based method, the discrimination of sleep stages was performed by calculating the modulation index (MI) in 30-second windows for each pair of frequencies listed in Table 3. This calculation was firstly carried out only during wake periods and then applied throughout the whole recording. Subsequently, based on the information provided in Table 3, criteria for stage identification were defined. For instance, the REM stages were identified when the MI values of the whole recording (calculated for frequencies 7.5-70 Hz and 7.5-140 Hz) exceeded their respective maximum thresholds. The upper and lower threshold were determined respectively by calculating the mean plus and the mean minus the standard deviation of the MI values obtained during wake periods for each frequency pair. As we can observe visually from the figure below (figure 48), the threshold method enables accurate discrimination of only the REM phase. The percentage accuracy with which this method can determine the REM phase is indeed very high. By applying the thresholds obtained from the MI values of a mouse in the Berger dataset, this method is capable of discriminating REM phases with an average precision of 94.3 +- 1.4 %, even on other days for the same mouse. However, this method is not as accurate in identifying the slow-wave sleep (SWS) phase or even the wake phase itself. This limitation is likely due to the absence of strong neural synchronization patterns observed during these phases, unlike the REM phase. Overall, since the threshold-based method that utilizes MI values derived from specific frequency pairs has demonstrated its effectiveness in accurately identifying the REM phase in mice, we aimed to

develop more robust algorithms based on neural networks for the precise identification of the whole sleep wake cycle.

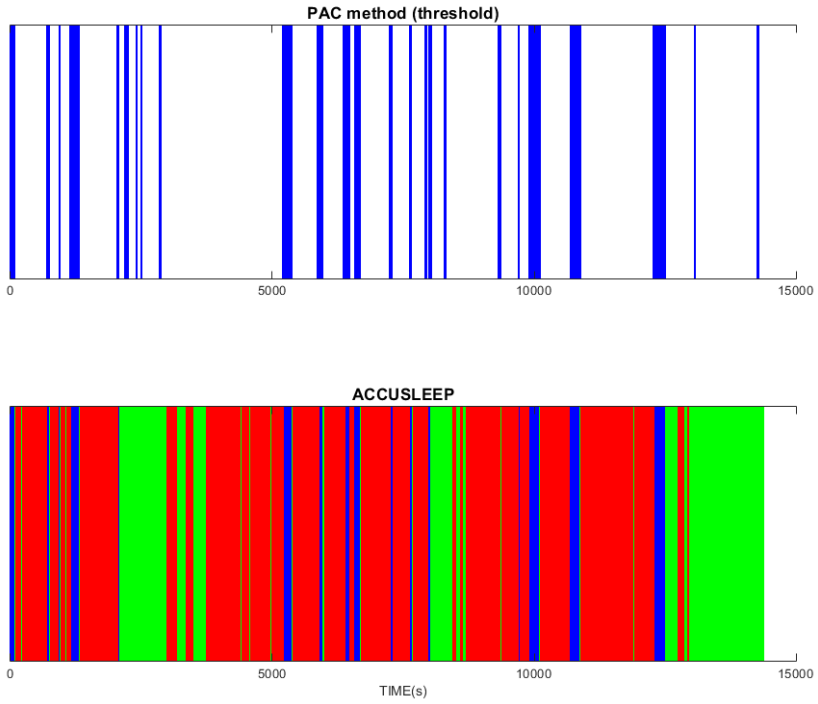

Figure 48 – Mouse 1 day1 REM detection with value of MI

7.2. Creating a routine for SWC staging using PAC (neural network).

I attempted to develop a perceptron-based neural network with limited success. Since the perceptron is primarily suitable for binary classification problems, I adopted the "one-vs-all" approach. I trained a perceptron network for each output class (in this case 3), so that each perceptron network could recognize whether an input data belongs to its respective class. As for the network input, I calculated the significant MI for each frequency pair in 30-second windows. I combined all the values into a matrix, which served as the input for my neural network. However, the results were uninteresting as the network struggled to discriminate between sleep stages. Subsequently, I develop a multiclass neural network called a Multilayer Neural Network (MNL) (figure 49). The purpose of this paragraph is to provide a detailed description of the model used in the study. The model is designed to classify different sleep stages, WAKE, SWS, REM based on PAC

information. This paragraph outlines the training process, the architecture of the neural network, and the activation functions employed.

Data preparation and training Process

The network employed in this model utilizes batch training, which is a method of training a neural network where the entire training dataset is presented to the network at once, and the network weights are updated after each epoch. Batch training can be a beneficial approach, as demonstrated in this case, when the pertinent information necessary for making accurate predictions is consistently distributed across the entire dataset, and there are sufficient computational resources available to process the entire dataset simultaneously. For the input, I tried three different approaches to determine the method that yielded the best performance. Firstly, I constructed the input using the same method as described earlier. Therefore, the input consisted of six neurons, each representing the (MI) value calculated in non-overlapping sliding windows of 30 seconds throughout the whole recording. These calculations were performed for six different frequency pairs as summarized in Table X. Secondly, I experimented with using frequency ranges instead of specific points as inputs. Finally, I incorporated the entire comodulogram as the input, so encompassing not only the selected frequency pairs but the entire range of calculated frequencies. More specifically, each comodulogram representing a 30-second signal was concatenated into a single column, so that the input consisted of a matrix where each column represented a comodulogram of a 30-second time window. For the calculation of the comodulogram, we calculated the coupling between phase frequencies 1.5 - 20.5 Hz and amplitude frequencies 10-200 Hz for each mice using non-overlapping time windows of 30 seconds. So, each column represents an example in the training dataset, while each row represents an attribute or feature. Before training the network, the class labels were converted into a target matrix, where each column represents an example in the training dataset, and each row represents a class. The target matrix is composed of binary values, containing only 0s and 1s. In this matrix, a value of 1 in the i-th row and j-th column indicates that the j-th example belongs to the i-th class. This conversion allows the network to effectively learn and classify the different classes based on the target values provided during training. I then standardized the input, split it randomly into training and testing sets, with 70% for training and 30% for testing the network. Unlike the perceptron network, this type of network can have one or more hidden layers, each with a varying number of neurons. I implemented a network with two layers: input, one hidden layer, and output (figure 43). For the choice of the number of

neurons in the hidden layer, there are some empirically derived rules of thumb. Among these, the most commonly relied upon is 'the optimal size of the hidden layer is usually between the size of the input and size of the output layers'. In sum, for most problems, one could probably get decent performance (even without a second optimization step) by setting the hidden layer configuration using just two rules: (i) the number of hidden layers equals one; and (ii) the number of neurons in that layer is the mean of the neurons in the input and output layers [45]. Once the data was prepared, the 'train' function in MATLAB was used to train the neural network. During the training process, for each epoch (up to a maximum of 1000), the entire training dataset is presented to the network. The input neurons transmit the output to the neurons in the hidden layer. The hidden neurons further process the information using the logistic sigmoid activation function and send the output to the output layer neurons. The output neurons process the information using the softmax activation function and generate the final output of the network for all examples in the training dataset. The final output of the network is then compared to the target values, and the total error is computed using the cross-entropy loss function. This error is used to update the network's weights using the scaled conjugate gradient algorithm. The process is repeated for subsequent epochs until the maximum number of epochs is reached or one of the stopping criteria is satisfied (the performance of the network gradually worsened over six consecutive epochs, indicating a declining trend in accuracy and predictive capability). The logistic sigmoid function is commonly used for the hidden neurons in neural networks because it introduces nonlinearity, enabling the network to model nonlinear relationships between inputs and outputs. The logistic sigmoid function maps the input to a range between 0 and 1, which can be useful for representing probabilities. The softmax function is a common activation function for output neurons in neural networks for multiclass classification. It maps the input to a vector of values between 0 and 1 that sum up to 1. This can be useful for representing the probabilities of different classes. The cross-entropy loss function is a common performance measure for classification problems. It measures the divergence between the predicted probability distributions of the network and the target probability distributions. Minimizing the error computed by the cross-entropy loss function during training helps the network produce outputs that closely approximate the target distributions.

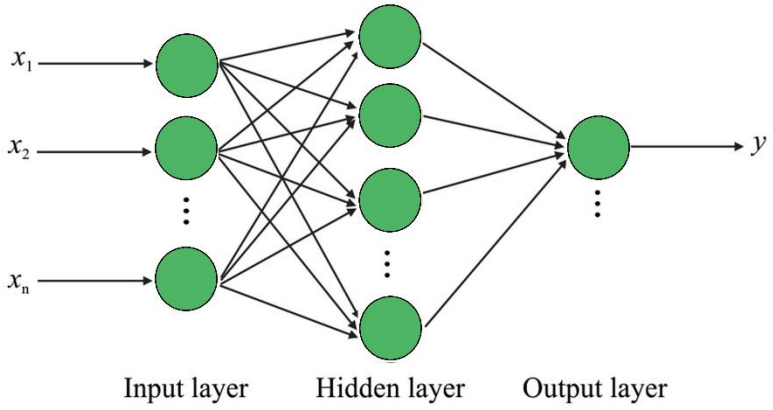

Figure 49 – Multilayer neural network

Results

Afterward, I tested the network multiple times, each with a different number of neurons, ranging from one to the maximum specified. For each network trained with a different number of neurons, I calculated the area under the curve (AUC). The AUC (Area Under the roc Curve) is a metric commonly used in evaluating the performance of classification models. The AUC provides a measure of how well a classifier can distinguish between positive and negative samples. It ranges from 0 to 1, where a value of 0.5 indicates random guessing and a value of 1 signifies a perfect classifier that can perfectly separate the two classes. Values below 0.5 indicate poor performance, as the classifier's predictions are worse than random guessing. The network that generated the highest AUC was selected. I repeated this process for several iterations (in my case 15), and the chosen network was the one that yielded the best performance. The best performance was achieved by training the network using input with the comodulogram (figure 50, 51, 52, 53). By training the network with mouse1 data from day 1, it is interesting to observe that we achieve accurate classification not only of the rapid eye movement (REM) phase but also of the slow wave sleep (SWS) and wake phase. Notably, the created network demonstrates not only good performance when applied to recordings of the same mouse on different days but also the ability to accurately discriminate the sleep-wake cycle when applied to recordings from other mice in the dataset. This is particularly interesting because the algorithm used as the ground truth is unable to achieve this. Subsequently, by training the network with day one data from all 10 mice in the dataset, the performance further improved while maintaining stability in terms of performance across different mice (figure 54). So, the best performance was achieved by training the network using input with six different frequency pairs, resulting in a mean performance of 92.6+-0.6.

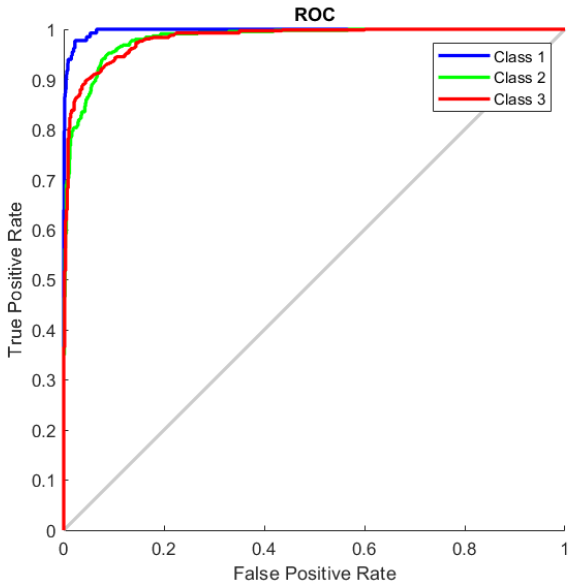

Figure 50 – The ROC curve of the MLN PAC method with comodulograms computed using sliding windows of 30 seconds.

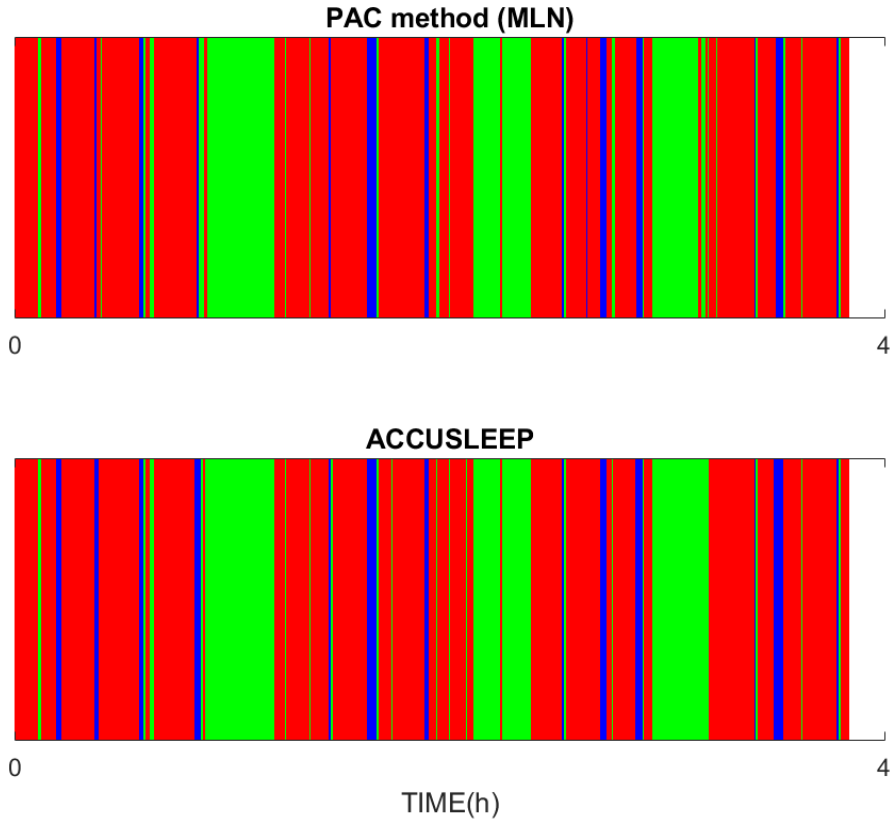

Figure 51 - Comparison of hypnograms, mouse 2 day3. The upper one is obtained using the MLP neural network with the input of comodulograms from all mice on day 1. The lower one represents the ground truth. The similarity between them is 96.2%, demonstrating that this method is highly reliable.

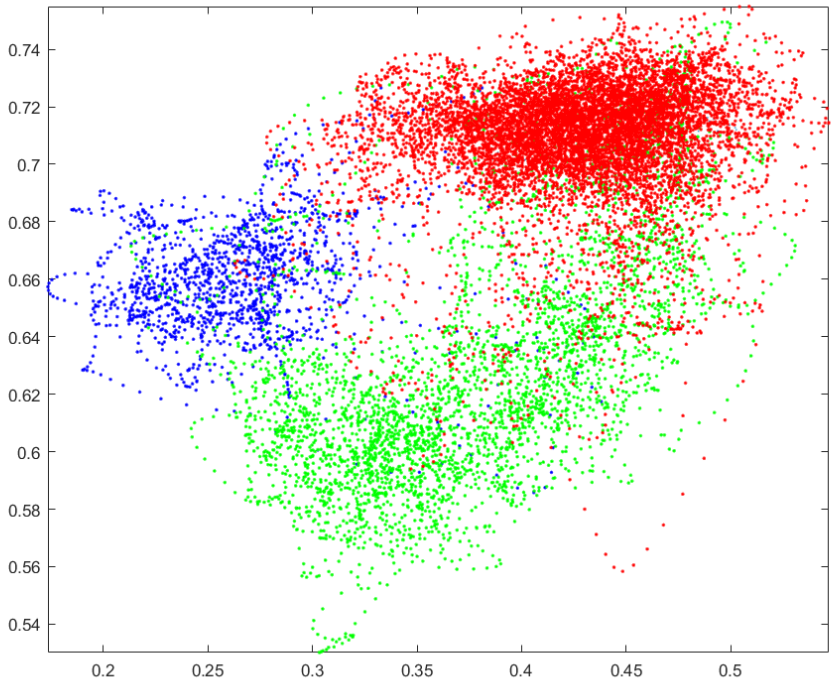

Figure 52 - Classification of MLN PAC method in the state space created in Gervasoni algorithm of mouse 2 day3.

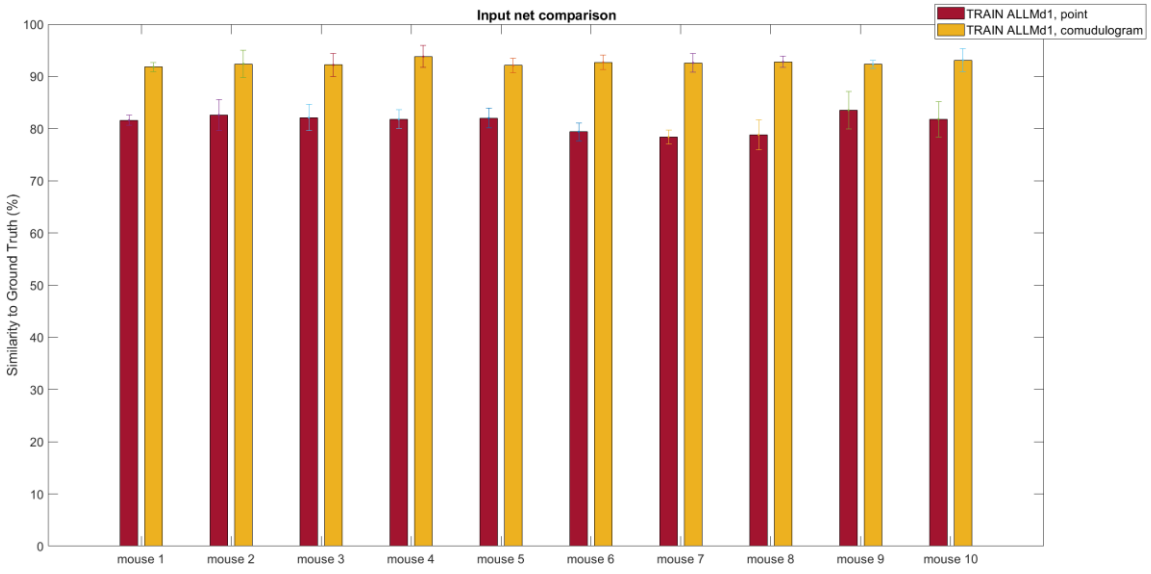

Figure 53 – Comparing training performance between single point of frequencies and comodulogram in input; as observed, a significant improvement in performance is evident when

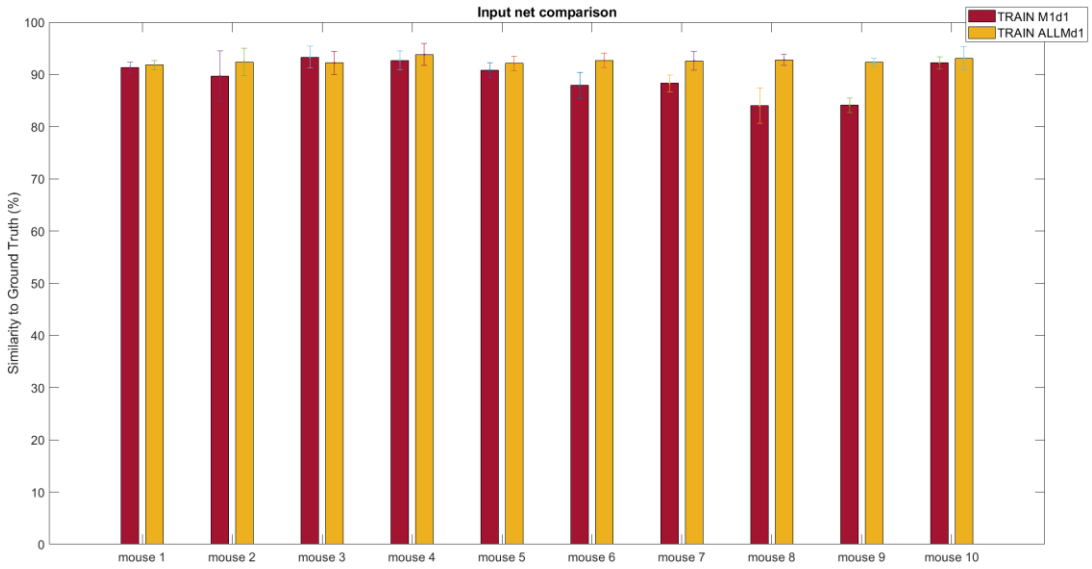

applying the comodulogram as input.

Figure 54 – Comparing training performance between single mouse and multiple mice input.

Conclusions

In this thesis work, the main neural synchronization patterns occurring during the sleep-wake cycle were identified, and their variations across different stages were investigated. Particularly, we observed that phase-amplitude coupling (PAC) between theta phase and gamma amplitude (both high and low) significantly increased during REM sleep compared to both wakefulness (WK) and slow wave sleep (SWS), and it also increased in WK compared to SWS. These findings can be straightforwardly interpreted in relation to the acquisition of memory traces during active exploration in WK and their subsequent consolidation during sleep, processes in which theta and gamma oscillations play important roles [14]. Although theta is a rhythm generated within hippocampal circuitry, its influence in cortical areas (such as the prefrontal region) can be captured by cortical electrodes such as those used in the acquisition of the recordings. Additionally, PAC values between delta and theta were significantly increased during SWS compared to both WK and REM. Delta waves are the predominant rhythms observed during SWS, and theta activity during non-REM sleep may play a role in sleep-dependent memory consolidation in humans [2]. Therefore, it can be concluded that the sleep-wake cycle strongly modulates PAC patterns, but PAC fails to detect the triple oscillation (slow oscillation-spindle-ripple) phenomenon. The alternative method implemented, to detect the SO-spindle-ripple coupling, demonstrated its capability to identify and analyze the coordination of slow oscillations, spindles and ripples. The results obtained from the four tested animals align with existing literature and provide insights into the coupling dynamics within the SWC. The investigation of temporal delays further contributes to understanding the robustness and sensitivity of the method. However, it is crucial to emphasize the need for future studies involving animal models with brain damage to validate the routine's performance in accurately detecting and quantifying the impact of such injuries on the coordination of slow oscillations, spindles and ripples. This validation would provide further confidence in the method's effectiveness and its potential as a tool for investigating dysfunctional SWCs in the context of neurological disorders and injuries. In our research, we developed a multilayer neural network based SWC stage detection algorithm that leveraged the patterns of neural synchronization. This algorithm offers significant utility as it does not rely on machine learning or spectral methods, providing additional insights into the specific associations between detected couplings and the stages in which they occur. This information can be particularly valuable when applying the method to animal models with brain lesions, such as stroke. In fact, this method, in addition to generating the same level of recognition as traditionally used techniques when applied to healthy animals, has

the potential to identify dysfunctional Sleep-Wake Cycles (SWCs) through its ability to associate main synchronizations within their respective stages. For instance, while a standard algorithm may indicate a normal wakefulness phase, the observed cerebral oscillations might resemble those typically seen in the REM sleep phase, suggesting a dysfunctional SWC associated with daydreaming or other types of pathologies that may not be evident through other algorithms. This research underscores the importance of incorporating neurobiologically plausible measures, such as PAC, into stage detection algorithms, as they provide a deeper understanding of the underlying neural dynamics and facilitate the identification of aberrant SWC patterns. The proposed algorithm holds promise for identifying and characterizing such patterns, offering potential applications in neurological research, clinical diagnostics, and therapeutic interventions targeting SWC dysfunctions.

References

[1] Siegel JM. Phylogeny and the function of REM sleep. Behav Brain Res. 1995 Jul-Aug;69(1-2):29-34.

[2] Kandel, E. R., Schwartz, J. H., & Jessell, T.M. eds., 2000. "Sleep and Dream". Principles of Neuroscience, 5th edn. New York: McGraw-hill.

[3] Rechtschaffen A. Current perspectives on the function of sleep. Perspect Biol Med. 1998 Spring;41(3):359-90.

[4] Ribeiro S, Gervasoni D, Soares ES, Zhou Y, Lin SC, Pantoja J, Lavine M, Nicolelis MA. Long-lasting novelty-induced neuronal reverberation during slow-wave sleep in multiple forebrain areas. PLoS Biol. 2004 Jan;2(1): E24.

[5] Born J, Wilhelm I. System consolidation of memory during sleep. Psychol Res. 2012 Mar;76(2):192-203.

[6] Blanco W, Pereira CM, Cota VR, Souza AC, Rennó-Costa C, Santos S, Dias G, Guerreiro AM, Tort AB, Neto AD, Ribeiro S. Synaptic Homeostasis and Restructuring across the Sleep-Wake Cycle. PLoS Comput Biol. 2015 May 28;11(5):e1004241.

[7] Thau L, Reddy V, Singh P. Anatomy, Central Nervous System. [Updated 2022 Oct 10]. In: StatPearls [Internet]. Treasure Island (FL): StatPearls Publishing; 2023 Jan-. Available from: https://www.ncbi.nlm.nih.gov/books/NBK542179/

[8] Cologne, Germany: Institute for Quality and Efficiency in Health Care (IQWiG); 2006-. How does the nervous system work? 2009 Oct 28 [Updated 2016 Aug 19].

[9] M.F. Bear, B.W. Connors, and M.A. Paradiso. Neuroscience exploring the brain. Lippincott Williams & Wilkins, third edition, 2007.

[10] Chen I, Lui F. Neuroanatomy, Neuron Action Potential. [Updated 2022 Aug 8]. In: StatPearls [Internet]. Treasure Island (FL): StatPearls Publishing; 2023 Jan-. Available from: https://www.ncbi.nlm.nih.gov/books/NBK546639/

[11] Steriade M, Nuñez A, Amzica F. A novel slow (< 1 Hz) oscillation of neocortical neurons in vivo: depolarizing and hyperpolarizing components. J Neurosci. 1993 Aug;13(8):3252-65. doi: 10.1523/JNEUROSCI.13-08-03252.1993. PMID: 8340806; PMCID: PMC6576541.

[12] Maldonado KA, Alsayouri K. Physiology, Brain. [Updated 2023 Mar 17]. In: StatPearls [Internet]. Treasure Island (FL): StatPearls Publishing; 2023 Jan-. Available from: https://www.ncbi.nlm.nih.gov/books/NBK551718/

[13] National Institute of Neurological Disorders and Stroke. (n.d.). Brain Basics: Understanding Sleep. Retrieved

[14] Jones BE. Basic mechanisms of sleep-wake states. In: Kryger MH, Roth T, Dement WC, editors. Principles and Practice of Sleep Medicine. 4th ed. Philadelphia: Elsevier/Saunders; 2005. pp. 136–153

[15] Institute of Medicine (US) Committee on Sleep Medicine and Research; Colten HR, Altevogt BM, editors. Sleep Disorders and Sleep Deprivation: An Unmet Public Health Problem. Washington (DC): National Academies Press (US); 2006. 2, Sleep Physiology. Available from: https://www.ncbi.nlm.nih.gov/books/NBK19956/

[16] Rasch B, Born J. About sleep's role in memory. Physiol Rev. 2013 Apr;93(2):681-766. doi: 10.1152/physrev.00032.2012. PMID: 23589831; PMCID: PMC3768102.

[17] Rångtell, F.H., Karamchedu, S., Andersson, P., van Egmond, L., Hultgren, T., Broman, JE., Cedernaes, J., Benedict, C. (2017) Learning performance is linked to procedural memory consolidation across both sleep and wakefulness. Sci Rep, 7(1):10234

[18] Kandel, E. R., Schwartz, J. H., & Jessell, T.M. eds., 2000. “Sleep and Dream”. Principles of Neuroscience, 5th edn. New York: McGraw-hill.

[19] Patel AK, Reddy V, Shumway KR, et al. Physiology, Sleep Stages. [Updated 2022 Sep 7]. In: StatPearls [Internet]. Treasure Island (FL): StatPearls Publishing; 2023 Jan.

[20] Iber C, Ancoli-Israel S, Chesson Jr. AL, Quan SF. The AASM Manual for the Scoring of Sleep and Associated Events. Rules Terminology and Technical Specifications. 2007.

[21] Britton JW, Frey LC, Hopp JLet al., authors; St. Louis EK, Frey LC, editors. Electroencephalography (EEG): An Introductory Text and Atlas of Normal and Abnormal Findings in Adults, Children, and Infants [Internet]. Chicago: American Epilepsy Society; 2016. The Normal EEG.

[22] Duss SB, Seiler A, Schmidt MH, Pace M, Adamantidis A, Müri RM, Bassetti CL. The role of sleep in recovery following ischemic stroke: A review of human and animal data. Neurobiol Sleep Circadian Rhythms. 2016 Nov 29; 2:94-105. doi: 10.1016/j.nbscr.2016.11.003. PMID: 31236498; PMCID: PMC6575180.

[23] Rasch B., Born J. About sleep's role in memory. Physiol. Rev. 2013; 93:681–766.

[24] Mölle M, Eschenko O, Gais S, Sara SJ, Born J. The influence of learning on sleep slow oscillations and associated spindles and ripples in humans and rats. Eur. J. Neurosci. 2009; 29: 1071–81.

[25] Improved sleep scoring in mice reveals human-like stages. Marie Masako Lacroix, Gaetan de Lavilléon, Julie Lefort, Karim Kanbi, Sophie Bagur, Samuel Laventure, Yves Dauvilliers, Christelle Peyron, Karim Benchenane bioRxiv 489005; doi: https://doi.org/10.1101/489005

[26] Tonegawa S, Liu X, Ramirez S, Redondo R. Memory engram cells have come of age. Neuron 87: 918–931, 2015. doi: 10.1016/j.neuron.2015.08.002.

[27] Timofeev I, Bazhenov M, Seigneur J, et al. Neuronal Synchronization and Thalamocortical Rhythms in Sleep, Wake and Epilepsy. In: Noebels JL, Avoli M, Rogawski MA, et al., editors. Jasper's Basic Mechanisms of the Epilepsies [Internet]. 4th edition. Bethesda (MD): National Center for Biotechnology Information (US); 2012. Available from: https://www.ncbi.nlm.nih.gov/books/NBK98144/

[28] Roumis DK, Frank LM. Hippocampal sharp-wave ripples in waking and sleeping states. Curr Opin Neurobiol. 2015 Dec; 35:6-12. doi: 10.1016/j.conb.2015.05.001. Epub 2015 May 23. PMID: 26011627; PMCID: PMC4641767.

[29] Joel Frohlich, Daniel Toker, Martin M Monti, Consciousness among delta waves: a paradox? Brain, Volume 144, Issue 8, August 2021, Pages 2257–2277.

[30] Buzsáki G, Wang XJ. Mechanisms of gamma oscillations. Annu Rev Neurosci. 2012; 35:203-25. doi: 10.1146/annurev-neuro-062111-150444. Epub 2012 Mar 20. PMID: 22443509; PMCID: PMC4049541.

[31] Mably AJ, Colgin LL. Gamma oscillations in cognitive disorders. Curr Opin Neurobiol. 2018 Oct; 52:182-187. doi: 10.1016/j.conb.2018.07.009. Epub 2018 Aug 16. PMID: 30121451; PMCID: PMC6139067.

[32] Gerashchenko D, Wisor JP, Kilduff TS. Sleep-active cells in the cerebral cortex and their role in slow-wave activity. Sleep Biol Rhythms. 2011 Jan;9(s1):71-77. doi: 10.1111/j.1479-8425.2010.00461. x. PMID: 21625335; PMCID: PMC3103062.

[33] Goyal, A., Miller, J., Qasim, S.E. et al. Functionally distinct high and low theta oscillations in the human hippocampus. Nat Commun 11, 2469 (2020). https://doi.org/10.1038/s41467-020-15670-6

[34] Danielle K. Sandsmark, MD, PhD, Jonathan E. Elliott, PhD, Miranda M. Lim, MD, PhD, Sleep-Wake Disturbances After Traumatic Brain Injury: Synthesis of Human and Animal Studies, Sleep, Volume 40, Issue 5, 1 May 2017, zsx044.

[35] Kim J, Guo L, Hishinuma A, Lemke S, Ramanathan DS, Won SJ, Ganguly K. Recovery of consolidation after sleep following stroke-interaction of slow waves, spindles, and GABA. Cell Rep. 2022 Mar 1;38(9):110426. doi: 10.1016/j.celrep.2022.110426. PMID: 35235787; PMCID: PMC9281513.

[36] Gruber R, Wise MS. Sleep spindle characteristics in children with neurodevelopmental disorders and their relation to cognition. Neural Plast 2016: 4724792, 2016. doi:10.1155/2016/4724792.

[37] Wilhelm I, Groch S, Preiss A, Walitza S, Huber R. Widespread reduction in sleep spindle activity in socially anxious children and adolescents. J Psychiatr Res 88: 47–55, 2017. doi: 10.1016/j.jpsychires.2016.12.018.

[38] Nishida M, Nakashima Y, Nishikawa T. Slow sleep spindle and procedural memory consolidation in patients with major depressive disorder. Nat Sci Sleep 8: 63–72, 2016. doi:10.2147/NSS.S100337.

[39] Urakami Y. Relationship between, sleep spindles and clinical recovery in patients with traumatic brain injury: a simultaneous EEG and MEG study. Clin EEG Neurosci 43: 39–47, 2012. doi:10.1177/1550059411428718.

[40] Ducharme-Crevier L, Press CA, Kurz JE, Mills MG, Goldstein JL, Wainwright MS. Early presence of sleep spindles on electroencephalography is associated with good outcome after pediatric cardiac arrest. Pediatr Crit Care Med 18: 452–460, 2017. doi:10.1097/PCC.0000000000001137.

[41] Réboli LA, Maciel RM, de Oliveira JC, Moraes MFD, Tilelli CQ, Cota VR. Persistence of neural function in animals submitted to seizure-suppressing scale-free nonperiodic electrical stimulation applied to the amygdala. Behav Brain Res. 2022 May 24;426:113843. doi: 10.1016/j.bbr.2022.113843. Epub 2022 Mar 15. PMID: 35304185.

[42] Barger Z, Frye CG, Liu D, Dan Y, Bouchard KE. Robust, automated sleep scoring by a compact neural network with distributional shift correction. PLoS One. 2019 Dec 13;14(12):e0224642. doi: 10.1371/journal.pone.0224642. PMID: 31834897; PMCID: PMC6910668.27

[43] Fernandez LMJ, Lüthi A. Sleep Spindles: Mechanisms and Functions. Physiol Rev. 2020 Apr 1;100(2):805-868. doi: 10.1152/physrev.00042.2018. Epub 2019 Dec 5. PMID: 31804897.

[44] Kim J, Guo L, Hishinuma A, Lemke S, Ramanathan DS, Won SJ, Ganguly K. Recovery of consolidation after sleep following stroke-interaction of slow waves, spindles, and GABA. Cell Rep. 2022 Mar 1;38(9):110426.

[45] Uygun DS, Katsuki F, Bolortuya Y, Aguilar DD, McKenna JT, Thankachan S, McCarley RW, Basheer R, Brown RE, Strecker RE, McNally JM. Validation of an automated sleep spindle detection method for mouse electroencephalography. Sleep. 2019 Feb 1;42(2):zsy218. doi: 10.1093/sleep/zsy218. PMID: 30476300; PMCID: PMC6611948.

[45] J. LaRocco, P. J. Franaszczuk, S. Kerick, and K. Robbins, “Spindler: a framework for parametric analysis and detection of spindles in EEG with application to sleep spindles,” Journal of Neural Engineering, vol. 15, no. 6, article 066015, 2018.

[46] Sampson AL, Lainscsek C, Gonzalez CE, Ulbert I, Devinsky O, Fabó D, Madsen JR, Halgren E, Cash SS, Sejnowski TJ. Delay differential analysis for dynamical sleep spindle detection. J Neurosci Methods. 2019 Mar 15;316:12-21. doi: 10.1016/j.jneumeth.2019.01.009. Epub 2019 Jan 30. PMID: 30707917; PMCID: PMC6447286.

[47] Gervasoni D, Lin SC, Ribeiro S, Soares ES, Pantoja J, Nicolelis MA. Global forebrain dynamics predict rat behavioral states and their transitions. J Neurosci. 2004 Dec 8;24(49):11137-47.

[48] Tort AB, Komorowski R, Eichenbaum H, Kopell N. Measuring phase-amplitude coupling between neuronal oscillations of different frequencies. J Neurophysiol. 2010 Aug;104(2):1195-210.

[49] Aguilera M, Douchamps V, Battaglia D, Goutagny R. How Many Gammas? Redefining Hippocampal Theta-Gamma Dynamic During Spatial Learning. Front Behav Neurosci. 2022 Feb 1;16:811278.

[50] Bandarabadi M, Boyce R, Gutierrez Herrera C, Bassetti CL, Williams S, Schindler K, Adamantidis A. Dynamic modulation of theta-gamma coupling during rapid eye movement sleep. Sleep. 2019 Dec 24;42(12):182.

[51] Tort AB, Scheffer-Teixeira R, Souza BC, Draguhn A, Brankačk J. Theta-associated high-frequency oscillations (110-160Hz) in the hippocampus and neocortex. Prog Neurobiol. 2013 Jan;100:1-14.

[52] Destexhe, A. Sejnowski, T. J. Sleep and sleep states: Thalamic regulation Squire, L. H. (Ed.), In: Encyclopedia of Neuroscience, 973-976, 2009

[53] Khodagholy D, Gelinas JN, Buzsáki G. Learning-enhanced coupling between ripple oscillations in association cortices and hippocampus. Science. 2017 Oct 20;358(6361):369-372. doi: 10.1126/science.aan6203. PMID: 29051381; PMCID: PMC5872145.

[54] Heaton, Jeff, Introduction to Neural Networks for Java, 2nd Edition, 2008, Heaton Research, Inc, 2nd.

Acknowledgments

I would like to express my sincere gratitude to the individuals who have contributed to the completion of this thesis. First of all, I would like to thank my supervisor, Prof.ssa Michela Chiappalone, for providing me with the opportunity to work on this project. Her guidance, support, and expertise have been invaluable throughout this journey. I would also like to extend a heartfelt thank you to my co-supervisor, Phd Vinicius Rosa Cota, for his unwavering support and assistance. His constant presence and willingness to help, approaching me not as a superior but as a colleague, have greatly contributed to the quality and progress of my work.